

ISSN 2523-0344

Volume 9, Issue – 19 July – December – 2023

Journal Industrial Engineering

ECORFAN®

ECORFAN-Perú

Chief Editor

SERRUDO-GONZALES, Javier. BsC

Executive Director

RAMOS-ESCAMILLA, María. PhD

Editorial Director

PERALTA-CASTRO, Enrique. MsC

Web Designer

ESCAMILLA-BOUCHAN, Imelda. PhD

Web Diagrammer

LUNA-SOTO, Vladimir. PhD

Editorial Assistant

SORIANO-VELAZCO, Jesús. BsC

Philologist

RAMOS-ARANCIBIA, Alejandra. BsC

Journal Industrial Engineering, Volume 7, Issue 19, December, 2023, is a biannual magazine published by ECORFAN-República del Perú. AV. La Raza, No 1047 - Santa Ana, Cusco-Peru, CP: 11500. WEB: http://www.ecorfan.org/republicofperu/rj_ingenieria_industrial.php, revista@ecorfan.org. Editor in Chief: SERRUDO-GONZALES, Javier. BsC. ISSN: 2523-0344. Responsible for the last update of this issue Unidad Informática ECORFAN. Imelda Escamilla Bouchán, PhD. Vladimir Luna Soto, PhD. Updated December 30, 2021.

The views expressed by the authors do not necessarily reflect the views of the publisher.

The total or partial reproduction of the contents and images of the publication without permission of the Instituto Nacional de Defensa de la Competencia y Protección de la Propiedad Intelectual is strictly prohibited.

Journal Industrial Engineering

Definition of Research Journal

Scientific Objectives

Support the international scientific community in its written production Science, Technology and Innovation in the Field of Engineering and Technology, in Subdisciplines Production systems design, product quality management, operations research, computer simulation, supply chains, quality certification, hydrometeorology.

ECORFAN-Mexico, S.C. is a Scientific and Technological Company in contribution to the Human Resource training focused on the continuity in the critical analysis of International Research and is attached to CONAHCYT-RENIECYT number 1702902, its commitment is to disseminate research and contributions of the International Scientific Community, academic institutions, agencies and entities of the public and private sectors and contribute to the linking of researchers who carry out scientific activities, technological developments and training of specialized human resources with governments, companies and social organizations.

Encourage the interlocution of the International Scientific Community with other Study Centers in Mexico and abroad and promote a wide incorporation of academics, specialists and researchers to the publication in Science Structures of Autonomous Universities - State Public Universities - Federal IES - Polytechnic Universities - Technological Universities - Federal Technological Institutes - Normal Schools - Decentralized Technological Institutes - Intercultural Universities - S & T Councils - CONAHCYT Research Centers.

Scope, Coverage and Audience

Journal Industrial Engineering is a Journal edited by ECORFAN-Mexico, S.C. in its Holding with repository in Republic of Peru, is a scientific publication arbitrated and indexed with semester periods. It supports a wide range of contents that are evaluated by academic peers by the Double-Blind method, around subjects related to the theory and practice of Production systems design, product quality management, operations research, computer simulation, supply chains, quality certification, hydrometeorology with diverse approaches and perspectives , That contribute to the diffusion of the development of Science Technology and Innovation that allow the arguments related to the decision making and influence in the formulation of international policies in the Field of Engineering and Technology. The editorial horizon of ECORFAN-Mexico® extends beyond the academy and integrates other segments of research and analysis outside the scope, as long as they meet the requirements of rigorous argumentative and scientific, as well as addressing issues of general and current interest of the International Scientific Society.

Editorial Board

AYALA - GARCÍA, Ivo Neftalí. PhD
University of Southampton

CASTILLO - LÓPEZ, Oscar. PhD
Academia de Ciencias de Polonia

CENDEJAS - VALDEZ, José Luis. PhD
Universidad Politécnica de Madrid

DIAZ - RAMIREZ, Arnoldo. PhD
Universidad Politécnica de Valencia

HERNÁNDEZ - PRIETO, María de Lourdes. PhD
Universidad Gestalt

LAGUNA, Manuel. PhD
University of Colorado

LARA - ROSANO, Felipe. PhD
Universidad de Aachen

RIVAS - PEREA, Pablo. PhD
University of Texas

TIRADO - RAMOS, Alfredo. PhD
University of Amsterdam

VEGA - PINEDA, Javier. PhD
University of Texas

Arbitration Committee

DÍAZ - CASTELLANOS, Elizabeth Eugenia. PhD
Universidad Popular Autónoma del Estado de Puebla

MALDONADO - MACÍAS, Aidé Aracely. PhD
Instituto Tecnológico de Ciudad Juárez

NAKASIMA – LÓPEZ, Mydory Oyuky. PhD
Universidad Autónoma de Baja California

OCHOA - CRUZ, Genaro. PhD
Instituto Politécnico Nacional

REALYVÁSQUEZ - VARGAS, Arturo. PhD
Universidad Autónoma de Ciudad Juárez

TABOADA - GONZÁLEZ, Paul Adolfo. PhD
Universidad Autónoma de Baja California

VALDEZ - ACOSTA, Fevrier Adolfo. PhD
Universidad Autónoma de Baja California

VASQUEZ - SANTACRUZ, J.A. PhD
Centro de Investigación y Estudios Avanzados

ARREDONDO - SOTO, Karina Cecilia. PhD
Instituto Tecnológico de Ciudad Juárez

RODRÍGUEZ – DÍAZ, Antonio. PhD
Universidad Autónoma de Baja California

RUELAS-SANTOYO, Edgar Augusto. PhD
Instituto Tecnológico Superior de Irapuato

Assignment of Rights

The sending of an Article to Journal Industrial Engineering emanates the commitment of the author not to submit it simultaneously to the consideration of other series publications for it must complement the Originality Format for its Article.

The authors sign the Authorization Format for their Article to be disseminated by means that ECORFAN-Mexico, S.C. In its Holding Republic of Peru considers pertinent for disclosure and diffusion of its Article its Rights of Work.

Declaration of Authorship

Indicate the Name of Author and Coauthors at most in the participation of the Article and indicate in extensive the Institutional Affiliation indicating the Department.

Identify the Name of Author and Coauthors at most with the CVU Scholarship Number-PNPC or SNI-CONAHCYT- Indicating the Researcher Level and their Google Scholar Profile to verify their Citation Level and H index.

Identify the Name of Author and Coauthors at most in the Science and Technology Profiles widely accepted by the International Scientific Community ORC ID - Researcher ID Thomson - arXiv Author ID - PubMed Author ID - Open ID respectively.

Indicate the contact for correspondence to the Author (Mail and Telephone) and indicate the Researcher who contributes as the first Author of the Article.

Plagiarism Detection

All Articles will be tested by plagiarism software PLAGSCAN if a plagiarism level is detected Positive will not be sent to arbitration and will be rescinded of the reception of the Article notifying the Authors responsible, claiming that academic plagiarism is criminalized in the Penal Code.

Arbitration Process

All Articles will be evaluated by academic peers by the Double Blind method, the Arbitration Approval is a requirement for the Editorial Board to make a final decision that will be final in all cases. MARVID® is a derivative brand of ECORFAN® specialized in providing the expert evaluators all of them with Doctorate degree and distinction of International Researchers in the respective Councils of Science and Technology the counterpart of CONAHCYT for the chapters of America-Europe-Asia- Africa and Oceania. The identification of the authorship should only appear on a first removable page, in order to ensure that the Arbitration process is anonymous and covers the following stages: Identification of the Research Journal with its author occupation rate - Identification of Authors and Coauthors - Detection of plagiarism PLAGSCAN - Review of Formats of Authorization and Originality-Allocation to the Editorial Board- Allocation of the pair of Expert Arbitrators-Notification of Arbitration -Declaration of observations to the Author-Verification of Article Modified for Editing-Publication.

Instructions for Scientific, Technological and Innovation Publication

Knowledge Area

The works must be unpublished and refer to topics of Production systems design, product quality management, operations research, computer simulation, supply chains, quality certification, hydrometeorology and other topics related to Engineering and Technology.

Content Presentation

As the first article, we present, *Topological and structural optimization of the brake pedal of a vehicle for the BAJASAE 2023 competition*, by CORDERO-GURIDI José de Jesús, ALVAREZ-SANTIAGO Jesús Daniel, MARTINEZ-DIAZ Ana Paola and HERNANDEZ-URBANO Cesar, with adscription in the Universidad Popular Autónoma del Estado de Puebla, as second article we present, *Design of a nozzle for Stratasys uPrint SE Plus 3D printer*, by CORTEZ-SOLIS, Reynaldo, ARENAS-ISLAS, David, BETANZOS-CASTILLO, Francisco and FUENTES-CASTAÑEDA, Pilaro, with adscription in the Posgrado CIATEQ, A.C., Tecnológico Nacional de México- TES Valle de Bravo, as third article we present, *Photovoltaic Autonomous Electric Charging Station*, by GARCÍA-CONTRERAS, Cecilia Pamela, ONTIVEROS-SÁNCHEZ, Kenneth Arturo and ALVAREZ-MACÍAS, Carlos, with adscription in the Instituto Tecnológico Nacional de México - Instituto Tecnológico de la Laguna, as fourth article we present, *Simulation model in ProModel to generate proposals for improving the H₂O purification process*, by RUIZ-DIAZ, Montserrat, SOTO-LEYVA, Yasmin, BONEMARTÍNEZ, Rosalía, and SANTOS-OSORIO, Arturo, with adscription in the Tecnológico Nacional de México - Instituto Tecnológico Superior de Huauchinango.

Content

Article	Page
Topological and structural optimization of the brake pedal of a vehicle for the BAJASAE 2023 competition CORDERO-GURIDI José de Jesús, ALVAREZ-SANTIAGO Jesús Daniel, MARTINEZ-DIAZ Ana Paola and HERNANDEZ-URBANO Cesar <i>Universidad Popular Autónoma del Estado de Puebla</i>	1-12
Design of a nozzle for Stratasys uPrint SE Plus 3D printer CORTEZ-SOLIS, Reynaldo, ARENAS-ISLAS, David, BETANZOS-CASTILLO, Francisco and FUENTES-CASTAÑEDA, Pilar <i>Posgrado CIATEQ, A.C.</i> <i>Tecnológico Nacional de México-TES Valle de Bravo</i>	13-37
Photovoltaic Autonomous Electric Charging Station GARCÍA-CONTRERAS, Cecilia Pamela, ONTIVEROS-SÁNCHEZ, Kenneth Arturo and ALVAREZ-MACÍAS, Carlos <i>Instituto Tecnológico Nacional de México - Instituto Tecnológico de la Laguna</i>	38-52
Simulation model in ProModel to generate proposals for improving the H₂O purification process RUIZ-DIAZ, Montserrat, SOTO-LEYVA, Yasmin, BONES-MARTÍNEZ, Rosalía, and SANTOS-OSORIO, Arturo <i>Tecnológico Nacional de México - Instituto Tecnológico Superior de Huauchinango</i>	53-59

Topological and structural optimization of the brake pedal of a vehicle for the BAJA SAE 2023 competition

Optimización topológica y estructural del pedal de freno de un vehículo para la competencia BAJA SAE 2023

CORDERO-GURIDI José de Jesús †*, ALVAREZ-SANTIAGO Jesús Daniel, MARTINEZ-DIAZ Ana Paola and HERNANDEZ-URBANO Cesar

Universidad Popular Autónoma del Estado de Puebla

ID 1st Author: *José de Jesús, Cordero-Guridi* / ORC ID: 0000-0001-5201-1906

ID 1st Co-author: *Jesús Daniel, Álvarez-Santiago* / ORC ID: 0009-0002-3182-6043

ID 2nd Co-author: *Ana Paola, Martínez-Díaz* / ORC ID: 0009-0009-5803-0601

ID 3rd Co-author: *Cesar, Hernández-Urbano* / ORC ID: 0009-0002-2346-5364

DOI: 10.35429/JIE.2023.19.7.1.12

Received September 10, 2023; Accepted December 30, 2023

Abstract

The brake system is a critical area in the operation of a vehicle. To consider correct operation, various variables and components must be taken into account, including the brake pedal that activates the operation of the area. This study shows the conception of the design of the brake pedal of a BAJA SAE type vehicle and the optimization of its geometry using a methodology of analytical calculations with the essential variables of the system, taking into account SAE regulations for the competition, and subsequently through finite element analysis (FEA) and topological optimization methods using ANSYS software. Results of structural static studies, modal analysis and fatigue are presented for an initial model of the brake pedal and subsequently the topological optimization, presenting studies with similar conditions. The studies showed and structurally validated the optimized proposal of the pedal with a 30% reduction in mass and minimal variations in deformation and life cycles, as well as in behavior under vibrations. This pedal was manufactured and used in the BAJA SAE Mexico 2023 competition, showing adequate performance for its technical requirements.

BAJA SAE, Topology optimization, Fatigue, Modal, ANSYS

Resumen

El sistema de frenos es un área crítica en el funcionamiento de un vehículo. Para la consideración de la operación correcta se deben tomar en cuenta diversas variables y componentes, entre ellos el pedal del freno que acciona el funcionamiento del área. Este estudio muestra la concepción del diseño del pedal de freno de un vehículo tipo BAJA SAE y la optimización de la geometría del mismo empleando una metodología de cálculos analíticos con las variables esenciales del sistema, tomando en cuenta normatividades SAE para la competencia, y posteriormente mediante análisis por elementos finitos (FEA) y métodos de optimización topológica empleando el software ANSYS. Se presentan resultados de estudios tipo estático estructural, análisis modal y fatiga para un modelo inicial del pedal de freno y posteriormente la optimización topológica, presentando estudios con condiciones similares. Los estudios mostraron y validaron estructuralmente la propuesta optimizada del pedal con una reducción del 30% de masa y variaciones mínimas en deformación y ciclos de vida, así como en comportamiento bajo vibraciones. Este pedal se fabricó y se utilizó en la competencia BAJA SAE México 2023, mostrando un desempeño adecuado para los requerimientos técnicos del mismo.

BAJA SAE, Optimización topológica, Fatiga, Modal, ANSYS

Citation: CORDERO-GURIDI José de Jesús, ALVAREZ-SANTIAGO Jesús Daniel, MARTINEZ-DIAZ Ana Paola and HERNANDEZ-URBANO Cesar. Topological and structural optimization of the brake pedal of a vehicle for the BAJA SAE 2023 competition. Journal Industrial Engineering. 2023. 7-19: 1-12

* Author Correspondence (e-mail: josejesus.cordero@upaep.mx).

† Researcher contributing as first author.

Introduction

The BAJA SAE competition is an automotive event where different universities in Mexico plan, design, build and fine-tune a vehicle with the particular characteristics of an off-road car. In the 70s, the SAE organization (Society of Automotive Engineers) created an international competition for higher education students called Baja SAE where it was required to conceptualize and materialize a car capable of traveling on rugged terrain for leisure purposes. There are dynamic and design evaluations during the contest [1]. Figure 1 shows an image of the vehicle in competition.



Figure 1. BAJA SAE type vehicle

In the BAJA SAE competition, teams traditionally manage the vehicle in different systems, in order to adequately address the logistics, design and manufacturing of its different components. These systems are: vehicle structure, steering, drivetrain, suspension and brakes.

Braking is a critical system in the vehicle, a mandatory element and a test in the competition that validates the safe operation of the car. According to BAJA SAE competition regulations, the car must be equipped with a hydraulic brake system that acts on all wheels and is operated by a single pedal. The pedal is rigidly connected to directly push the brake master cylinder; The braking system must be able to lock all four wheels at static and road and unpaved speeds [2].

Within the components of the braking area, the pedal has specific operating requirements for its operation by regulation and by essential functioning of the system, which when met have been subject to optimization to have a light and resistant component that fulfills the function of braking, but seeking to add the least amount of mass to the final vehicle. Various authors have developed similar studies to optimize the braking system in BAJA SAE competition, Wang et al. [2] developed a simulation and evaluation of the behavior of the brake pedal for the BAJA SAE competition in China, evaluating different materials and geometric changes in the joints with the vehicle structure, seeking to optimize optimal structural results within the design range original. Correa-Arciniegas et al. [3] developed an optimization through design tools such as QFD and later the analysis of fluid flow in the brake disc, although the results were maintained in forces and pressures in the system by analytical calculation.

Regarding the brake pedal, Asanov [4] developed the study of the proposal for a brake pedal for a general vehicle, considering structural evaluations and deformations under the loads proposed in his study. On the other hand, Gupta et al. [5] developed the study and analysis of a brake system for the Formula SAE competition, with a methodology for calculating essential properties of the brake system, material selection, CAD modeling and finally finite element simulations. The optimization of the pedal was based on the definition of the pedal radius through iterations with MATLAB and analysis with various materials. Additionally, other components of the brake system were evaluated looking for mass reduction in the complete system.

Regarding topological optimization, Romero & Queipo [6] sought the optimization of brake pedal mass through a numerical model using variables related to structural analysis in the pedal of a Formula SAE vehicle, reporting as a conclusion an application of a design of experiments for the optimization of the variables and the corresponding pedal geometry. Finally, Sudin et al. [7] showed a study on a brake pedal of a conventional vehicle, with the application of the Altair Optistruct software to define optimization objectives and the corresponding comparison of the original model and its structural behavior, against the model with mass reduction.

Method Description

For the development of the braking system for BAJA SAE 2023, the requirements and standards indicated for the 2023 competition were taken into consideration.

Regarding applicable standards with respect to Baja SAE competition, there are the following:

- J1703 - Motor Vehicle Brake Fluid - Standard: Establishes the standards for brake fluids that are used in motor vehicles [8].
- J429 - Mechanical and Material Requirements for Externally Threaded Fasteners - Standard: Establishes the mechanical and material requirements for externally threaded fasteners, such as bolts and screws [9].

Likewise, the Baja SAE regulation [10] mentions two requirements with which the braking system must comply, these requirements talk about materials, forces and function of the object of study (brake pedal), these sections of the regulation are:

B.7.1 - Brake system

The vehicle must have a hydraulically actuated primary friction braking system that acts on all wheels and is operated with a single pedal. The pedal must directly actuate the master cylinder via a rigid link (i.e. no cables allowed). The brake system must be capable of locking and sliding all wheels, both in static condition and at high speed, regardless of surface conditions or transmission mode. The braking system will have sufficient force to keep the vehicle at idle or at low part throttle. Brake pedals and associated components shall be constructed of steel or aluminum and shall be designed to withstand a minimum brake pedal force of 450 lbf (2000 N) [10].

B.7.1.1 - Independent Circuits

The braking system must be segregated into at least two (2) independent hydraulic circuits so that, in the event of a leak or failure at any point in one system, effective braking power is maintained on at least two wheels.

The development of this work was contemplated in 7 steps; which can be seen in the following diagram in figure 2. The first step is the collection of information from past competitions, later we continued with the calculations of the braking forces, once these variables were obtained, we continued with the analysis of the technical requirements, as well as the investigation and selection of materials, with the information obtained, the CAD modeling of the components and the numerical analysis were carried out and, finally, we present results that we obtained from both analyzes and the conclusions.

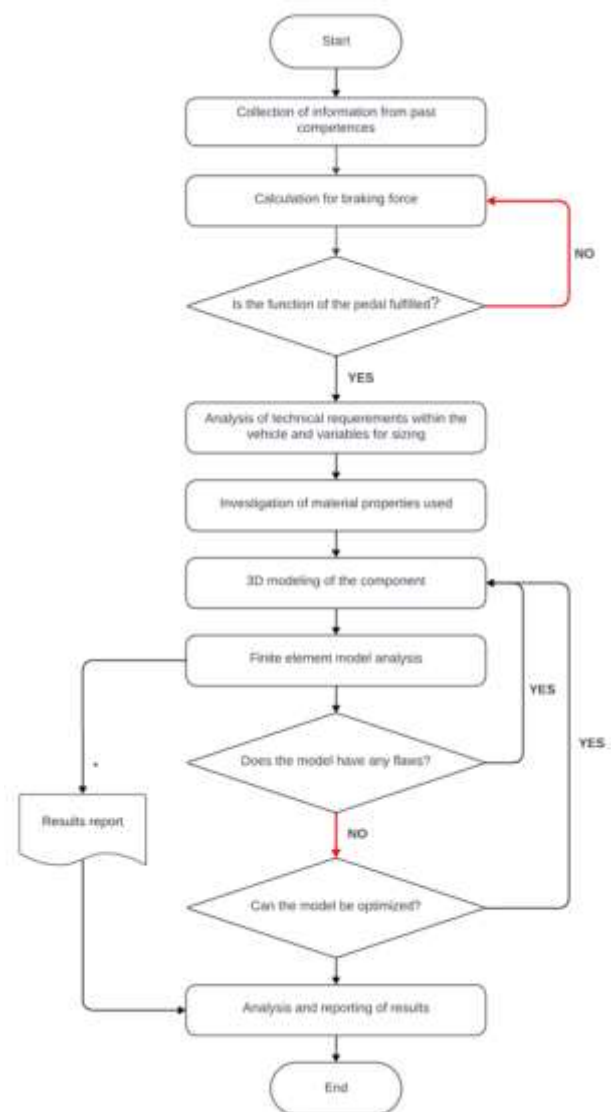


Figure 2. Method used for optimization

Analytical Approach to the Problem

Within the numerical evaluations, and for greater mastery in the development of the brake pedal, various fundamental equations of mechanics and statics for Baja SAE type vehicles were investigated, which are presented below:

Pedal operation

The pedal is the control element of the braking system of a vehicle, which is why great attention must be paid when considering the principle of operation, design of the mechanism and its geometries. The braking force of the system will be proportional to the force exerted on the pedal, this is because the mechanism will function as a lever that transmits the force that comes from the foot to the hydraulic pumps.

In order to obtain a multiplier effect on the braking force, it is necessary that the distance between the axis of rotation to the actuator of the master cylinders be less than the distance from the axis of rotation to the area where the pedal is operated by the foot. By dividing both values, a value known as ratio will be obtained, which represents the relationship between the input force and the multiplication of the force that goes out to the master cylinder. The brake pedal has 2 different configurations; figure 3 shows a representation of each one along with the variables for calculating the pedal ratio.

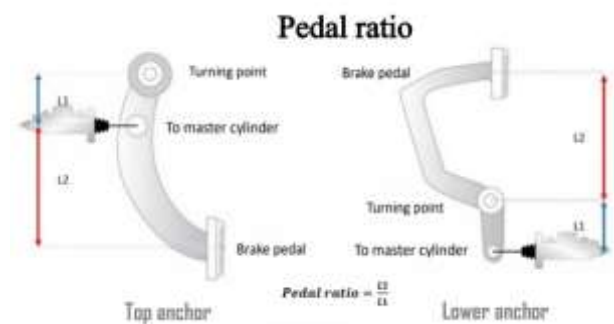


Figure 3 Types of brake pedal anchoring [11]

The pedal ratio is a very important factor which is calculated based on variables such as diameter of the master cylinders, diameter of pipes, type of brake system, etc. where the brake ratio can vary between 4 and 6.

There are 2 types of brake pedal mechanism:

- Pedals with top anchorage: the pivot point is located near the steering column in the area that separates the cabin from the engine,
- Pedals with lower anchorage: fixed to the vehicle floor so the pivot point is more coupled to the natural movement of the heel.

Braking forces

Braking is a common action while driving a vehicle, the objective of this action is to reduce the speed of the vehicle through the contact of 2 pads on a disc which rotates at the same speed as the tires, this through a hydraulic system which is activated by means of the brake pedal.

A hydraulic braking system bases its operation on the transformation of a force exerted on the brake pedal into a pressure on a fluid by means of a pump (in the case of the system the function is performed by the master cylinders), this pressure goes to move the cylinders of the brake calipers in such a way that friction is generated between the disc and the brake pad.

The principle of operation of the transmission of the force of a pedal is through a lever, like the one shown in figure 4, a lever is a simple machine which can transmit force or displacement, in this application it is used for the increase of a mechanical force, the objects of interest for the analysis of pedal force are:

- Applied force
- Resistance force
- Support point

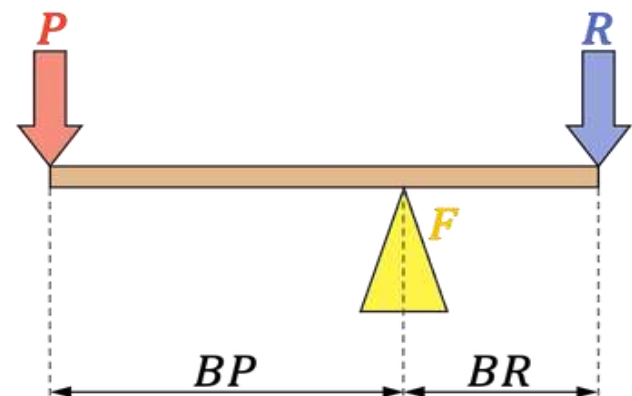


Figure 4 Representation of the variables of a lever[12].

The following equation presents a system in equilibrium of a plate.

$$F \times B_P = R \times B_R$$

Figure 5 Equilibrium equation of a lever

Where:

F = Foot force applied to the pedal

B_p = Distance from the application of force to the support point

R = Braking force transmitted by the pedal

B_r = Distance from the support point to the force transmitted to the brake master cylinder

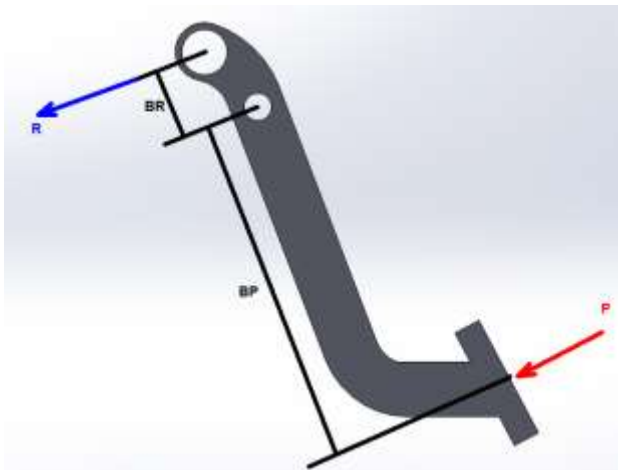


Figure 6 Lever representation in 3D model

Through the equation presented it will be possible to calculate the force transmitted by the pedal, which serves as input for the calculation of the braking force in the entire system.

Technical Characterization

For the Baja SAE 2023 competition, a disc brake system with calipers on all four wheels was chosen. Figure 7 shows a general diagram of the brake system.

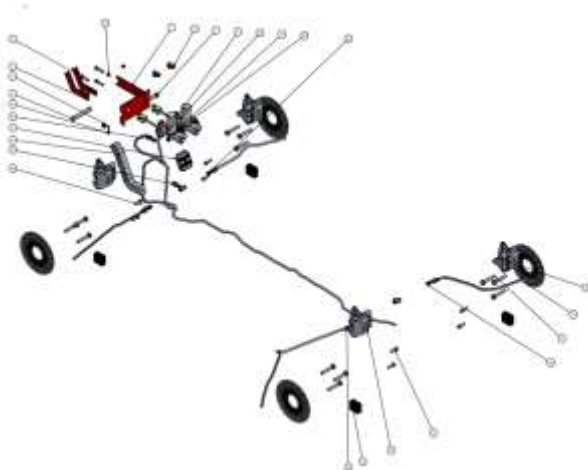


Figure 7 Exploded brake system

In this way, it can be established in an introductory manner that the braking system had the following elements described in table 1:

Ítem	Component	Amount
TIRE ZONE	Left caliper	2
	Right caliper	2
	Brake pad	8
	Brake disc	4
	Mass-disc fixing screws	12
	Caliper-knuckle fixing scrow	8
FRONT PART	Master cylinders	2
	Brake post	1
	Brake footrest	1
	Cylinder connection bolt	1
	Pivot screw	1
	Nut for pivot screw	1
	Pedal union screw	1
	Cylinder-bolt union screw	2
	Nut for cylinder-bolt union	2
	Cylinder fixing screw	4
Cylinder fastening screw nut	4	
HYDRAULIC LINE	T hydraulic line	4
	Hydraulic system hoses	7
	Line-caliper union screw	4
	Hydraulic system adapter	2

Table 1. Brake system BOM

Regarding the components related to the pedal, Figure 8 shows a CAD model with the two independent brake pumps mounted on the brake pedal assembly.

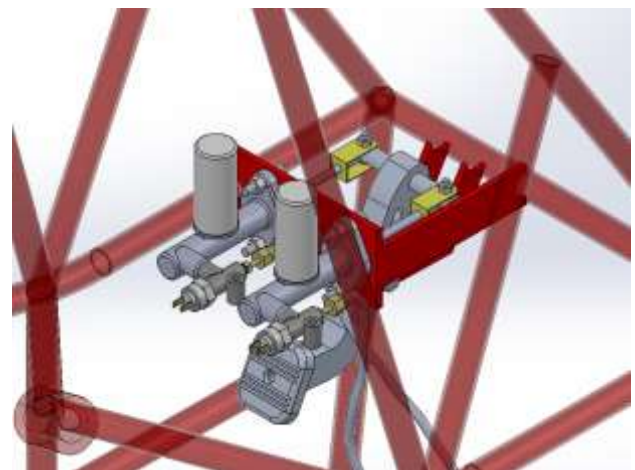


Figure 8 CAD model of pedal assembly with hydraulic pumps

Numerical Analysis

For the development of the CAD assembly of the pedal, shown in figure 9, certain requirements were taken into account, which were described in the regulations of the BAJA SAE 2023 competition.

The main consideration that was mentioned in the regulations is that the pedal the brake must withstand a force of at least 2000 N and must be manufactured in steel with a minimum of 20% carbon concentration or 6061 aluminum, in addition to the requirements of the regulations for the competition, the design and modeling of the pedal was limited by variables both in the calculation of the force necessary to brake the vehicle, which influenced the distance from the support point and the area of contact of the foot with the pedal as well as the angle of inclination that would be between the area of the lever of the pedal and the foot support surface.



Figure 9 First CAD model of the pedal

Another issue which was of great relevance for the design of the pedal was the environment by which it was going to be surrounded, the first element that restricts the dimensions of the pedal was the chassis (made up of a tubular structure) of the vehicle and the position in the which the brake pump fastenings were positioned, having to take into consideration ergonomic elements due to the driver's driving position in such a way that the brake pedal will be in a position and have the appropriate geometry for the pilot to perform the action of pressing the pedal comfortably and that the pedal will perform its function, the result of these considerations are shown in figure 10 where the dimensions of the pedal are shown.

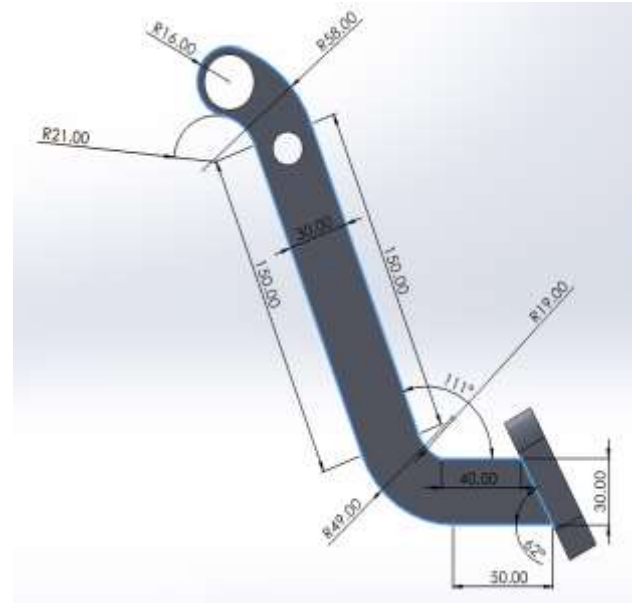


Figure 10 Pedal dimensions

When evaluating the pedal, 6061 aluminum was considered due to its malleability and easy access. It was proposed to carry out 3 studies in the ANSYS software in order to evaluate the vibration modes, the useful life behavior that the material will have and the loading forces that it will have. Table 2 shows the characteristics of the meshing used in the analysis carried out.

Analysis	Modal	Structural static
Aspect ratio (max)	6.3029	6.3029
Element size	7	7
Element type	Tetrahedron	Tetrahedron
Number of mesh elements	377446	377446
Element quality	0.99999	0.99999

Table 2 Meshing characteristics

Regarding the requirements for the analysis, Table 3 shows the boundary conditions that were considered for the pedal analyses. It should be noted that in the modal analysis only the fixations were considered while in the structural static analysis the loads that were used were previously calculated. These values were stipulated due to the positioning of the pedal with respect to the vehicle. Figure 11 shows the approach graphically.

Type of load / fastening	Value	Location
Force in the X axis	2000 N	Pedal pad
Force in the X axis	9619 N	Top hole
Cylindrical support	0 mm	Top hole
Cylindrical support	0 mm	Bottom hole

Table 3 Specification of location of loads and supports exerted on the pedal



Figure 11 Global view of the pedal representing loads and supports exerted on the model for study

Initial model results

Structural

The total deformations presented by the loads described above are shown in figure 12.

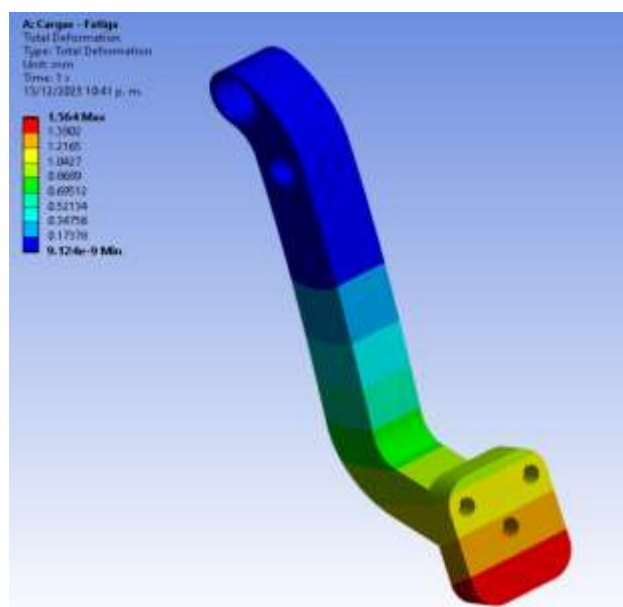


Figure 12 Global view of the pedal representing the results of the deformations due to the applied loads

The equivalent forces presented by the loads described above are shown in figure 13.

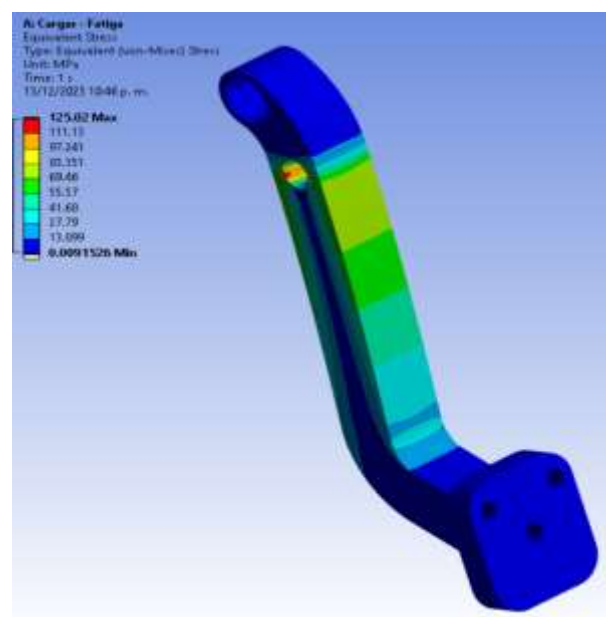


Figure 13 Global view of the pedal representing the results of the applied loads

As seen in Table 4, a maximum value of 1.564 mm was obtained in the total deformation, 0.0055919 mm in the directional deformation and 125.02 MPa in the equivalent stress, this based on the loads applied in the areas where the pedal is activated and where The force is multiplied by the effect of the lever arm.

Structural static analysis	
Type	Value
Total deformation	1.564 mm
Equivalent stress	125 MPa
Directional deformation	0.0055919 mm
Life	1e+008 cycles

Tabla 4 Resultados evaluación estática estructural

Fatigue

Figure 14 shows the results of the pedal fatigue analysis, a value of 1e+008 cycles was obtained, based on the stress-strain curve of the AL6061. The distribution of the cycles is observed globally throughout the geometry of the pedal, with very few points below this limit.

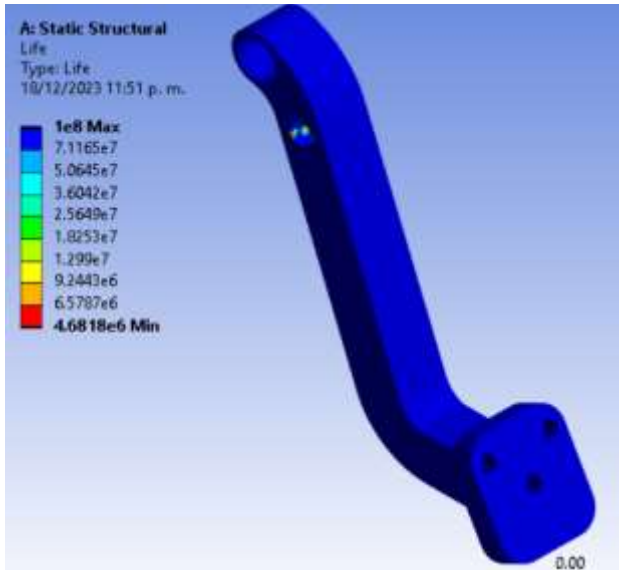


Figure 14 Global view of the pedal representing the results of the applied loads

Modal

For the modal analysis of the pedal structure, Figure 15 presents the different vibration modes of the analyzed structure. As part of this evaluation, the typical operating revolutions of the vehicle's engine were identified, for which its operating frequency was found to be 64.16 Hz.

Table 5 describes the numerical values found in the vibration modes of the structure.

BAJA engine working analysis	Vibration modes results	Numerical values in HZ
3850 rpm = 64.16 Hz	1	336.49
	2	347.06
	3	1192.6
	4	1443.6
	5	2526.3
	6	4624.2

Table 5 Modal evaluation results

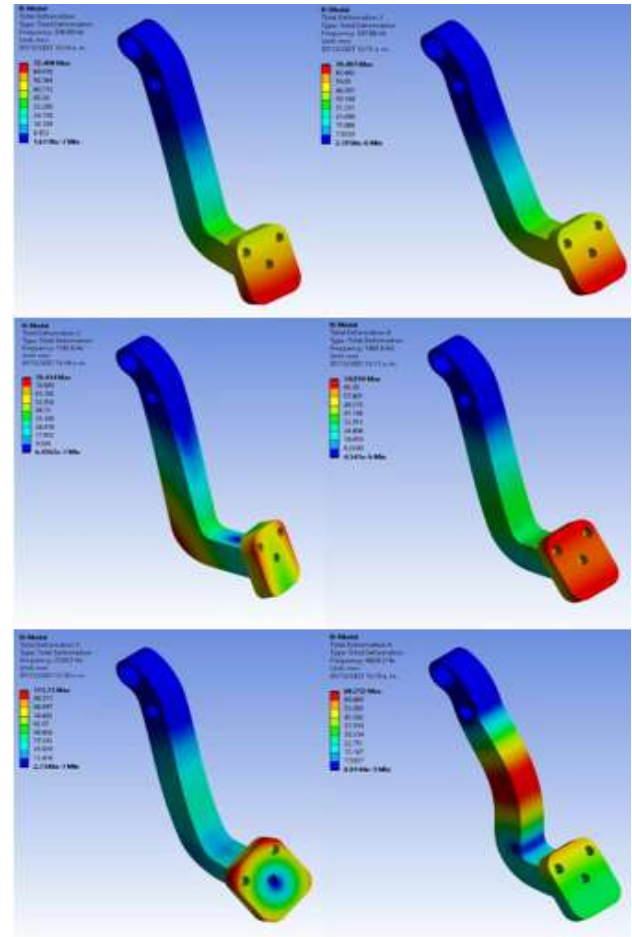


Figure 15 Modal evaluation results

Topology optimization

After evaluating the design of the brake pedal through the different studies presented, the topological optimization of the pedal was carried out, the analysis focused on reducing mass as a key factor. A target reduction of 30% of the original mass was set, with the aim of reducing weight inside the vehicle without compromising the function of the optimized elements.

Figure 16 shows the conditions under which the study was carried out. The areas where the forces and supports are placed in the structural static evaluation were taken into consideration, as well as areas where it is not of interest to eliminate material within the geometry.



Figure 16 Global view of the pedal representing topological region (blue A) and exclusion region (red A)

The analysis yielded a model with the topological density where an optimized design is shown in Figure 17.



Figure 17 Topological Density

Based on the results obtained in the topological optimization analysis, the change in the geometry of the pedal was made to reduce the weight. The proposed model is shown in Figure 18.



Figure 18 New pedal model proposal

In order to validate that the new pedal model met the requirements set out at the beginning of the document, the analyzes shown in the previous model were carried out again, taking into consideration similar conditions for the meshing and the same boundary conditions used with the original geometry.

Optimized model results

Structural

Figures 19 and 20 show the results of the total deformations and the stresses applied to the optimized geometry of the pedal.

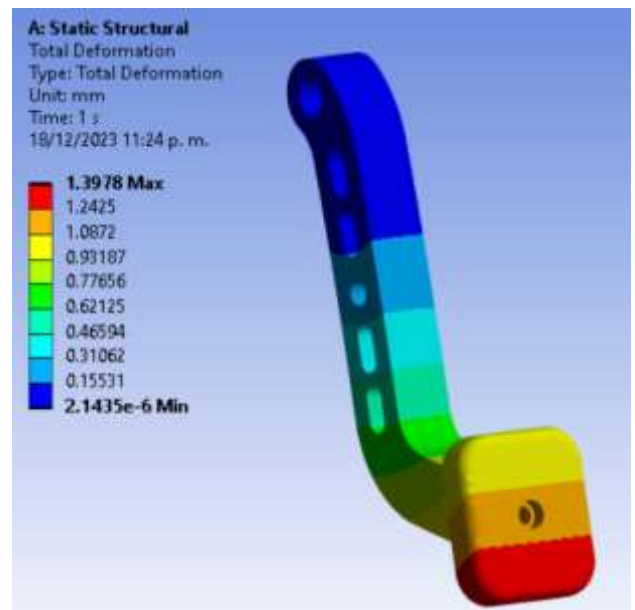


Figure 19 Global view of the pedal representing the results of the applied loads

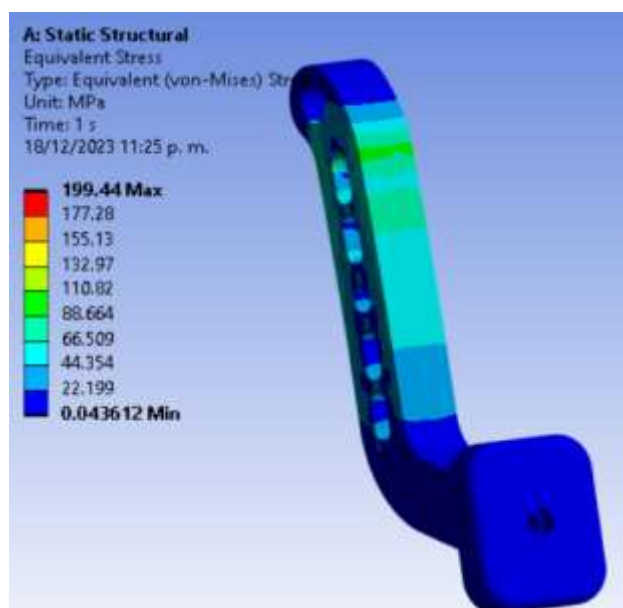


Figure 20 Global view of the pedal representing the results of the applied loads

Subsequently, the fatigue evaluation is applied with the same conditions, which is shown in Figure 21. In this result, variations are observed with respect to the previous analysis, especially in the minimum number of cycles to be fulfilled in some points.

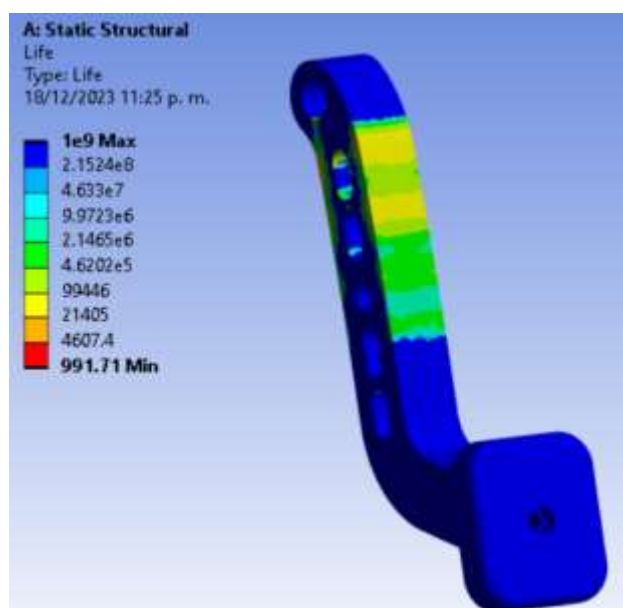


Figure 21 Global view of the pedal representing the results of the applied loads

As seen in Table 6, a maximum value of 1.3978 mm was obtained in the total deformation and 199 MPa in the equivalent stress, this based on the loads applied in the areas where the pedal is activated and where the force is multiplied by the effect of the lever arm.

Structural static analysis	
Type	Optimized model
	Value
Total deformation	1.3978 mm
Equivalent stress (276 MPa del AL6061)	199.44 MPa
Life	1e+009 cycles

Table 6 Structural static evaluation results

Modal

The modal evaluation of the optimized model was carried out, finding the results shown in table 7 and figure 22 of the different vibration modes.

BAJA engine working analysis	Vibration modes	Optimized model Numerical values in HZ
3850 rpm = 64.16 Hz	1	278.38
	2	373.47
	3	987.2
	4	1389.1
	5	2171.6
	6	4799.1

Table 7 Modal evaluation results

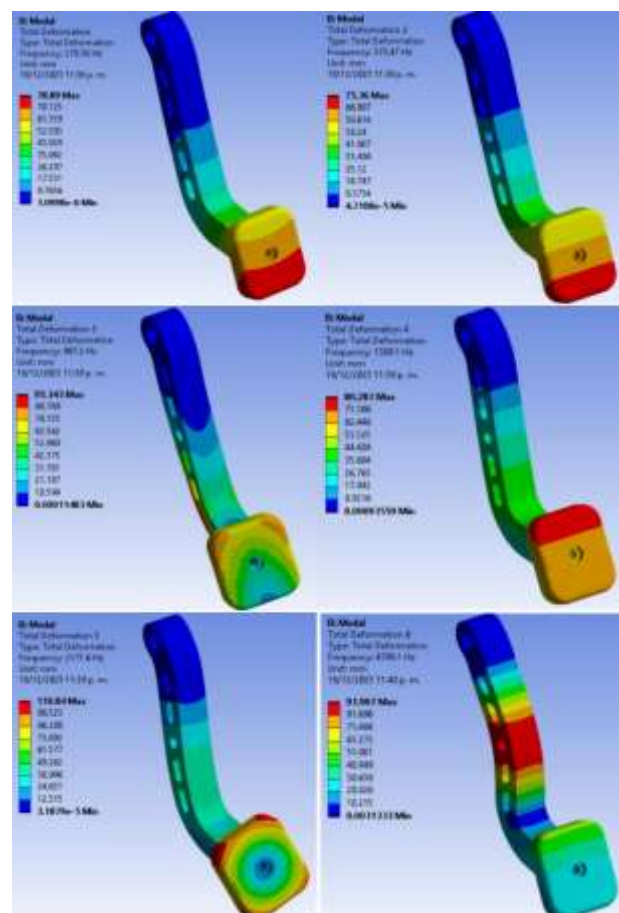


Figure 22 Global view of the pedal representing the results of the applied loads

Conclusion and discussion

In the studies presented, the performance of the pedal structure was analyzed under three main studies, structural statics, operating cycles and modal evaluation.

Structural static analysis		
Type	Initial model	Optimized model
	Value	
Total deformation	1.564 mm	1.3978 mm
Equivalent stress (276 MPa yield of AL6061)	125 MPa	199.44 MPa
Life	1e+008 cycles	1e+009 cycles

Table 8 Structural evaluation results

BAJA engine working revolutions	Vibration modes	Initial model	Optimized model
		Numerical values in HZ	
3850 rpm = 64.16 Hz	1	336.49	278.38
	2	347.06	373.47
	3	1192.6	987.2
	4	1443.6	1389.1
	5	2526.3	2171.6
	6	4624.2	4799.1

Table 9 Modal evaluation results

As seen in tables 8 and 9, the results obtained between the initial proposal of the model and the final optimized geometry present a minimum variation taking into consideration the reduction of the material, this meets the objective of generating a lighter model but that I preserved the necessary properties so that the pedal does not fail and fulfills its function.

Of these three criteria, in the calculated values, it was found when comparing them against the requirements stipulated in the competition regulations that the pedal can perform its function without it failing when activated, in the structural static analysis parameters were calculated of total deformation which gave values which are minimal and do not affect the behavior or integrity of the pedal, in addition in the result of the Von-Misses criterion it was observed that the value did not exceed the yield limit of the material used for the pedal and as the last section of the structural static analysis, the number of operating cycles of the pedal was calculated, ensuring that the number of times the pedal was activated is not enough for the element to fail.

With respect to the topological optimization carried out, the objective of reducing the weight of the element studied, maintaining similar characteristics in terms of the behavior of the pedal and ensuring correct operation, as well as the elimination of possible failures due to the forces to which it was subjected during the BAJA SAE 2023 competition.

In the same way, Asanov [4] analyzed a model of a brake pedal under certain parameters, where it was analyzed whether the pedal is prepared to resist loads in a sudden braking process. Regarding these studies, there is a similarity in their approach having a force greater than that indicated in their investigation. As for future work, it could be the evaluation using certain failure parameters or even the use of another material and determining the dynamic behavior of the pedal.

Although this brake pedal was designed in accordance with the vehicles manufactured for the Baja SAE competition, taking into account the loads that the driver will apply to the pedal and the weight it must support in order to have correct braking performance.

This optimized model was manufactured and used in the 2023 competition and of which figure 23 is shown.



Figure 23 Baja SAE 2023 Vehicle Mounted Pedal

In future work, we will seek to maintain the resistance characteristics of the brake pedal by further reducing the weight through a different optimization, change of material or geometry, but improving the output force that is transmitted through the pedal to the hydraulic system.

Acknowledgements

The authors wish to thank the Popular Autonomous University of the State of Puebla for the use of the facilities and facilities provided in the development of this work.

Funding

This work was fully funded by the Universidad Popular Autónoma del Estado de Puebla A.C.

References

[1] Gutiérrez, L. C., & Guridi, J. D. J. C. (2019). Reducción de transmisión para vehículos todo terreno con realidad aumentada e ingeniería asistida por computadora. *Revista Politécnica*, 15(30), 32-40. <https://revistas.elpoli.edu.co/index.php/pol/article/view/1588>

[2] Wang, S., Liu, X., Chen, W., Tang, J., Liu, Q., Ning, T., & Yao, H. (2022, February). Force Analysis and Optimization of BSC Brake Pedal Based on ANSYS. In *Journal of Physics: Conference Series* (Vol. 2187, No. 1, p. 012033). IOP Publishing. 10.1088/1742-6596/2187/1/012033

[3] Correa-Arciniegas, J., Mago, M., Ríos, R., & Vallés, L. Brake system proposal for a Baja SAE vehicle. <https://doi.org/10.54139/revinguc.v28i2.28>

[4] ASANOV, S. (2021). The Stress and deformation analysis of the brake pedal using Finite Element Method. *Acta of Turin Polytechnic University in Tashkent*, 11(3), 30-32. <https://www.acta.polito.uz/index.php/journal/article/view/64/29>

[5] Gupta, E., Bora, D. K. S., & Rammohan, A. (2022). Design and analysis of brake system for FSAE race car. *Engineering Research Express*, 4(2), 025039. 10.1088/2631-8695/ac6ecd

[6] Romero, J. L., & Queipo, N. V. (2017). Surrogate-based optimization of a brake pedal. *Revista Técnica de la Facultad de Ingeniería Universidad del Zulia*, 40(1), 11-15. https://ve.scielo.org/scielo.php?pid=S0254-07702017000100003&script=sci_abstract&tlng=en

[7] Sudin, M. N., Tahir, M. M., Ramli, F. R., & Shamsuddin, S. A. (2014). Topology optimization in automotive brake pedal redesign. *International Journal of Engineering and Technology (IJET)*, 6(1), 398-402. https://www.researchgate.net/publication/260449002_Topology_Optimization_in_Automotive_Brake_Pedal_Redesign

[8] J1703_201909: Motor Vehicle Brake Fluid. SAE International. (n.d.). https://www.sae.org/standards/content/j1703_201909/

[9] J429a (WIP) mechanical and material requirements for externally threaded fasteners. SAE International. (n.d.-a). <https://www.sae.org/standards/content/j429/>

[10] Baja SAE rules. saemx. (n.d.). <https://www.saemx.org/baja-sae-rules>

[11] El sistema de Frenos en el Automóvil (ii). espíritu RACER. (2019, December 8). <https://espirituracer.com/reportajes/el-sistema-de-frenos-en-el-automovil-ii/>

[12] Cejarosu. (n.d.). Ley de la palanca. Estudio de la palanca de primer grado. http://concurso.cnice.mec.es/cnice2006/material107/operadores/ope_pal_primergrado.htm

Design of a nozzle for Stratasys uPrint SE Plus 3D printer

Diseño de una boquilla para impresora 3D de la marca Stratasys uPrint SE Plus

CORTEZ-SOLIS, Reynaldo†*, ARENAS-ISLAS, David, BETANZOS-CASTILLO, Francisco and FUENTES-CASTAÑEDA, Pilar

Posgrado CIATEQ, A.C.

Tecnológico Nacional de México-*TES Valle de Bravo*

ID 1st Author: *Reynaldo, Cortez-Solis* / ORC ID: 0000-0001-7519-1815, CVU CONACYT ID: 1113392.

ID 1st Co-author: *David, Arenas-Islas* / ORC ID: 0000-0001-6169-2045, CVU CONACYT ID: 408571.

ID 2nd Co-author: *Francisco, Betanzos-Castillo* / ORC ID: 0000-0002-7245-703X, CVU CONACYT ID: 206209. ID 3rd

Co-author: *Pilar, Fuentes-Castañeda* / ORC ID: 0000-0001-6567-9614, CVU CONACYT ID: 428699.

DOI: 10.35429/JIE.2023.19.7.13.37

Received July 15, 2023; Accepted December 30, 2023

Abstract

The work is supported by the comparison of conventional metrology methods and the use of virtual optical comparison technologies virtual optical comparison technologies, these methods are used for the design of a nozzle for the Stratasys the design of a nozzle for the Stratasys 3D printer analysis by means of CAE and the Finite Element Method (FEM) Finite Element Method (FEM) to be able to evaluate some more adequate parameters that will serve as the serve as the main basis for the development of the same nozzle. On the other hand, it is also based on the CFA analysis with the type of polymer used to verify if the design is feasible, taking into account the necessary configurations for the use of the most appropriate manufacturing. The difference between using a conventional metrology method is the decrease of the error in obtaining geometries of a certain model, on the other hand, when using an optical comparator, it was taken as a main point that it is only to obtain geometries of smaller elements, this makes that with the use of new technologies it is not 100% accurate in obtaining a perfect geometry.

Engineering and Technology, Mechanical Engineering, Others

Resumen

El trabajo se sustenta con la comparación de los métodos de metrología convencional y uso de tecnologías virtuales de comparación óptica, dichos métodos son usados para realizar el diseño de una boquilla para la impresora 3D de la marca Stratasys, asimismo se pretende tomar como soporte el tipo de análisis mediante CAE y el Método de Elementos Finitos (MEF) para poder valorar algunos parámetros más adecuados que sirvan como base principal para el desarrollo de la misma boquilla. Por otra parte, también se sustenta en el Análisis de CFA con el tipo de polímero usado y así poder verificar si el diseño es viable, tomando en cuenta las configuraciones necesarias para el uso de la manufactura más adecuada. La diferencia entre usar un método convencional de metrología precisa la disminución del error en la obtención de geometrías de cierto modelo, por otra parte, al hacer uso de un comparador óptico se tomó como punto principal que es solo para obtener geometrías de elementos más pequeñas, esto hace que con el uso de nuevas tecnologías no se precise al 100% en la obtención de una geometría perfecta.

Ingeniería y Tecnología, Ingenierías Mecánicas, Otras

Citation: CORTEZ-SOLIS, Reynaldo, ARENAS-ISLAS, David, BETANZOS-CASTILLO, Francisco and FUENTES-CASTAÑEDA, Pilar. Design of a nozzle for Stratasys uPrint SE Plus 3D printer. Journal Industrial Engineering. 2023. 7-19: 13-37

* Correspondence to Author (e-mail: reynaldo.c-s@hotmail.com)

† Researcher contributing as first author.

Introduction

New technologies in manufacturing are developing very fast in the application of new methods of 3D modeling and rapid prototyping.

According to (Ortega) the process of creating a mathematical representation of surfaces using geometries is called 3D modeling, this can be represented in two ways: on screen as a two-dimensional image through a process known as 3D rendering or as a physical object, through a 3D printer or numerical control manufacturing tool.

On the other hand, additive manufacturing is the technical name that encompasses all 3D printing technologies, it is the manufacture of three-dimensional objects by adding material instead of subtraction in order to model and prototype.

With the application of these technologies so far it has not been possible to obtain a 100% perfect replica in the manufacture of prototypes and 3D models, each of these techniques that are applied have different application methodologies when developing a model; today we can say that manufacturing plays great roles, such is the case of additive manufacturing, as a proposal and application support in this project, with the design of a 3D printer nozzle using CAD design methods and conventional metrology to apply reverse engineering to a sample object.

Finally, different materials are required for its application and design of the nozzle to support internal and external variables when manufacturing a model, for these variables it is intended to make use of a CAE software for the analysis of CFD fluid simulations of the nozzle and thermal resistance of the same to opt for the best design material proposal.

In this project we took as main points, the lack of acquisition with suppliers because they are obsolete equipment, the acquisition time and cost, as fundamental factors to take as main idea the design of the nozzle and to have in existence a model to be able to manufacture it in the future.

Introduction to Prototyping

The conception of the manufacturing of a model starts by analyzing its characteristics and attributes of design, ergonomics, costs, etc. To date, the design of a mold was made in a CAD software to be taken to a machine that could be an injection molding machine and see the results of that model. The costs of product design and development increased drastically when a product did not meet specifications, so it was necessary to redesign the mold, manufacture it and test the product again. All these costs, which are charged to the cost of the finished product, can be considerably reduced if the part is first designed at the prototype level and then the mold of that product is generated for mass production. This advantage is offered by the new technology that performs a three-dimensional printing called 3D printer. (Costa, 2018)

What is a 3D printer nozzle?

The nozzle is the last step where the filament is extruded, after heating in the melter. As in most 3D printers, the nozzle can be changed, depending on different properties such as the material to be printed, the diameter, or the utility of the nozzle.

The inner diameter of the nozzle affects the amount of plastic extruded per second, the flow, the quality and the maximum extrusion speed. Specifically, the nozzle diameter determines the layer height, which as a general rule will be 1/2 of the nozzle diameter. Smaller diameters allow thinner layers and thinner walls to be printed. Nozzles for 3D printers are available in various diameters between 0.2mm, 0.25mm, 0.3mm, 0.35mm, 0.4mm, 0.5mm, 0.6mm and 0.8mm. This determines the layer height and therefore the printing speed.

In 3D printing, we usually say that the maximum layer height given by a nozzle, to avoid problems in printing, is 80% of the nozzle diameter, so we would find the following maximum layer heights per nozzle diameter:

$$0.2 \text{ mm: } 0.2 * 0.8 = 0.16 \text{ mm}$$

$$0.4 \text{ mm: } 0.4 * 0.8 = 0.32 \text{ mm}$$

$$0.6 \text{ mm: } 0.6 * 0.8 = 0.48 \text{ mm}$$

These characteristics can have a big impact on the time it takes for the part to print, as well as the quality of the final object.

Generally, the most commonly used diameter in desktop 3D printers is 0.4. A nozzle diameter that gives us a good finish in terms of resolution and speed. The layer height for this type of nozzle caliber is usually 0.2mm, which implies an optimal detail per layer in the final design.

You can buy 0.2, 0.15 and even 0.1 nozzles that have demonstrated great performance, since the smaller the size, the more detail, although it also depends on the level of resolution that the 3D printer can offer.

Even 0.6 nozzles are a good option for printing, although these types of nozzles are more focused to be used in industrial 3D printing.

Elements of a nozzle

The thread pitch: is the distance between the crests of the area to be threaded. Generally, and with some exceptions, this distance is 1mm. It is important because this part is screwed to the heater block, and it has to fit perfectly.

The distance from the head, or the end of the thread and the end of the nozzle. This measurement is very important, this is the part that will protrude from your hotend, so if you buy a nozzle with this section larger or smaller, you will have to modify the end of the stroke or re-level.

Thread distance: this distance usually varies depending on the brand. Most 3D printers require a nozzle with a thread distance of 5 mm. The standard Ender 3 nozzle, for example, has 5 mm.

The thread metric: most nozzles are metric 6 (M6). This is a 6 mm diameter thread. Mk8 nozzles are also metric 6. MK10 nozzles are metric 7 (M7).

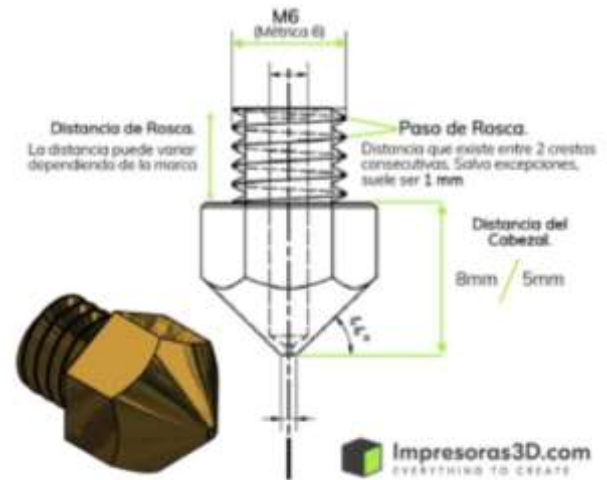


Figure 1 Nozzle elements.(IMPRESORAS3D.COM, 2021)

Types of Nozzles

When we talk about size, we are referring to the physical mass and length of the part. This is not to be confused with the nozzle diameter orifice, which is a measurement of the space inside the nozzle through which the filament is extruded.

Standard

The length of the nozzle is determined by the type and size of the fuser heater block. The current standard dimensions of these parts fit V6 and MK8 extruders, with an overall length of 12 to 13 mm.

Volcano

Volcano nozzles are designed for higher speeds and temperatures, with the ability to process at least three times more plastic than standard nozzles. Volcano nozzles require a longer nozzle, typically 21mm from end to end to promote better thermal conduction.

Supervolcano





Supervolcano nozzles are varied in both material and outlet diameters. It is one of the best nozzles that offers the best ratio of quality, detail and speed.

BondTech's CHT nozzles have a triple inlet orifice, allowing up to 30% increase in flow, ultra-precise machining, higher melt capacity, and also enjoy the advantages of nickel plating.



Figure 2 Type of nozzles according to their shape and size.(IMPRESORAS3D.COM, 2021)

Due to their relatively high thermal conductivity and tight manufacturing tolerances, 3D printer nozzles are made of different metals that affect the printing process. Let's take a look at the different materials that are used depending on the filament we are going to extrude. (IMPRESORAS3D.COM, 2021)

Nozzle type	Characteristics
Brass nozzles 	<ul style="list-style-type: none"> Maximum temperature: Max: 300°C. High thermal conductivity. Not suitable for abrasive materials. Low cost. Low wear resistance.
Stainless steel nozzles. 	<ul style="list-style-type: none"> Maximum temperature: Max: 500°C. High thermal conductivity. Not suitable for abrasive materials. Suitable for materials in contact with food. Low cost. Low wear resistance.
Nickel nozzles. 	<ul style="list-style-type: none"> Abrasion resistant. Greater fluidity. Suitable for abrasive materials More affordable than similar ones. High wear resistance.
Vanadium nozzles 	<ul style="list-style-type: none"> Extremely resistant. Suitable for abrasive filaments. High precision. High durability.

Tungsten Nozzles. 	<ul style="list-style-type: none"> Maximum temperature: Max: 550°C. Excellent Conductivity. Suitable for all types of materials. Made of tungsten carbide and copper alloy. Uniform temperature and low friction coefficient.
Hardened steel nozzles. 	<ul style="list-style-type: none"> Maximum temperature: Max: 500°C. Medium thermal conductivity. Suitable for abrasive materials. High cost. High wear resistance.
Ruby-tipped nozzles 	<ul style="list-style-type: none"> Maximum temperature: Max: 500°C. High thermal conductivity. Suitable for abrasive materials. High cost. High wear resistance.

Table 1 Nozzle types and characteristics. (IMPRESORAS3D.COM, 2021)

Properties of the materials used in nozzles

Properties of brass

Brasses are binary alloys of copper and zinc combined in different proportions which, practically speaking, range from: Cu 50 - 95% and Zn 50 - 5%. These alloys are more fusible than copper; they have a high resistance to corrosion, and even in marine atmospheres they have good lubricating properties. Commercial brasses can be divided in two broad groups, cold work brasses (α) and latones for hot work (brasses α plus β).

The ductility and Mechanical strength varies with zinc content, increasing with the percentage of zinc, reaching a maximum when the zinc content is 30%, providing a good combination of mechanical strength and ductility when maximum corrosion resistance is not essential.

As the zinc content increases above 30%, the ductility of the metal decreases, becoming brittle and hard; however, the tensile strength reaches its maximum with approximately 45% zinc. The Brinell hardness of brass ranges between 50 and 60. These changes in mechanical properties are caused by the alteration of the internal structure.

The electrical conductivity of brasses decreases as the zinc content increases. As the zinc content increases above the solid solution range α , the structure of the brasses changes to a mixture of the α and β phases. The Muntz metal composition (60% Cu and 40% Zn), brings together the mechanical strength of the α and β mixture, at room temperature and the higher ductility of a single-phase structure, at elevated temperatures. (Ledo, 2011)

Properties of stainless steel

Stainless steels are alloys based on iron, chromium and carbon, to which other elements are added, such as nickel, molybdenum, manganese, silicon and titanium, among others, which give them good resistance to some types of corrosion in certain industrial applications. The presence of each element in certain percentages produces different variations in the intrinsic characteristics of the various types. According to EN 10088, stainless steels are defined as those ferrous alloys containing chromium in a minimum proportion of 10.5%.

This good corrosion resistance is due to the ability of these alloys to form a passive layer which is a stable, adherent film of chromium oxide (Cr₂O₃), also called chromite, which protects the steel in an oxidizing environment. This passive film rebuilds itself when damaged, if the environment is sufficiently oxidizing, maintaining a permanent protection of the steel.

There is a wide variety of stainless steels, each of which has properties for some specific application, to improve their characteristics some elements are added: a) Increased corrosion resistance: Cr, Ni, Ti and Mo. b) Improve machinability: Se and S. c) Increase hardness: Cu, Al and Mo. d) Increase formability and weldability: Cr and Ni. e) Improve mechanical characteristics: Mn, N and C. f) Decrease intergranular corrosion: Ti, Nb and Ta.

The most common way to classify stainless steels is by the crystallographic structure or microstructure of the material, they are divided into 5 families: g) Austenitic (FCC). h) Ferritic (BCC). i) Martensitic (Tetragonal centered in the body). j) Double phase or Duplex (Austeno-ferritic and ferritic-martensitic). k) Precipitation hardened (Austenitic or martensitic base).

As the definition of stainless steel is given by the percentage of chromium, which must exceed 10.5%, the increase of this percentage and the combination with nickel determine the nature and proportion of the phases present and consequently define the type of stainless steel.

The chromium content in these steels varies between 16 and 26%; nickel and manganese contents can reach levels of 35 and 16% respectively. The austenitic structure in these steels is stabilized at room temperature by the addition of elements such as nickel, manganese and nitrogen. They are not ferromagnetic in their annealed condition and only work harden. Their cryogenic characteristics are excellent and they exhibit good mechanical strength at high temperatures. They are very resistant to impact and difficult to machine, unless they contain S and Se, and can be hardened by adding C and N.

The family of austenitic steels is divided into two groups: a) Austenitic chromium-manganese-nickel steels, designated by a three-digit number starting with 2, known as the 200 series, characterized by high mechanical strength, due to the presence of sulfur and manganese, with the last two digits depending on other elements. b) Austenitic chromium-nickel steels, designated by a number 3, 300 series, with a basic composition of 12% Cr and 8% Ni, being the most commercially successful range of steels.

For this series, the chemical composition is modified according to the type of use of the material by adding or reducing elements such as carbon and/or nitrogen and/or modifying the nickel/chromium balance. The 200 series steels acquire their austenitic characteristics through the addition of nitrogen and manganese (between 4 and 16%), while nickel is limited to below 7%. The 300 series steels contain high levels of nickel and up to 2% manganese.

Elements such as molybdenum, copper, silicon, aluminum, titanium and niobium are added to improve resistance to halide corrosion, pitting or to improve their resistance to oxidation.

They are not ferromagnetic in their annealed condition and can only be hardened by cold working. The yield strength, yield strength or yield values (σ_y) of the 300 series austenitic steels are comparable to those of low carbon steels.

Typical values of σ_y in the annealed condition vary between 200 and 280 MPa, mechanical strength varies from 500 to 750 MPa and exhibit elongations from 40 to 60%. Values of σ_y in manganese steels can vary from 350 to 500 MPa. These steels are not susceptible to hardening by heat treatment, but exhibit mechanical work hardening. AISI 302 (17% Cr, 8% Ni) and AISI 304 (18% Cr, 8% Ni) steels are considered basic alloys of the austenitic stainless steels.

The particular composition of these steels is due to the minimum nickel content (hence lower cost) required to retain the γ -phase at room temperature; so for low or high Cr contents the addition of more nickel is required. For example, for higher corrosion resistance, a steel is designed with 25% Cr, but it needs about 15% Ni to retain the austenite at room temperature and this means a higher cost. (Leal Alanís, 2011)

Properties of nickel

Nickel is a hard, malleable and ductile metal, which can have a high luster. It has magnetic properties below 345 °C. It has a melting point of 1,455 °C and a boiling point of 2,730 °C. Passing carbon monoxide through impure nickel forms nickel carbonyl, a volatile gas. This gas, heated to 200°C, decomposes, depositing pure metallic nickel. Steels containing between 2% and 4% nickel are used in automotive parts, such as axles, crankshafts, gears, keys and rods, in machine parts and in armor plates. (GARCÍA, 2006)

Properties of Vanadium

Vanadium is a grayish metal with a density of 6.11 g/cm³. In the periodic table, it is the first transition element of group VB, it has atomic number 23, electronic configuration [Ar] 4s² 3d³, atomic weight 50.95, melting point 1950 °C and boiling point 3600 °C. It exists in different oxidation states ranging from -1 to +5, and generally passes from one state to another by the transfer of an electron through oxidation-reduction processes. However, only the three highest states, VIII, VIV and VV, respectively, have biological functions recognized.

Similar to molybdenum (Mo), vanadium has an exceptional position within the biometals, as it participates in biological processes as an anion or cation.

Under physiological conditions VV predominates as vanadate anion (H₂ VO₄⁻) and VIV as vanadyl cation (VO₂⁺); although, other species of cations (VO₃⁺, VO₂⁺) and anions (HVO₄²⁻, V₄ O₁₂⁴⁻ and V₁₀ O₂₈⁶⁻) of VV and anions ([VO₂(OH₅)]⁻) for VIV may be present. At pH near 7 VIII is found exclusively in the form of V³⁺ cation and in the cellular environment in the form of complexes. Under acidic conditions of pH 3.5, the vanadyl ion is very stable, in basic solutions the orthovanadate ion (VO₄³⁻) predominates, which is very similar in its geometry to phosphate (PO₄³⁻). The coordination chemistry of vanadium is extensive and very interesting, commonly presenting octahedral, pyramid or square bipyramid geometry, where an oxygen always forms a double bond with VV or VIV, giving rise to oxovanadate or oxovanadil compounds.

A large number of inorganic vanadium compounds are known. Table I shows some of the physical and chemical properties of the most commercial compounds used in industry and which are of toxicological interest. Vanadium pentoxide (V₂ O₅), the most commercially available compound, is a reddish-yellow salt with a melting point of 1750 °C and a boiling point of 690 °C. It is a hazardous chemical agent and its occupational exposure limit for dusts and fumes is 0.05 mg/m³. Vanadium trioxide (V₂ O₃) melts at 1970 °C, is a black salt that crystallizes gradually into indigo-blue on contact with air to form vanadium tetroxide (V₂ O₄) and decomposes on heating to produce very toxic fumes. (Lozano, 2006)

Nozzle diameters

When selecting the nozzle, the exit diameter through which the filament will pass must be taken into account, as this will determine the maximum quality that can be obtained. When heated, the filament is pushed through the nozzle, generating an elevated pressure inside the material passage channel. This pressure must be kept constant, otherwise the extruder will not have the necessary force to push the filament. This situation results in loss of extruder motor steps and inconsistency in the amount of material deposited. To avoid this problem, it is essential to select the correct nozzle diameter in the laminating software, and to correct this parameter each time the nozzle is changed to a different size.

When using smaller diameter nozzles, the extruder deposits less filament in each pass, so it covers less surface area and must make more strokes to cover the printed layer. As a result, printing times increase considerably. As an advantage, the resolution in the X and Y axes will be much higher, so more detailed parts can be printed.

On the other hand, if we wish to print very large parts, with a medium or low level of detail, it would be convenient to use a nozzle with a larger exit diameter. In addition to covering a larger surface area per pass, thus reducing the times of each individual layer, a larger nozzle allows the height of the printed layers to be increased. As a general rule, the maximum layer height that can be printed is approximately 75% of the nozzle diameter, although sometimes it can cause problems of poor adhesion between layers and subsequent delamination of the part. It is advisable not to exceed 60%, so if we use a 0.8 mm nozzle, a maximum layer height of 0.48 mm would give us a very good relationship between speed and printing quality.

Otra forma de ahorrar tiempo en cada pieza es reducir la cantidad de paredes impresas. Lo habitual al usar boquillas estándar de 0,4 mm es establecer dos paredes de ancho en los laterales del objeto. Usando una boquilla de 0,8 mm se puede imprimir sólo una pared y lograr la misma resistencia. Debemos ajustar muy bien las retracciones para evitar faltantes de material en las paredes, ya que los defectos se magnifican al agrandar las capas.

Most laminating software includes the option to set the line width, which brings advantages in part strength or printing speed. To experiment with these parameters, this table can be of great help: (3D Solved, s.f.)

Nozzle size.	Minimum layer height.	Maximum layer height.	Minimum line width.	Maximum line width.
0.15 mm	0.04 mm	0.12 mm	0.1 mm	0.3 mm
0.20 mm	0.05 mm	0.16 mm	0.12 mm	0.4 mm
0.25 mm	0.06 mm	0.20 mm	0.15 mm	0.5 mm
0.30 mm	0.08	0.24 mm	0.18 mm	0.6 mm
0.35 mm	0.09 mm	0.28 mm	0.2 mm	0.7 mm
0.40 mm	0.10 mm	0.32 mm	0.24 mm	0.8 mm
0.50 mm	0.13 mm	0.40 mm	0.3 mm	1 mm
0.60 mm	0.15 mm	0.48 mm	0.36 mm	1.2 mm
0.80 mm	0.20 mm	0.64 mm	0.48 mm	1.6 mm
1.00 mm	0.25 mm	0.80 mm	0.6 mm	2 mm

Table 2 Line width. (3D Solved, s.f.)

Process

Additive manufacturing (AM), formerly known as rapid prototyping (RP), is one such technological development. AM is defined by the American Society for Testing and Materials (ASTM) as "a process of joining materials to fabricate objects from 3D model data, usually layer by layer, as opposed to subtractive manufacturing methodologies".

Also commonly referred to as 3D printing in the public literature, this emerging technology is revolutionizing the manufacturing industry with its ability to convert digital data into physical parts. Its distinct ability to fabricate complex shapes and structures has already made it invaluable for the production of prototypes such as engine connectors for the automotive industry and tools such as investment casting molds in the jewelry and aerospace industries.

Regardless of the different techniques used in the AM systems developed, they generally adopt the same basic approach, which can be detailed as:

A model or component is modeled in a computer aided manufacturing system (CAD-CAM). The model describing the physical part to be built must be represented as closed surfaces that ambiguously define a closed volume. This means that the data must specify the bottom, the outside and the boundary of the model. This requirement will be redundant if the modeling technique used is based on the solid model.

2. The solid or surface model to be built is then converted into a file format called "STL" (stereolithography) originated by 3D Systems. The STL file format approximates the surfaces of the model using the simplest of polygons, triangles. Highly curved surfaces must employ many triangles and this means that STL files for curved parts can be large. Some AM systems also accept data in the 2D/3D vector graphics format based on the Initial Graphics Exchange Specification (IGES).

A computer program analyzes an. STL file that defines the model to be manufactured and "slices" the model into cross sections. The cross sections are systematically recreated through solidification of liquids or powders and then combined to form a 3D model.

Fundamentally, AM development can be described in four areas. The key aspects of AM are four: input, method, material and applications, Figure 3.

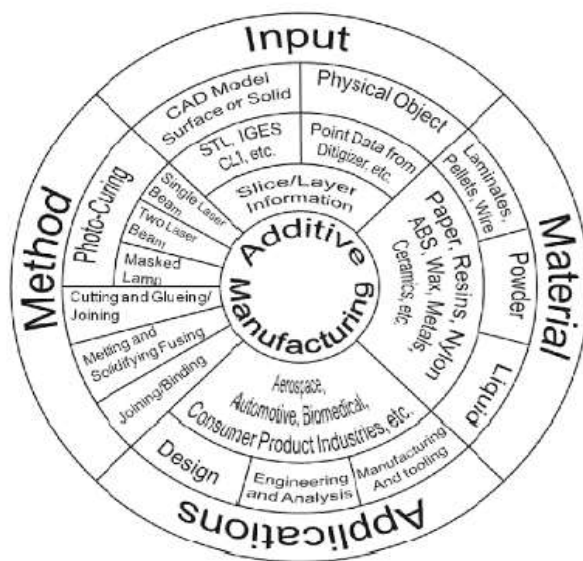


Figure 3 Key Aspects of Additive Manufacturing. (Chee Kai Chua, Kai Fai Leong. 3D Printing and Additive Manufacturing: Principles and Applications. World Scientific Publishing Co Pte Ltd. 2014)

How printers work

To create a 3D model, the first step is to design it with 3D rendering software (CAD type). The model is saved in a stereolithography (STL file). The printer software reinterprets the information in the. STL file and transforms it into 2D horizontal sections that will be printed by the printer in an additive way until the complete 3D object is formed.

There are many different techniques for printing three-dimensional models. The one used by the most common printers is fused deposition modeling (FDM) or thermoplastic extrusion. The printer has a nozzle that can be moved very precisely in three axes, through which it pours molten material in the form of wires that solidify immediately after exiting the nozzle. The most common materials used in this type of printer are various types of plastics, such as acrylonitrile butadiene styrene (ABS) and poly lactic acid (PLA).

But they can also be used with waxes, metals, ceramics, nylon, glass and even chocolate and other foods to create pastry pieces.

Components and Mechanical Positioning System

Positioning Algorithm

The design of the positioning system uses the Bresenham algorithm for its displacement, from which trajectory tracking and error minimization are guaranteed. This algorithm considers for the movement between two points in the XY plane, a line that goes from the initial point (x_1, y_1) to the point (x_2, y_2) , as shown in Figure 3-1. From these points $\Delta Px = x_2 - x_1$ and $\Delta Py = y_2 - y_1$ are calculated, whose results are compared to establish the axis of motion; if $|\Delta Px| \geq |\Delta Py|$ X is taken as the driving axis otherwise it is the Y axis that is the driver.

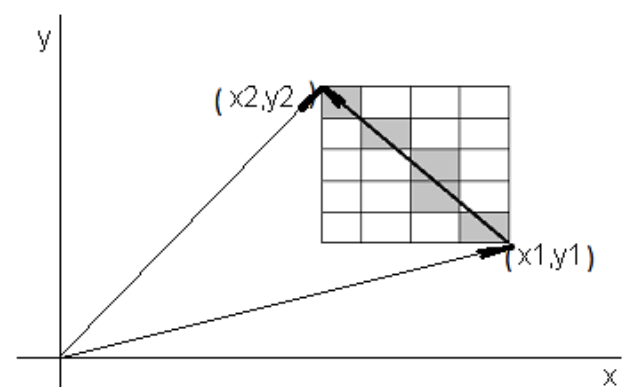


Figure 4 Movement established according to the Bresenham algorithm. (Jersson Xavier León Medina)

To determine the movement in the XY plane, we start from the real numbers provided by the G code, use absolute coordinates from which we define the initial position P1 and final position P2 of the extruder and discretize them to determine the displacement characteristics.

Within the main loop of the algorithm the coordinate corresponding to the driving axis is incremented by one unit and in the other axis, usually known as passive axis, it is only incremented as needed according to the following procedure:

The slope m of the line is calculated, which is given by:

$$m = \Delta Y / \Delta X \quad (1)$$

The initial error, given by:

$$\epsilon = - [1 - y_1 - m(1 - x_1)] \quad (2)$$

Where x_1 and y_1 correspond to the initial positions on the coordinate axes.

With these results, we define the beginning of the movement from the point (x_1, y_1) , and we start advancing one unit in the movement axis, we add the slope to the initial error and we establish if the new value is greater than 0, if it is not, we continue advancing in the movement axis and we add the slope again, until this sum becomes greater than 0, at that moment we increase one unit in the other axis and the error is decreased in one unit, starting the process again until we find the arrival point (x_2, y_2) .

The motion on the X and y axes is described by ΔP_x and ΔP_y according to the above algorithm; on the Z axis the motion is defined according to the thickness of the deposited material layer.

Axis Movements

X-axis motion

The selected mechanism corresponds to a pinion-gear belt motion transmission system, supported by bearings, configured as shown in Figure 5.

This movement is governed by a motor and a pinion-belt mechanism, which moves a mass determined by the sum of the components of the material extruder tool and its support structure, the movement is guided by bearings that move on longitudinal guides.

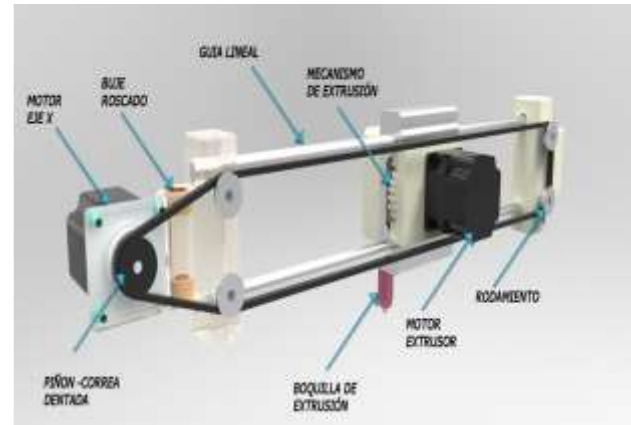


Figure 5 Actuator for X-axis motion. (Jersson Xavier León Medina)

The displacement ΔP_x is determined by the number of steps per revolution of the motor and the gear ratio given by the number of teeth of the pinion and the belt pitch, the linear speed is a function of the angular velocity of the motor, and the radius of the pinion; the actuator power depends on the inertia, and the frictional losses. The mathematical models to determine the above values are described below.

$$\Delta P_x = N_x P_c / (P_m) \eta \quad (3)$$

Where:

N_x = Number of sprocket teeth for the shaft.

P_c = Belt pitch.

P_m = Number of steps per revolution of the motor.

n = Steps for the given motion.

Linear velocity of the X axis.

$$V_X = \omega_{mx} r_{px} \quad (4)$$

Where:

v_x = Linear velocity of the x-axis.

r_{px} = Radius of the x-axis pinion.

ω_{mx} = Angular velocity of the x-axis motor.

The force required to move the x-axis is calculated as follows:

$$F_{cx} = W / \mu \quad (5)$$

Where:

F_{cx} = Force required to move the x-axis.

W = Total weight of the x-axis carriage.

μ = Coefficient of friction.

The total torque of the motor X T_{cx} required to move the load at constant speed is:

$$T_{cx} = F_{cx} * r_{px} \quad (6)$$

The torque required to move the load at an accelerated rate is greater than that required to move the load at constant speed, due to inertial effects, and is calculated as follows: The load inertia J_a takes into account the carriage hammer X and is modeled as follows:

$$J_a = \frac{D^2 M}{4} \quad (7)$$

Where:

D=Diameter of the pinion gear coupled to the X motor.

M = Mass to be moved of the X axis

The inertia J_b of the bearings, proper of the shaft on which the belt slides are modeled as a solid cylinder as follows:

$$J_b = \frac{\pi \rho D^4 L}{32} \quad (8)$$

Where:

ρ =Density of the bearing material.

D=Bearing diameter.

L=Thickness of the bearing.

The total inertia is the sum of all those involved.

$$J_T = \sum J_i \quad (9)$$

The linear acceleration α existing at the moment of starting or braking the mechanism is given by:

$$\alpha = \frac{\partial \omega}{\partial t} \quad (10)$$

The total torque T_{TX} required in motor X is themes:

$$T_{TX} = T_{CXV} + J_T \frac{\partial \omega}{\partial t} \quad (11)$$

Movimiento en el eje Y

El eje Y responde al mismo tipo de modelamiento paramétrico definido para el mecanismo de transmisión de movimiento del eje X, ya que poseen el mismo mecanismo de transmisión con polea-correa dentada.

Y-axis motion

The Y-axis responds to the same type of parametric modeling defined for the X-axis motion transmission mechanism, since they have the same transmission mechanism with toothed belt-pulley.

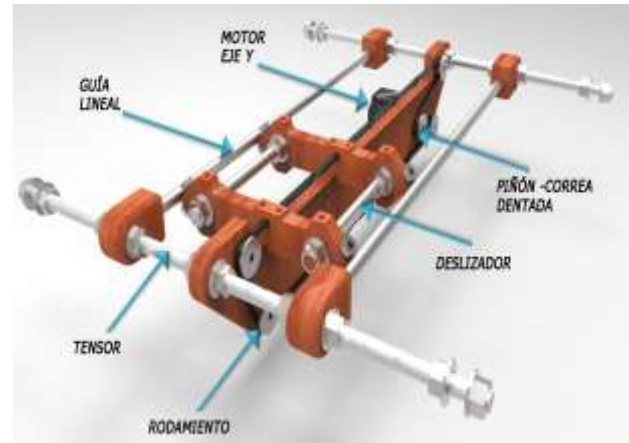


Figure 6 Y-motion actuator. (Jersson Xavier León Medina)

Z-axis motion

This motion is governed by a stepper motor, a motion transmission system integrated by two gearwheels that provide rotational motion to a transverse axis, and this through two worm-worm-crown mechanisms, located at the ends of the prototype, provides motion to two vertical threaded rods that transmit motion in the Z direction to the coupled X axis.

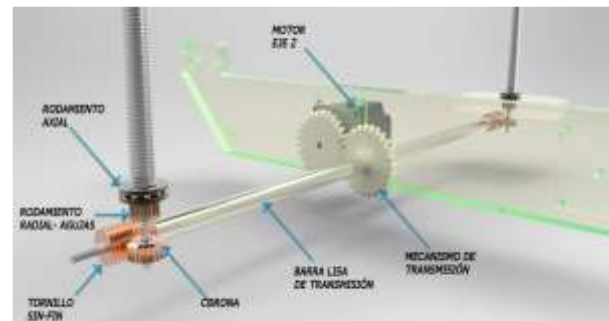


Figure 7 Actuator for Z-axis motion. (Jersson Xavier León Medina)

In this direction the change of position ΔP_z is determined by the state of the coordinates delivered by the G-code, which vary according to the characteristics of the thickness of the molten layer. The displacement and speed is dependent on the number of steps per revolution of the motor, the gear ratio of the gears and the pitch of the vertical rod thread, as follows:

$$\Delta P_z = \frac{P_t}{P_m N_z} \eta \quad (12)$$

Where:

N_z = Number of crown teeth.

P_t = Pitch of the vertical rod thread.

P_m = Number of motor steps per revolution.

n = Number of steps for the given motion.

Z-axis linear velocity.

$$V_z = \frac{1}{2\pi} \frac{\omega_{mz}}{N_z} P_t \quad (13)$$

Material extrusion mechanism

The extrusion mechanism is composed of: the extruder motor with a pinion coupled to the driving shaft and a toothed wheel coupled to a shaft supported by two bearings and which in turn drives a small toothed wheel that comes into contact with the material filament, thus allowing the supply of the material to the heater.

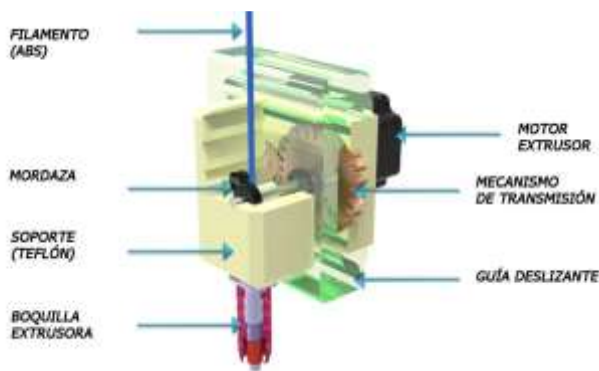


Figure 8 Extrusion Mechanism. (Jersson Xavier León Medina)

Control Design

Within the design of the printer, some control strategies are contemplated to supervise the system, in order to ensure some safety parameters and correct operation of the printer. Some of them are:

– Open loop control

In this control strategy there is no feedback from the plant to a control card, only the latter exerts its function on the actuators, but the final response of action is not measured.

– Closed loop control

In this control strategy there is a feedback to the controller so that the performance signal measured through sensors is compared with a base signal or reference signal, to establish the control actions based on the error signal to tend to be equal and thus minimize possible errors.

– Control Proporcional Integral Derivativo (PID)

A PID (Proportional Integrative Derivative Proportional) controller is a generic control mechanism on a closed loop feedback, widely used in industry for system control. The PID is a system that enters an error calculated from the desired output minus the output obtained and its output is used as input to the system to be controlled. The controller attempts to minimize the error by adjusting the system input:

We can highlight the following equation of the PID control strategy, it shows the model of the controller output that will serve as control input signal to the process. (Jersson Xavier León Medina)

$$u(t) = K_p e(t) + K_i \int_0^t e(t) dt + K_d \frac{de(t)}{dt} \quad (14)$$

Where:

$e(t)$ is the signal error.

$u(t)$ controller output and control input to the process.

K_p is the proportional gain.

K_i is the integral time gain.

K_d is the derivative time gain.

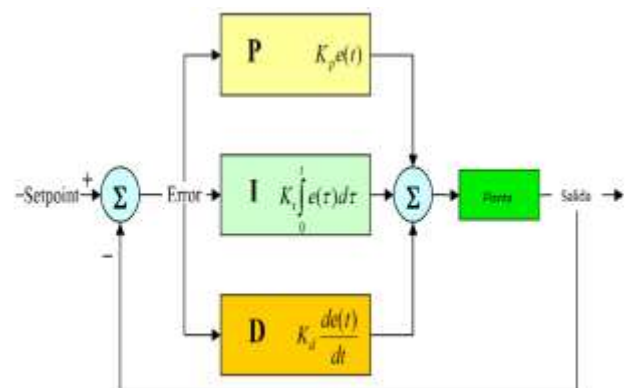


Figure 9 PID Control Diagram. (Jersson Xavier León Medina)

3D Printing

3D printing has been one of the most significant inventions in recent years. This is why the incipient creation of three-dimensional objects through additive or layer compaction techniques could surpass the development of products through the use of molds or the extrusion or subtraction of raw material.



Figure 10 3D printing appears at the top of the trend curve. (Joquera Ortega, 2016)

This revolution in the manufacture of parts has covered many areas, from engineering to medicine, bringing as a guarantee a breakthrough towards new knowledge. Today it is possible to re-transform bits into atoms, i.e. into physical objects, in homes, workshops or SMEs, thanks to 3D printers and rapid prototyping machines.

3D printing or additive manufacturing (AM) is a process of creating three-dimensional objects by adding materials layer by layer. Physical objects are produced using data from a digital model of a 3D model or other data sources, such as an AMF (Additive Manufacturing File). The personal computer plus the Internet and this new invention allow society to have the solutions to its problems at its fingertips. From this conjugation of technologies, a part is obtained, starting from a digital file (3D model), different additive processes are used in which successive layers of material are applied to create a tangible object. (Joquera Ortega, 2016)



Figure 11 3D Printer - UP Plus 2 manufactured by Tiertime. (Joquera Ortega, 2016)

From this invention, the technology was modified until today, where the printing is made of plastic material. This situation has certain advantages and limitations as shown in Table 3.

Advantages	Limitations
Complexity and freedom of design.	Higher cost of large productions.
Customization and personalization	Less choice of materials, colors, finishes
No need for tools.	Limited resistance and durability
Speed and cost savings.	Accuracy of printed objects.
Faster and less risky market access.	Most 3D printers are limited by scale and size.
Less waste, sustainability, environmentally friendly.	

Table 3 Ventajas y Limitaciones de la Impresión 3D. (Introducción a la Impresión 3D)

In the same way, the synergy between a mechanical design software with the communication to the 3D printer generates the manufacturing process of the part. This consists of the creation of a mathematical representation of surfaces using geometry, where the result is known as a 3D model, which can be represented on screen as a two-dimensional image or as a physical object, through a 3D printer.

In the same way, the synergy between a mechanical design software with the communication to the 3D printer generates the manufacturing process of the part. This consists of the creation of a mathematical representation of surfaces using geometry, where the result is known as a 3D model, which can be represented on screen as a two-dimensional image or as a physical object, through a 3D printer. When the 3D printer receives the correct information, it begins to produce the objects according to the design established by the user.

This process takes place inside the printer. The filament (spool of material) passes through the extruder, which pushes it through the head melting the material all the way out through the nozzle as it draws each layer onto the print tray. As the material exits, it cools to maintain its shape. The layers build up one on top of the other until the final object is obtained.

On the other hand, for SMEs dedicated to manufacturing, to be able to acquire this machine requires a strong investment, as well as papers that grant the required permits because most of them are manufactured abroad, so it is difficult to have this equipment in the workshops or production areas. From this, the idea of designing a 3D printer was born in order to guarantee the needs of any organization and the regional market. Therefore, the general objective of this research is to analyze the mechatronic design for the manufacture of a 3D printer.

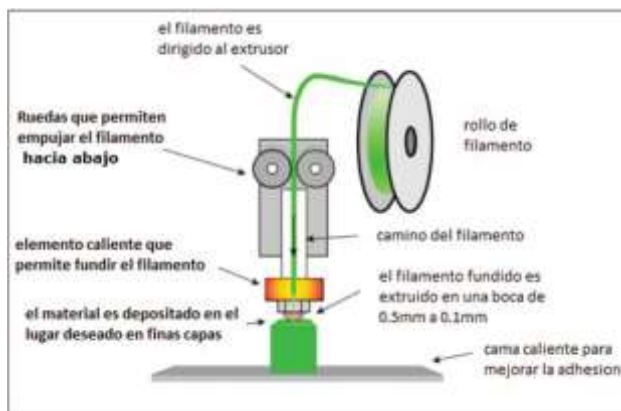


Figure 12 3D printing process. (Introducción a la impresión 3D)

3D printer application

The application of 3D printers are varied and in great quantity due to the versatility that can offer the products, because the user can manufacture the designs that guarantee the needs of the moment. From engineering, science, medicine and even education have had an answer thanks to the incorporation of parts produced by these machines.

This equipment can be used in the classroom as an educational tool in order to capture the student's attention and as a stimulator of their ideas. Table 4 details the advantages of using this technique as an educational tool in the classroom. In the same way, the fundamental material that can be used and experienced by students are thermoplastics (usually PLA or ABS) due to their versatility for being able to work with them.

Advantages	Features
Promote creativity.	The student will be able to capture their ideas in a digital context through a computer and witness how what was in their mind becomes a physical piece. From then on, their curiosity will take on infinite possibilities.
They develop spatial intelligence.	Another of the virtues offered by the "magic" of 3D printing. Children will develop their ability to recognize objects and unravel the similarities and/or differences between them, as well as improve their relationship with the space around them.
They solve problems while having fun and building knowledge.	The adaptation of 3D printers to the classroom opens up an unlimited field of possibilities for teachers. Students will be able to solve problems by creating individual pieces that break down the problem and speed up its resolution. Also, by solving this type of technological problems, they make a connection between theoretical and practical knowledge and reality.

Table 4 Advantages of the 3D printer in education. (Romero Perez)

Consequently, the development of this technology allows to improve the analysis of the parameters of various phenomena that occur in the sciences and thus provide more creative solutions to these problems. For example, in hydraulic engineering, through the design and construction of elements that are designed for specific situations, there is greater student participation due to the motivation to learn new knowledge thanks to the application of 3D printed models. In the field of medicine, it has provided answers to countless problems where solutions were difficult or highly expensive. Printing, for example, prostheses has helped to improve the quality of life of many patients. Table 5 details the use of 3D printing in the medical field.

Area	Features
Transplants.	There are two cases: you need to take skin from a part of the body and place it on the lesion, or you need to reconstruct a bone. In both cases, 3-D printers can help.
Organs.	Living cells are used as the material for printing. From these it is possible to generate an organ to be implanted in a person.
Others.	3D fabrication of corset for patients suffering from scoliosis. 3D printing of fetus in order to detect malformations in the unborn in order to follow up on the mother's gestation. 3D printing of plaster casts for fractures in the upper or lower limbs of the human body. Bone manufacturing.

Table 5 Use of printing in medicine. (Chimbo, Aveiga, Moreira y Tumbaco, 2016)

For the development of the machine, it is proposed to create a diagram that links the mechanical and electronic modules in order to respond to the design of the 3D printer. (Alex Mauricio Tipán-Suárez).

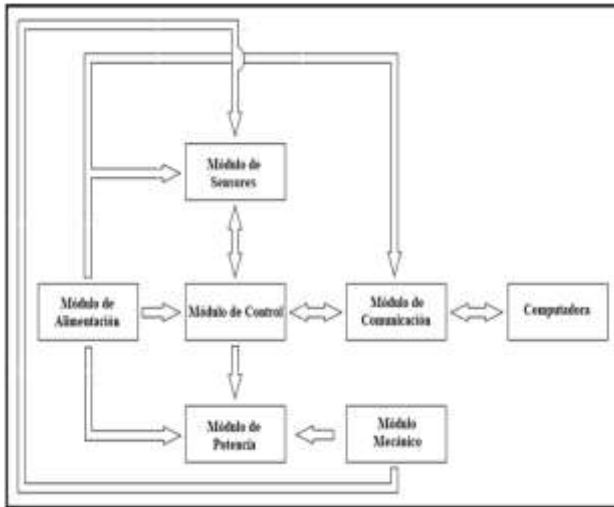


Figure 13 Diagram of the design of a 3D printer. (Naranjo y García)

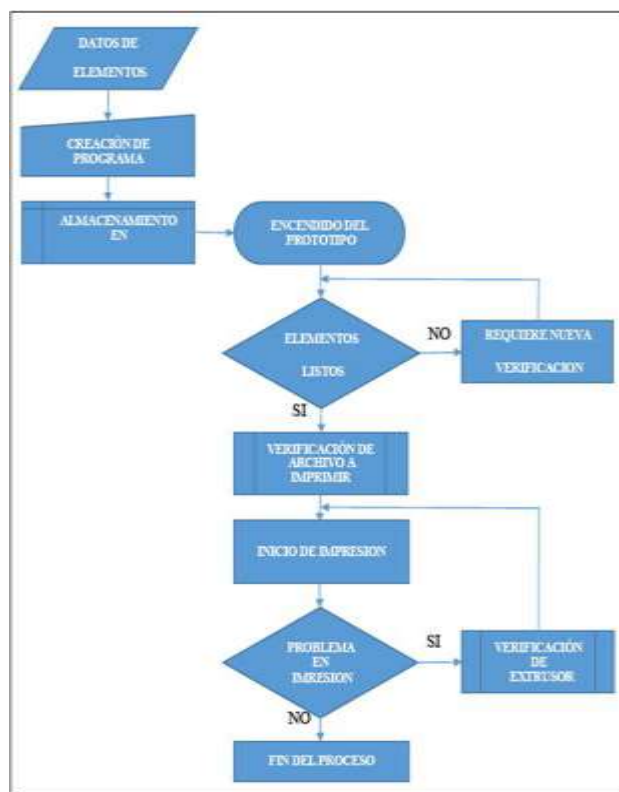


Figure 14 Printer flowchart. (Cañas Masapanta)

Rheology of Polymers

In order to support the research, this information is taken into account for the rheology of the polymers to determine the best material to be able to manufacture the nozzle in the future, if desired, in a physical way.

The etymological origin of rheology refers to the study of flow (from the Greek reos: to flow and logos: treatise, science) and was proposed by Eugene Cook Bingham, professor of chemistry at Lafayette College (Easton, PA, USA) to define that branch of physics whose objective is the fundamental and practical knowledge of the deformation or flow of matter.

Polymers and Biopolymers

Polymers result from the union of several units of a monomer, resulting in a chemical compound of natural or synthetic origin based on its constituent structural units. In the field of organic chemistry, polymers are called biopolymers. There are micromolecules of biological interest such as carbohydrates and proteins that, being intrinsic to animal and vegetable raw materials used for food formulation, generate food dispersions that have certain rheological behaviors.

A very common resulting colloid is sols, a dispersion formed by a solid dispersed in a liquid, in this case the particles of the dispersed phase are constituted by large macromolecules such as proteins, polysaccharides and lipids. In the case of sols and other fluid colloids, applying a force results in a deformation flow per unit time. The resistance of the solute to flow is defined as viscosity. If for a fluid the relationship between stress and shear rate is directly proportional, it has an ideal behavior known as "Newtonian", i.e. it obeys Newton's law of viscosity. (Zambrano-Herrera, 2020)

$$\tau = \eta \left(\frac{dv}{dy} \right) \tag{15}$$

where:
 τ=Shear stress.
 η=Coefficient of Viscosity (Pa.s)
 $\left(\frac{dv}{dy} \right)$ = Rate of speed or shear.

Classification of fluids

Fluids can be generally classified according to the relationship between the applied stress and the deformation ratio. We can classify fluids into 2 main groups, Newtonian fluids and non-Newtonian fluids.

Newtonian fluids are those in which the relationship between shear stress and velocity gradient is constant, the viscosity being constant.

$$\mu = \frac{\sigma}{\dot{\gamma}} \quad (16)$$

Non-Newtonian fluids are those in which the relationship between shear stress and velocity gradient is not constant. In this case, instead of viscosity coefficient or Newtonian viscosity, we speak of apparent viscosity coefficient.

$$\eta = \frac{\sigma(\dot{\gamma})}{\dot{\gamma}} \quad (17)$$

Non-Newtonian fluids, provided there is an influence due to shear time, can be divided into pseudoplastic fluids, dilatant fluids and plastic fluids.

Pseudoplastic fluids are those products in which the apparent viscosity decreases with the velocity gradient.

Dilatant fluids are those products in which the apparent viscosity increases with the velocity gradient.

Plastic fluids are those products that require a minimum stress to start flowing. This minimum stress is known as the stress threshold or creep threshold (σ_0). Below the creep threshold, the product exhibits solid-like characteristics. Once this creep threshold is exceeded, and the flow regime is reached, these fluids can behave as Newtonian (Bingham plastics) or as pseudoplastics (plastics in general). (Talens Oliag)

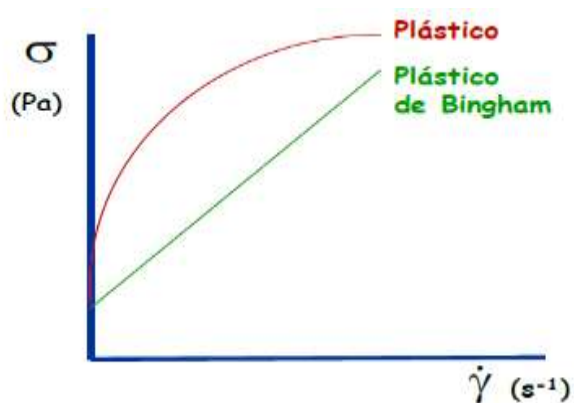


Figure 15 Flow curve or relationship between shear stress versus velocity gradient for a general plastic and Bingham plastic. (Talens Oliag)

Reverse Engineering

Parameter vs. function estimation

Inverse problems can be divided into two classes: parameter estimation and function estimation. The distinction is not always made, partly because many of the problems can be treated as function estimation problems and therefore include parameter estimation problems. Parameter estimation has a somewhat different connotation from heat transfer function estimation.

Mathematicians generally think of function estimation as the determination of an infinite dimensional solution (not just a finite dimensional discretization of a function, although the dimension can be quite large). But this is a theoretical concept and when one goes to implement the theory, one typically resorts to finite-dimensional approximations. This finite-dimensional approximation should converge to the infinite-dimensional function one is looking for. There are now some aspects that, although not exclusive to parameter estimation, are emphasized more than in the estimation of functions.

1. A limited number of parameters are estimated. In heat transfer, the number can be as small as one, it can be as large as half a dozen, and sometimes it could even go even higher.
2. The problems are usually not ill-posed, but they are usually nonlinear, even if the descriptive differential equation is linear.
3. Parameters often refer to a physical property, such as the thermal conductivity of a specific material at a particular temperature. These properties are not subject to human adjustment as, for example, a heat flow function is.
4. Parameter estimation analysis is not complete without giving an interval estimate or confidence region.
5. Model building is an important part of parameter estimation; that is, we have a physical process that we may not understand and wish to model more perfectly.

6. Careful examination of the residuals (measured minus estimated) values of the measured variables) is done to check the adequacy of the mathematical model and to better understand the measurement errors completely. The residuals should not have a characteristic signature that persists experiment after experiment. Such a characteristic signature indicates a bias that affects parameter estimates.
7. The sum-of-squares or weighted sum-of-squares function chosen should be selected based on measurement error.
8. A powerful way to investigate the adequacy of the model and experiment is to estimate the parameters sequentially. These parameter estimates should approximate constant values rather than moving up or down at the end of the analysis interval.
9. The optimal design of experiment is very important to obtain the best precision of the estimates.
10. Perception is the primary concern, while computational efficiency may not be.

Unlike parameter estimation, function estimation generally has the following characteristics:

1. The number of parameters to describe a function is usually large: perhaps in the hundreds or even thousands.
2. The problems are often ill-posed and may or may not be linear.
3. Computational efficiency is important. This may lead to avoid calculation of sensitivity coefficients. Intuition of the sensitivity of several components is usually not of interest.
4. Confidence intervals, model building, residual analysis, optimal design of experiments, statistics and sequential parameter estimates are rarely considered. (Woodbury, 2003)

Optical comparator

Optical comparators are a type of optical measuring instrument. The measuring principle is similar to that of optical microscopes. The object is placed on the platform and a light is shone onto the object from below. This causes the object's profile, or shadow, to be projected onto the screen. A telecentric optical system is used to enable accurate measurements.

Optical comparators were originally developed to inspect the contours of objects. Models equipped with measuring functions appeared later. Some large optical comparators have screen diameters exceeding 1m.

The following are some advantages of optical comparators.

- Non-contact measurement of the object.
- Measurement possible even for objects with small or complicated shapes.

Unlike measuring microscopes, it is not necessary to look through an eyepiece lens, making it possible for several people to make observations at the same time.

The use of optical comparators is widespread in the inspection and measurement of items such as electronic components and precision components. Conventionally, time and effort were required to reference the data and positioning of the object. (KEYENCE, 2023)

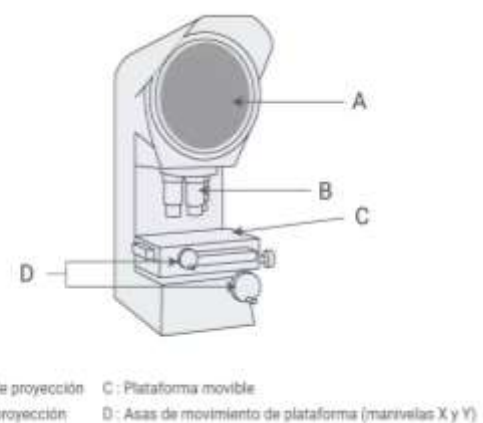


Figure 16 Parts of an optical comparator. (KEYENCE, 2023)

Finite Element Method

The finite element method (FEM), sometimes referred to as the finite element method (FEA), is a computational technique used to obtain approximate solutions of boundary value problems in engineering. Simply put, a boundary value problem is a mathematical problem in which one or more dependent variables must satisfy a differential equation everywhere within a known domain of independent variables and satisfy specific conditions on the boundary of the domain.

Boundary value problems are also sometimes referred to as field problems. The field is the domain of interest and most often represents a physical structure. The field variables are the dependent variables of interest governed by the differential equation. The boundary conditions are the specified values of the field. Variables (or related variables, such as derivatives) at the boundaries of the field.

Depending on the type of physical problem being analyzed, field variables may include physical displacement, temperature, heat flow and fluid velocity to name a few. The volume represents the domain of a boundary value problem to be solved. For simplicity, at this point, we assume a two-dimensional case with a single field variable (x, y) to be determined at each point $P(x, y)$ such that a known governing equation (or equations) is satisfied exactly at each of those points.

The mathematical solution is obtained; that is, the solution is a closed-form algebraic expression of the independent variables. In practical problems, the domain may be geometrically complex as is often the governing equation and the probability of obtaining an exact closed-form solution is very low. Therefore, approximate solutions based on numerical techniques and digital computation are most often obtained in engineering analysis of complex problems.

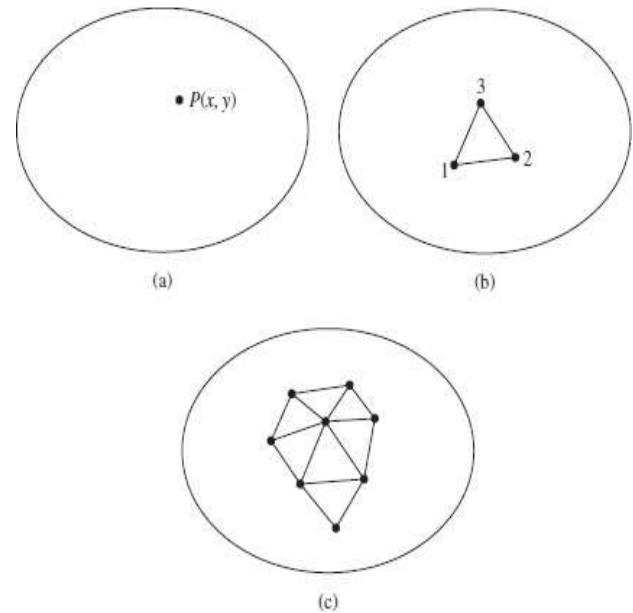


Figure 17 (a) A general two-dimensional domain of field variable (x, y)
 (b) A three-node finite element defined in the domain.
 (c) Additional elements showing a partial finite element mesh of the domain. (V.Hutton, 2004)

If the field variable values are computed only at the nodes, the field variable values computed at the nodes are used to approximate the values at non-nodal points (i.e., at the interior element) by interpolation of the nodal values. For the three-node triangle example, the nodes are all exterior and, at any other point within the element, the field variable is described by the approximate relationship:

$$\phi(x,y) = N_1(x,y)\phi_1 + N_2(x,y)\phi_2 + N_3(x,y)\phi_3 \quad (18)$$

Where ϕ_1 , ϕ_2 , and ϕ_3 are the values of the field variable at the nodes, and N_1 , N_2 , and N_3 are the interpolation functions, also known as shape functions or mixture functions. In the finite element approach, the nodal values of the field variable are treated as unknown constants to be determined. The interpolation functions are usually polynomial forms of the independent variables, derived to satisfy certain conditions required at the nodes.

These conditions are discussed in detail in later chapters. The main point to note here is that the interpolation functions are predetermined and known functions of the independent variables; and these functions describe the variation of the field variable within the finite element. (V.Hutton, 2004)

Displacement

A typical element, e , is defined by nodes, i, j, m , etc., and straight line boundaries. Let the displacement u at any point within the element be approximated as a column vector,

$$u \approx \hat{u} = \sum_k N_k a_k^e = [N_i, N_j, \dots] \begin{Bmatrix} a_i \\ a_j \\ \vdots \end{Bmatrix} = N a^e \quad (19)$$

Wherein the components of N are prescribed functions of position and a^e represents a listing of nodal displacements for a particular element.

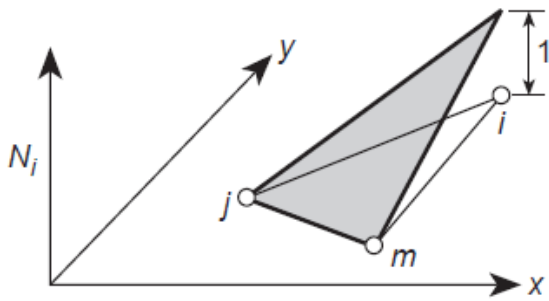


Figure 18 Form of the N_i function for an element. (O.C. Zienkiewicz, 2000)

In the case of air stress, for example, it represents the horizontal and vertical movements of a typical point within the element and the corresponding displacements of a node i .

$$u = \begin{Bmatrix} u(x, y) \\ v(x, y) \end{Bmatrix} \quad a_i = \begin{Bmatrix} u_i \\ v_i \end{Bmatrix} \quad (20)$$

The functions N_i, N_j, N_m should be chosen such that appropriate nodal displacements are given when the coordinates of the corresponding nodes are inserted into the general equation.

$$N_i(x_i, y_i) = I \text{ (matriz de identidad)} \quad (21)$$

Meanwhile:

$$N_i(x_i, y_i) = N_i(x_m, y_m) = 0 \quad (22)$$

If both displacement components are specified identically, then we can write and obtain N_i from the general equation, noting that $N_i=1$ at x_i, y_i but zero at other vertices. (O.C. Zienkiewicz, 2000)

Methodology to be developed

The type of nozzle to be used was determined, according to the existing printers in the machines laboratory of the prototyping area of the Tecnológico de Estudios Superiores de Valle de Bravo, taking into account as a reference the nozzle of a Stratasys 3D printer.



Figure 19 Stratasys 3D printer nozzle. (Own authorship)

The measurements of the nozzle were determined by metrology in order to start reverse engineering using the metrology technique.



Figure 20 Determination of the outer diameter of the nozzle

Own Authorship



Figure 21 Obtaining the general diameter of the nozzle

Own Authorship



Figure 22 Nozzle height determination
Own authorship

Reverse Engineering application for nozzle modeling

Nozzle modeling in Solidworks Software

Once reverse engineering was applied to the nozzle, the modeling of the nozzle in solidworks software was started, using the conventional metrology technique.

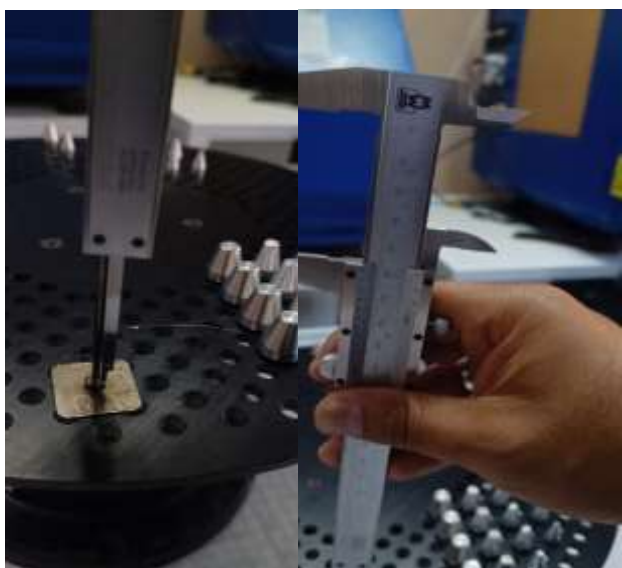


Figure 23 Obtaining nozzle height (filament guide)
Own Authorship

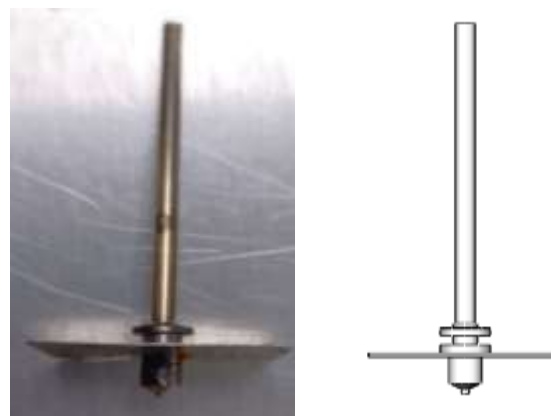


Figure 26 Stratasys machine nozzle modeling
Own Authorship

Determination of nozzle sizing, conical nozzle procurement.

We worked with documentary research to determine the flow and speed that will pass through the nozzle, according to the printing material, taking as a reference that waste plays a very important role for the development of this project.



Figure 27 Obtaining the conical part of the nozzle
Own Authorship

Due to the fact that there are only two nozzles of this printer, it is being analyzed that the printing parameters are very weak and some factors such as the speed are preventing the material from having a correct flow.

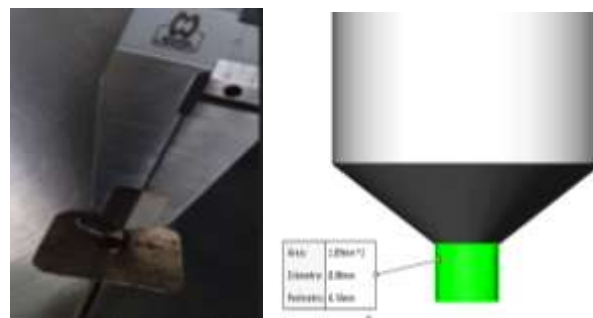


Figure 28 Obtaining the nozzle tip
Own Authorship

At this stage, the metrology methodology and the use of an optical comparator are being used to determine the measurements and obtain a geometry that can be compared between both techniques.

The nomenclature of the extruder was determined using a vernier, and the materials of which the nozzle is made were also analyzed.

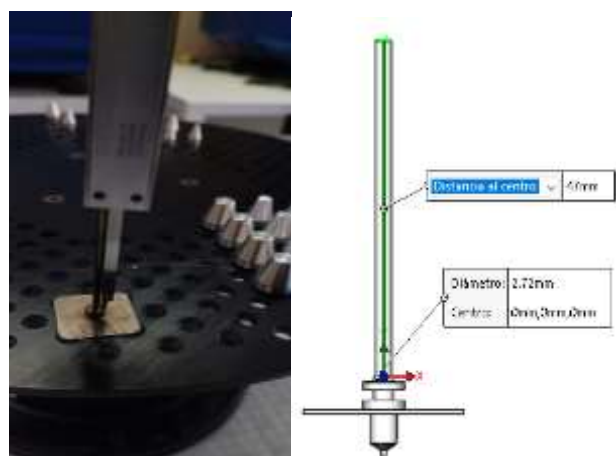


Figure 29 Determination of extruder height
Own Authorship

Determination of measurements between the two extruder supports for nozzle assembly.

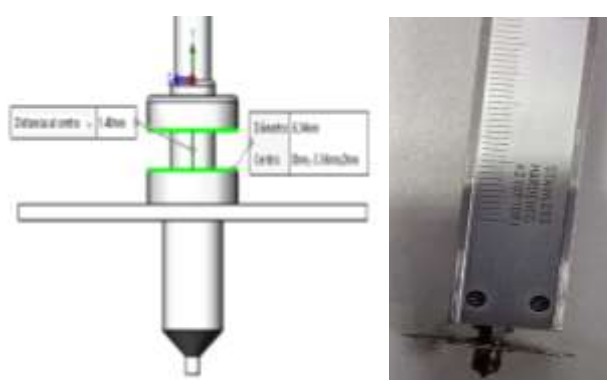


Figure 30 Determination of distance between extruder supports
Own Authorship

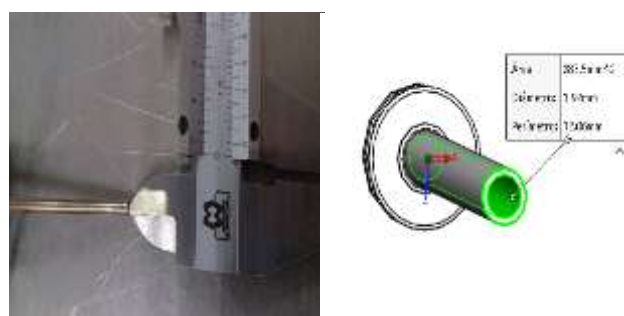


Figure 31 Obtaining the diameter of the extruder guide
Own Authorship

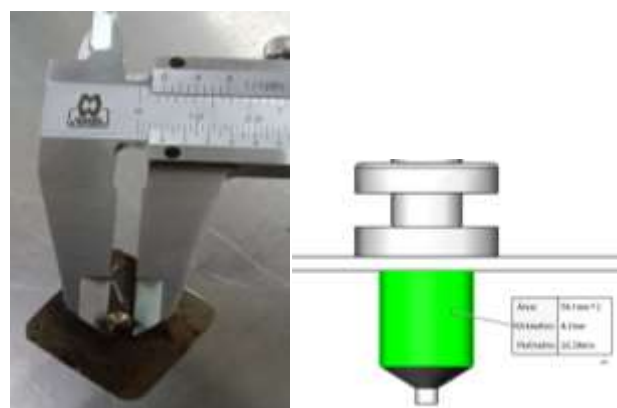


Figure 32 Determination of nozzle geometry
Own Authorship

Determination of geometries with optical comparator

The geometries of the nozzle were obtained using a Scarrett model 300 SERIES optical comparator, and the measurements obtained with conventional metrology and the optical comparator were compared, taking into account that there was a margin of error of 1% between the measurements with the optical comparator and those with conventional metrology instruments.



Figure 33 Obtaining geometries with optical comparator
Own Authorship



Figure 34 Obtaining nozzle geometries
Own Authorship



Figure 35 Obtaining digital parameters
Own Authorship

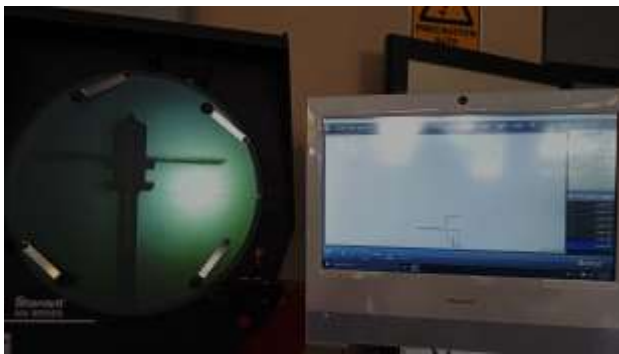


Figure 36 2D design of nozzle/comparison with conventional metrology
Own Authorship

Modeling of the nozzle in Ansys Workbench software

By means of SpaceClaim in the Fluid Flow library of Ansys Workbench, once the metrology and reverse engineering methodology was applied. The measurements obtained by metrology were taken as references, and in comparison with the optical comparator the correct measurements of the nozzle were verified, by referencing each of the nozzle geometries in a physical manner as detailed below.

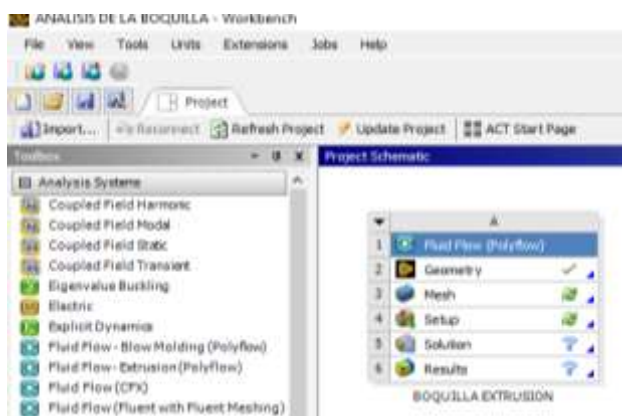


Figure 37 Interaction with Ansys Workbench-Fluid Flow
Own Authorship

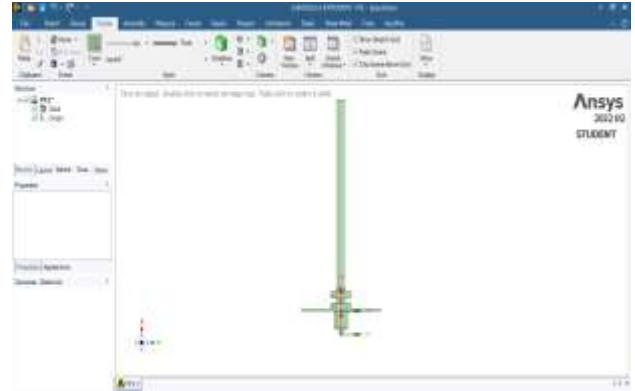


Figure 37 Ansys Workbench-SpaceClaim nozzle modeling
Own Authorship

Each of the angles were taken to verify the geometries of the nozzle and perform an analysis of each edge to apply the most appropriate material and perform a specific meshing, and finally perform an analysis by the Finite Element Method, this analysis will be to obtain the best results for a physical manufacture of the nozzle in the future.

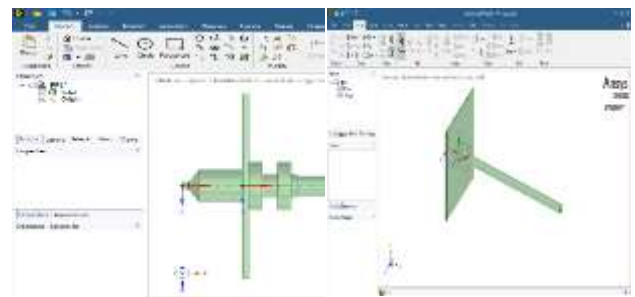


Figure 38 Trimetric and Top view of the nozzle
Own Authorship

Results

According to the results obtained, the 3% margin of error compared to conventional metrology with the use of optical technologies, a comparison was made and it was concluded that the use of this type of technology allows identifying more adequate geometries and with lower margins of error.

With the design in Ansys workbench, Spaceclim's CAD design library, it can be verified that with the 3D modeling 112746 nodes were obtained, 1 cm in size for each element, resulting in 57461 elements.

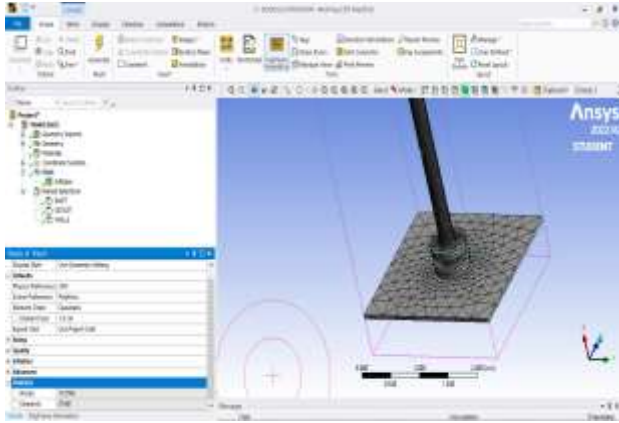


Figure 39 Nodes and Meshing Elements
Own Authorship

Subsequently, the meshing in each nozzle space was verified to identify possible collisions or geometries that present a margin of error, for each of the steps.

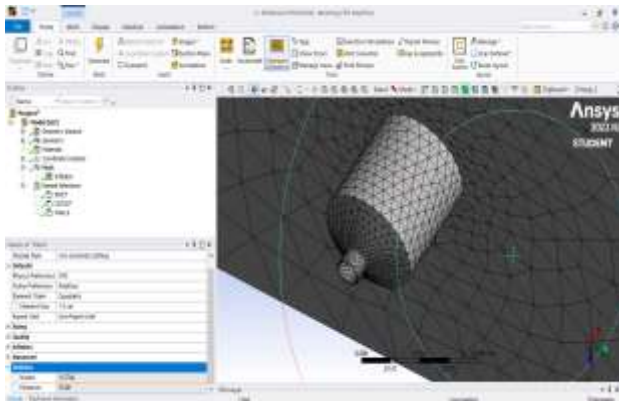


Figure 40 Verification of geometries and mesh elements
Own Authorship

Annexes

For the CAE section, the boundary conditions to be assigned to the element (nozzle) were taken as a reference, generating as fluid inputs. Equations (15), (16) and (17) referring to Newtonian and non-Newtonian fluids were used to determine the viscosity in the simulation, verifying the behavior of the material and the behavior of the nozzle.

The following parameters were taken into account in order to perform the simulation of fluid behavior, fluid velocity, displacement and to obtain a viscosity parameter.

Parameters with ABS impression material:

Density = 1030 kg/m³

Viscosity = 1.24 e-0.5

Nozzle Material: Aluminum

Mathematical Modeling:

Fluid flow

$$\tau = \eta \left(\frac{dv}{dy} \right) \quad (15)$$

where:

τ =Shear stress.

η =Viscosity coefficient (Pa.s).

$\left(\frac{dv}{dy} \right)$ =Velocity or shear rate

Newtonian Fluids

$$\mu = \frac{\sigma}{\gamma} \quad (16)$$

Non-Newtonian Fluids

$$\eta = \frac{\sigma(Y)}{\gamma} \quad (17)$$

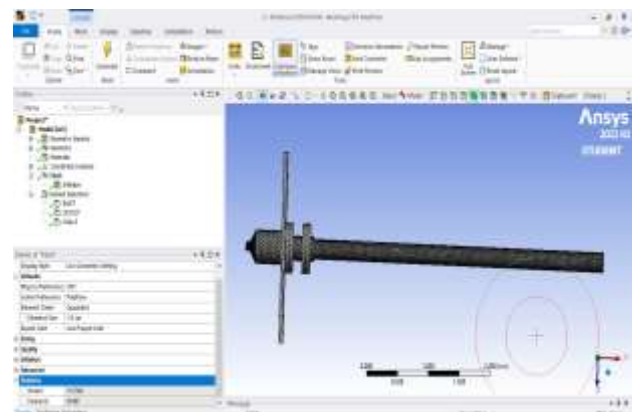


Figure 41 Assignment of input and output boundary conditions
Own Authorship

Once the inputs and outputs were identified with the behavioral parameters of the ABS material with a viscosity of 1.24 e-0.5 kg/(m s) and a flow density of 1030 kg/m³.

Subsequently it was moved for a results analysis to another Ansys Workbench library called Fluent to perform the material behavior through the Aluminum nozzle design as a results approach more with reality.



Figure 42 Analysis with inlet boundary conditions, outlet in Fluent
Own Authorship

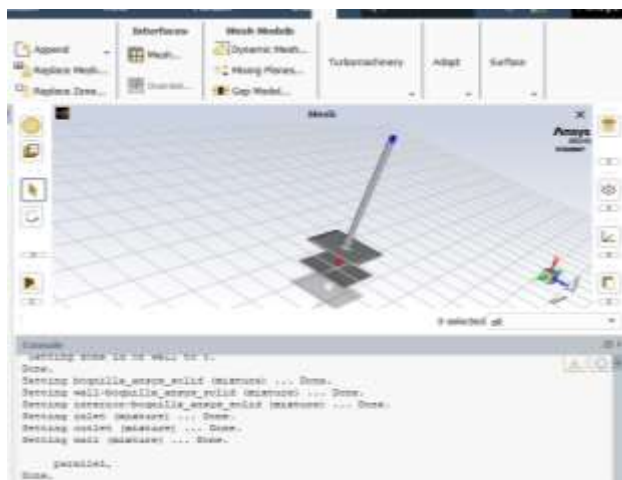


Figure 43 Verification of results and meshing in Fluent
Author's own work

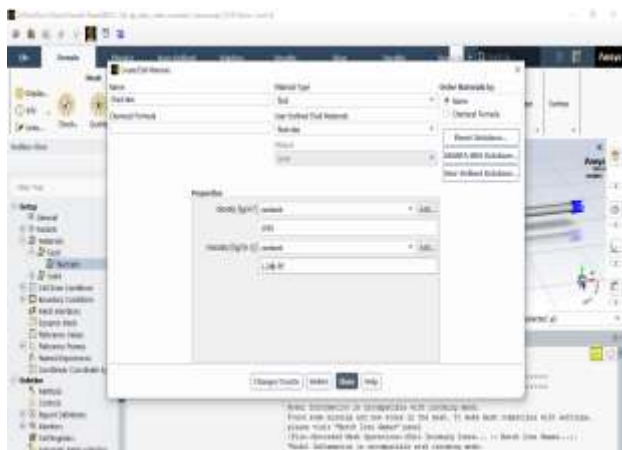


Figure 44 Configuration of viscosity and density parameters
Own Authorship

Once the material parameters were configured in the Fluent software, a temperature of 300° C was determined for the extrusion material of the nozzle for the ABS material.

Obtaining the following results of viscosity and behavior of the material, as a non-Newtonian material.

With a velocity of 10.91 m/s as maximum level, in a plane of 1.653 e-02.

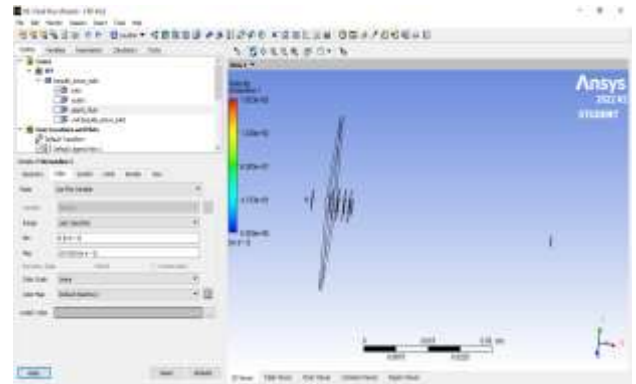


Figure 45 Velocity behavior
Own Authorship

As a result of a pressure of 3.201e+08 Pa maximum and a minimum of -3.592 e+07.

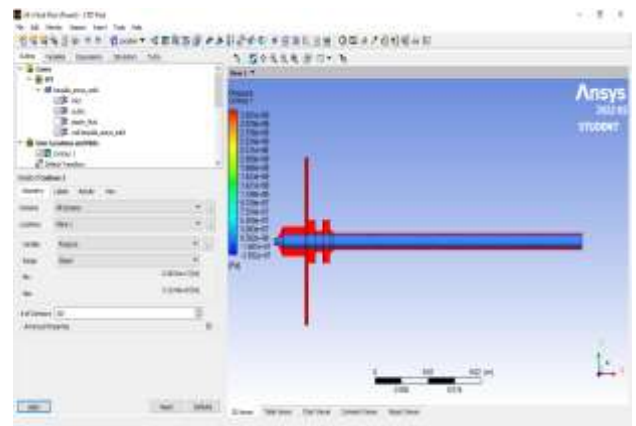


Figure 46 Material pressure analysis
Own Authorship

In the analysis it was determined how a parameter more turbulence in the nozzle of 8.262 e+02 maximum and 1.033 e+02 minimum, which could be observed that aluminum in this first analysis transfers heat more adequately throughout the nozzle in value of (m² s²).

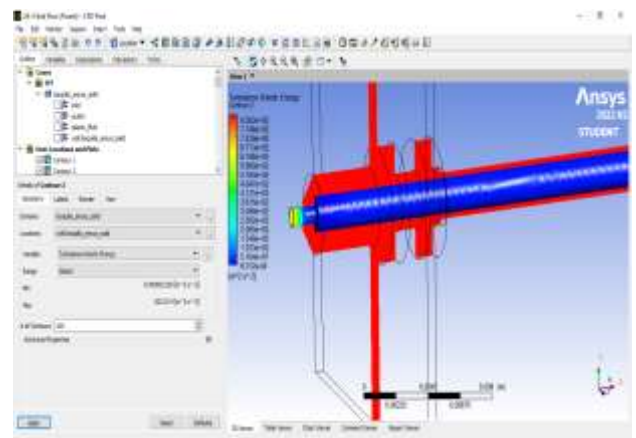


Figure 47 Maximum and minimum turbulence
Own Authorship

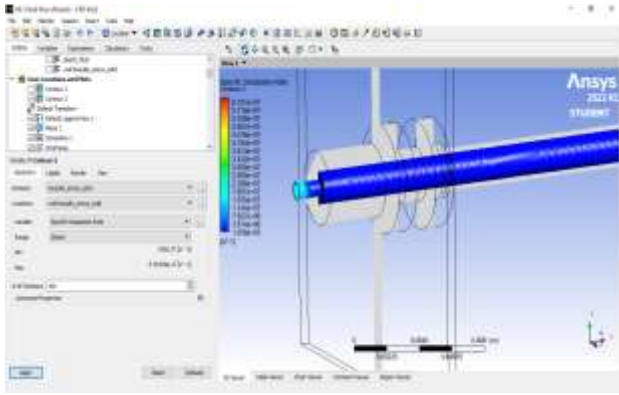


Figure 48 Dissipation rate
Own Authorship

Acknowledgement

I would like to thank the Advanced Technology Center (CIATEQ A.C.) based in Estado de México for allowing me to train as a Master in Advanced Manufacturing in their facilities, since with the support and knowledge of their professors they continue to train quality professionals, allowing the approach with this type of Advanced Technology centers and the Industry for the reinforcement of knowledge.

On the other hand, I also thank the Tecnológico de Estudios Superiores de Valle de Bravo, for allowing me to develop this project within their facilities and laboratories.

Conclusions

The objective and main point of this project was the modeling and design of a 3D printer nozzle of the Stratasys brand, and as breakdown points application of the different metrology techniques and the use of optics technologies for obtaining the geometry of the nozzle.

It is determined that the application of reverse engineering in the use of reverse engineering technique and modeling analysis was performed, therefore, it was identified that the accuracy of obtaining geometries is more accurate with the use of optical comparator due to its shadow projection for small parts, and compared to the use of measuring instrument can obtain a geometry, but with a deviation or a margin of error of 3% between the two techniques.

The main objective is concluded because the Tecnológico does not have these spare parts and the acquisition of these nozzles have a discontinuity in the market by the manufacturer, with the design and modeling of this nozzle can be sent to manufacture new nozzles with the standard plans in the field of mechanical drawing.

With the Finite Element Analysis, it can be observed that the nozzle is viable to be manufactured and constructed in a physical way, and that it will be possible to reduce the waste of material according to the manufacturing selected by the institution, carrying out the pertinent modifications of the project.

Recommendations

As recommendations to perform more future simulations with more materials, as first analysis was performed with aluminum material for the nozzle, but it is proposed to perform analysis with brass to verify the flow behavior of ABS material and compare both materials to verify which is the most suitable.

As well as the analysis with other libraries and different meshing with different steps between each element of each of the 3D models of the nozzle, taking as reference other types of nozzles.

References

- Ahmad, Z. (2006). *Principles of corrosion engineering and corrosion control*. Amsterdam: IChem; Elsevier.
- Alex Mauricio Tipán-Suárez, C. M.-C.-M.-S. (202). *Diseño Mecatrónico para la fabricación de una impresora 3D*. 6(3).
- Costa, J. A. (2018). *Tecnología para el prototipado rápido: Impresoras 3D*. 3(1).
- GARCÍA, E. P. (2006, junio). *CIMAV repositorio*. CIMAV Repositorio: <http://cimav.repositorioinstitucional.mx/jspui/handle/1004/606>

Hernández, A. Y. (2021). *METODOLOGÍA DE DISEÑO MODULAR PARA LA REDUCCIÓN DE PARTES Y ANÁLISIS ESTRUCTURAL EN UNA CAJA DE BATERÍAS DE USO AUTOMOTRIZ*. Nuevo León Monterrey: UANL.

<http://eprints.uanl.mx/21613/1/1080314528.pdf>

IMPRESORAS3D.COM. (2021, Julio 26). *Impresoras3D.Com EVERYTHING TO CREATE*. <https://www.impresoras3d.com/guia-de-boquillas-para-impresoras-3d/>

Iturriaga de la Fuente, G. (1999). *México Patente n° 2268902*.

Jersson Xavier León Medina, E. T. (2013). Diseño de un prototipo de impresora 3D que aplica la Técnica de Prototipado Rapido Mdelado Por Deposición Fundida. Colombia: Universidad Pedagógica y Tecnológica de Colombia.

KEYENCE. (2023, julio 20). *Conceptos Básicos de la Medición Dimensional y los Intrumentos de Medición (Fundamentos de Medición)*. <https://www.keyence.com.mx/ss/products/measure-sys/measurement-selection/type/projector.jsp>

Leal Alanís, S. A. (2011, junio). *eprints.uanl.mx*. <http://eprints.uanl.mx/2495/1/1080049438.pdf>.

Ledo, I. E. (2011). Caracterización del Latón. *Metalurgica*, 30(1), 57-54.

Lozano, J. J. (2006). VANADIO: CONTAMINACIÓN, METABOLISMO Y GENOTOXICIDAD. *Internacional Contaminación Ambiental*, 22(4), 173-189.

Mayer, M. (n.d.). *3D Solved*. The 3D Printing Search Engine!: <https://3dsolved.com/es/todo-sobre-boquillas-de-impresion-3d/>

Mazzola, I. L. (2021). Ventajas, desventajas y perspectiva estudiantil de la tecnología del CAD/CAM en el proceso enseñanza-aprendizaje de la educación dental. *Revista Cubana de Investigaciones Biomédicas.*, 1-13.

O.C. Zienkiewicz, R. T. (2000). *The Finite Element Method*. Barcelona España: McGraw Hill. <https://doi.org/ISBN-0750650494>

Ortega, A. J. (n.d.). *Fabricación Digital: Introducción al modelado e impresión 3D*. España: Secretaria General Tecnica, Subdirección General de Documentaciones y Publicaciones.

Sheila, W., Bisson, C., y Duffy, A. P. (2012). Applying a behavioural and operational diagnostic typology of competitive intelligence practice: empirical evidence from the SME sector in Turkey. *Journal of Strategic Marketing*, 20(1), 19-33. <https://doi.org/http://dx.doi.org/10.1080/0965254X.2011.628450>

SIEMENS. (2023, 06 22). *Diseño Asistido por Ordenador (CAD)*. Diseño Asistido por Ordenador (CAD): <https://www.plm.automation.siemens.com/global/es/our-story/glossary/computer-aided-design-cad/12507>

Song, Y., Rampley, C. P., & Chen, X. (2019). Application of bacterial whole-cell biosensors in health. In Y. Song, C. P. Rampley, & X. Chen, *Handbook of Cell Biosensors* (pp. 1-17). Springer Nature Switzerland AG.

Talens Oliag, P. (n.d.). Caracterización del comportamiento reológico de un alimento fluido plástico. *Universidad Politecnica de Valencia*, 1.

V.Hutton, D. (2004). *Fundamental of Finite Element Analysis*. USA: McGraw-Hill. <https://doi.org/0-07-239536-2>

Woodbury, K. A. (2003). *Inverse Engineering Handbook*. CRC PRESS, 1st Edition, 480. <https://doi.org/https://doi.org/10.1201/9781420041613>

Zambrano-Herrera, W. (2020). REOLOGÍA DE POLÍMEROS. *Agrollania*, 19, 48. <https://doi.org/ISSN: 2665-0053>

Photovoltaic Autonomous Electric Charging Station

Electrolinera Fotovoltaica Autónoma

GARCÍA-CONTRERAS, Cecilia Pamela^{†*}, ONTIVEROS-SÁNCHEZ, Kenneth Arturo and ALVAREZ-MACÍAS, Carlos

Instituto Tecnológico Nacional de México, Instituto Tecnológico de la Laguna.

ID 1st Author: Cecilia Pamela, García-Contreras / ORC ID: 0000-0003-3056-0896, CVU CONAHCYT ID: 1271712

ID 2nd Co-author: Kenneth, Ontiveros-Sánchez / ORC ID: 0009-0004-1105-7958

ID 3rd Co-author: Carlos, Alvarez-Macías / ORC ID: 0000-0002-2263-0316, CVU CONAHCYT ID: 165872

DOI: 10.35429/JIE.2023.19.7.38.52

Received July 20, 2023; Accepted December 30, 2023

Abstract

Over the past decade, emerging technologies in the automotive sector have evolved with the integration of electric vehicles, providing a sustainable option for consumers. This approach aims to reduce reliance on fossil fuels and extend their extraction and consumption. This study proposes the sizing of an autonomous photovoltaic system to power an electric vehicle charging station, assessing its feasibility and profitability. Given the significance of electric vehicles in the future of transportation, exploring ways to meet their energy needs is crucial in contributing to the reduction of fossil fuels. While the theoretical project proves to be technologically feasible, analyses of areas, components, costs, and return on investment reveal that recovering the initial investment is not economically viable.

Autonomous Photovoltaic System, EV Charging Station, Photovoltaic System Design

Resumen

Durante la última década, las tecnologías emergentes en el sector automotriz han evolucionado con la integración de vehículos eléctricos, ofreciendo una opción sostenible para los consumidores. Este enfoque busca reducir la dependencia de combustibles fósiles y extender su extracción y consumo. Este estudio propone el dimensionamiento de un sistema fotovoltaico autónomo para alimentar una estación de carga de vehículos eléctricos, evaluando su viabilidad y rentabilidad. Dada la importancia de los vehículos eléctricos en el futuro del transporte, es crucial explorar formas de satisfacer sus necesidades energéticas, contribuyendo así a la reducción de combustibles fósiles. Aunque el proyecto teórico demuestra ser factible desde el punto de vista tecnológico, los análisis de Areas, componentes, costos y retorno de inversión revelan que no es económicamente rentable recuperar la inversión inicial.

Sistema Fotovoltaico Autónomo, Electrolinera, Dimensionado

Citation: GARCÍA-CONTRERAS, Cecilia Pamela, ONTIVEROS-SÁNCHEZ, Kenneth Arturo and ALVAREZ-MACÍAS, Carlos. Photovoltaic Autonomous Electric Charging Station. Journal Industrial Engineering. 2023. 7-19: 38-52

* Author's Correspondence (e-mail: ceciliapamela.gc@gmail.com)

† Researcher contributing as first author.

Introduction

In the last decades, it has become common knowledge that the current global energy model, based on fossil fuels, is unsustainable in the long term. The most urgent and immediate reason is the climate change induced by the burning and massive use of fossil fuels, and the second reason (but almost equally urgent) is the impending depletion of fossil fuel reserves with their exhaustive use. With this context in mind, a variety of alternatives have been presented to replace our current energy model. These alternatives are based on the direct or indirect use of renewable energy sources, such as biomass, solar, wind, or tidal energy. The integration of alternative energy sources into a country's energy model, as well as better resource management, is known as sustainable development—a common goal for all countries and their respective companies.

In Mexico, according to data from the Secretary of Energy (SENER) for the year 2020 in the National Energy Balance: Final energy consumption by sector, shown in Figure 1, it is noted that almost 40% of the country's final energy consumption is required by the transportation sector (Final energy consumption by sector, National Energy Balance, 2020).

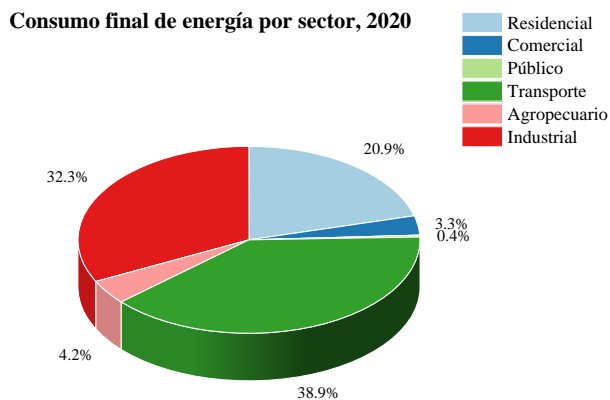


Figure 1 National Energy Balance: Final energy consumption by sector, year 2020

Source of reference: (*Final energy consumption by sector, National Energy Balance, 2020*)

Due to the high demands for energy and performance expectations, as well as the need to carry their energy source, it is logical to conclude that the transportation sector is the one with the most difficulties in terms of modification and improvement. However, being such an important sector, the transition to a sustainable model is inevitable.

Among the most popular and developed proposals for the transportation sector, specifically for the automotive section, is the so-called electric vehicle (EV).

Generally, all electric vehicles (EVs) have one or more electric motors instead of an internal combustion engine. All EVs use a rechargeable high-capacity battery pack to power the electric motor; this battery must be charged at a specialized charging station or a household outlet. Additionally, electric vehicles must have a controller that will manage the power supplied to the motor, i.e., the vehicle's speed. Electric vehicles that rely solely on rechargeable batteries for operation are called "Battery Electric Vehicles" or BEVs (Electric Vehicle Technology Explained, 2012). Figure 2 shows a basic diagram of a BEV.

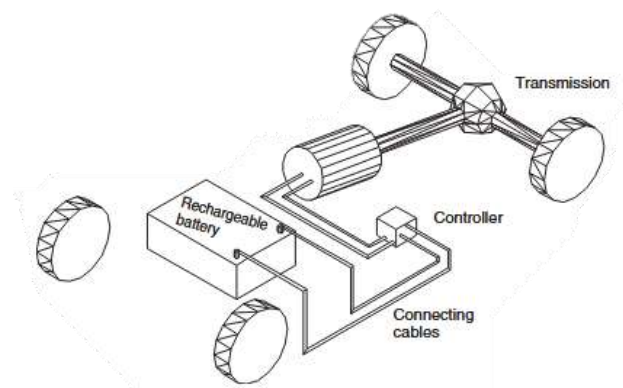


Figure 2 Battery-powered electric vehicle

Source of reference: (*Electric Vehicle Technology Explained, 2012*)

Rechargeable batteries are typically located underneath the center of the chassis, with more mass at the rear for better safety and weight distribution in the vehicle. A design challenge is that batteries usually account for about 40% of the weight in an electric vehicle (EV), whereas in a fossil fuel-based car, the engine, cooling system, and support systems only make up 25% to 30% of the car's weight (depending on the size of the gas tank), (Ultimate guide for Electric Cars, 38-43, 2020).

These rechargeable batteries do not have a definitive charging time that can be applied universally to all electric cars on the market. However, we know that three aspects affect their charging:

- Charging point power
- Battery capacity
- Maximum car charging power

In cases where the maximum power and charging point power differ, the lower power will determine the waiting time. Battery capacity determines the charging time and how often the process should be repeated (Electric Vehicle Technology Explained, 2012).

On the other hand, the average lifespan of batteries is estimated to be around 3000 full charge cycles. Therefore, if we consider daily charging and discharging, we find that the battery lasts just over 8 years. This may seem like a relatively short time, especially for the primary energy source of a car (which is typically seen as a long-term investment). However, this is considering the worst-case scenario, as the usual recommendation is that electric vehicle batteries never fully discharge, just as no one would let their internal combustion car run completely out of fuel.

Currently, there are different types of batteries available for use in EVs, including lead-acid, nickel-cadmium, nickel-metal hydride, lithium-ion, lithium-ion with cathode (LiFePO₄), and lithium polymer (J. Larminie, 2012). For comparative purposes, these batteries, along with some important specifications, are presented in Table 1.

Battery	Specific Energy (Wh/kg)	Energy Density (Wh/L)	Lifespan (charge-discharge cycles)
Lead-Acid	30-40	75	500-800
Nickel-Cadmium (NiCd)	40-60	80	1500-200
Nickel-Metal Hydride (NiMh)	30-80	150	300-500
Lithium-Ion	100-250	150	400-1200
Lithium-Ion with Cathode	90-100	250	2000
Lithium Polymer (LiPo)	300	300	1000

Table 1 Comparison of commercially available batteries
Source of reference: (Electric Vehicle Technology Explained, 2012)

*These data are only guidelines, as battery performance depends significantly on usage (appropriate or not)

While battery technology continues to advance, and the future trend is for prices to gradually decrease, batteries are still relatively expensive and not fully adapted for trips of more than 200 km per charge. Fortunately, in an urban environment and for the average use of a car, over 90% of trips do not exceed 200 km (How Green are Electric or Hydrogen-Powered Cars?, 2016).

Generally, lithium-ion batteries (one of the most commonly used types of batteries for electric cars) undergo an aging and wear process over their lifespan due to physical and chemical reasons. The following guidelines help maintain batteries in a reliable long-term state and preserve the highest possible capacity and autonomy:

- For short trips in daily use, it is advisable to charge the high-voltage battery to a maximum of 80% on average.
- For parking periods exceeding 12 hours, it is recommended to park the vehicle with a state between a minimum of 30% and a maximum of 80%.
- For charging the battery to 100%, it is preferable to set the timer on the charging manager and start driving immediately after the charge is complete.

On the other hand, the charging infrastructure or charging station is a facility that provides electricity for recharging the batteries of electric vehicles (EVs), including plug-in hybrid vehicles. Charging stations used as fast electricity dispensers typically have a battery fast-charging time of no more than ten minutes, and both these and domestic stations must be directly connected to a power source (usually the electrical grid) (The Electric Vehicle and its Interaction with the Electrical Grid, 2010).

Currently, each car brand or manufacturer usually has its own connector for charging the desired vehicle. In other words, a charging station for a specific electric car cannot be directly connected to a car from a different brand, as there are different inputs for different brands or manufacturers.

In the future, it is intended that charging station formats and their connection to cars will be limited and consolidated to a single standard protocol to keep prices lower (Ultimate Guide for Electric Cars, 38-43, 2020). Currently, the standard protocol with the most opportunities to consolidate is IEC 62196, developed by the International Electrotechnical Commission (IEC), which allows charging stations described in Table 2.

Name	Supply (kW)	Voltage (V)	Current (A)	Phase
CHAdEMO "Charge de move"	62.5	500	125	DC
VDE-AR-E 2623-2-2	43.5	400	63	3 fases
SAE J1772- 2009	16.8	240	70	1 fase
Serie Libera	22	400	32	3 fases

Table 2 Charging station systems developed from the international standard IEC 629196

Source of reference: (*El vehículo eléctrico y su interacción con la red eléctrica*, 2010)

While they may seem few, the future goal is for only one type of universal connector to exist. The estimated trend is that CHAdEMO and Tesla charging stations (not included in Table 1.3 due to limited available information) will be the final contenders, but it is still too early to definitively state which of the two will win the competition (Ultimate Guide for Electric Cars, 38-43, 2020). On the other hand, the charging stations described in Table 1.3 still do not fully meet the commonly accepted definition of "fast charging systems" by the industry, as they require more than 10 minutes for an average user to recharge during a mid-journey stop. Meanwhile, the Tesla Supercharger, by Tesla Motors, can supply up to 120 kW and achieve an 80% battery recharge time in 5-10 minutes (The Electric Vehicle and its Interaction with the Electrical Grid, 2010). For security and copyright reasons, official information on the operation method and exact demand for Tesla Superchargers is scarce.

In all European countries, the electric vehicle charging infrastructure is very advanced. Spain, in particular, has 11,517 out of 224,237 publicly accessible charging points available in Europe, with 71,079 registered electric vehicles by the end of 2021 (Annual Evolution of the Total Number of Electric Vehicle Registrations in Spain between 2013 and 2021, 2022).

The sector advocates for a minimum network of 70,000 publicly accessible charging points by 2023, 120,000 by 2025, and 340,000 by 2030 (Fast Charging Points in Spain for Electric Cars: Where They Are and What Price They Offer, 2022). Installation and charging companies in Spain support these ideas and have plans such as Iberdrola's Smart Mobility Plan, which aims to have a fast charging station every 50 km to enable travel throughout the country with autonomy (Nuno, 2010).

In contrast, Mexico only has 2,100 charging points (it is not specified in the figures if these are public or private). This is despite reports that 2021 was a "good year for the commercialization of electric vehicles in Mexico" (Electric Cars Exist, but No Plugs: The Dilemma of the Automotive Sector in Mexico, 2022). It is a common idea that one of the main reasons why only 1 in every 20 cars sold in the country is "green" is the limited accessibility to charging or a lack of charging stations in Mexico (Electric Cars Exist, but No Plugs: The Dilemma of the Automotive Sector in Mexico, 2022).

Despite bureaucratic barriers and misinformation, access to charging stations is a problem that the country will have to face sooner or later, as electric cars will be the only option for personal transportation in the not-so-distant future. This is considering that countries like France and Japan have already set a deadline for the commercialization of internal combustion cars—sooner or later, countries worldwide will have to adopt similar measures, including Mexico (Charging Stations: The Great Business Stalled by the Electrical Counter-Reform, 2021). Pure Battery Electric Vehicles (BEVs) are commonly charged from the electrical grid overnight at the owner's residence, provided they have their charging station or an adapter to plug directly into the grid outlets.

The energy from the grid is generated from a combination of sources; major generators use nuclear, coal, and gas energy. In some places, power production in the electrical grid may also come from renewable sources such as hydro, wind, and solar (Ultimate Guide for Electric Cars, 38-43, 2020). However, it's essential to remember that a fast-charging supply requires an industrial-type electrical service, as it demands large amounts of energy in a very short time (10 minutes or less).

The required power from the grid when charging a car with this type of service can go up to 210 kW. If we consider a charging station similar to current gas stations, with multiple simultaneous fast-charging points, the station might demand power peaks on the order of megawatts—which, if the electrical grid is not prepared, can cause voltage drops or outages during busy hours when several vehicles decide to charge simultaneously (The Electric Vehicle and its Interaction with the Electrical Grid, 2010).

For this reason, we believe that installing this charging station can be more beneficial if connected to an autonomous solar photovoltaic system, which stores energy from the photovoltaic panels when demand is low and releases/supplies it once demand is high. As the name implies, it would be a system off the electrical grid so that, if megawatts of energy were demanded at once and these could potentially cause an imbalance in the electrical grid, the electrical grid would not be affected because it is not connected to the system. For an autonomous system, various factors, mainly geographical and climatological, must be considered to adequately size the type and quantity of equipment (modules, batteries, cables, controller, protection, etc.) to meet the energy demand required by the user. Additionally, it must adhere to pre-established values and standards for safe sizing and installation.

The objective of this work is to conduct a case study for the locality of Torreón, Coahuila, and verify, theoretically, if it would be possible to install a fast-charging station for electric vehicles powered by an autonomous solar photovoltaic system.

Methodology

Currently, there are many options in the market for sizing software for photovoltaic installations, such as PVsyst, RETScreen, or HOMER (economic and environmental viability of off-grid PV-BESS for charging electric vehicles: Case Study of Spain, 2018). However, these programs are not the only option for sizing a photovoltaic system. To size the system traditionally, we will have to consider each part together and go back or change some parameter or device if it turns out to be cumbersome later.

We start with the batteries, first obtaining the capacity required by the battery in Ampere-hours, with Equation 1.

$$Ah \text{ en batteries } s = \frac{\text{Required Energy (Wh)}}{\text{Battery Bank Voltage} \times \% \text{ Discharge} \times 0.77} \quad (1)$$

It is recommended not to discharge the battery beyond 50% to have a longer lifespan without sacrificing too many hours of use (Style, 2012). With this data, a battery model and a connection scheme are chosen to meet the discharge demand. Then we must size the battery charge and, therefore, the supply it must have, taking into account the peak solar hours of the region (PSH). This with Equations 2 and 3.

$$\text{Load} = \text{Battery Bank Voltage} * \% \text{ charge} * \text{capacity} \quad (2)$$

$$\text{Supply} = \frac{\text{Battery Bank Capacity} * \% \text{ charge}}{\text{PSH}} \quad (3)$$

In a correct sizing, after sizing the batteries (with the help of Equation 1 and having a clear understanding of the energy required by the system), we move on to size the charge controller.

The work of the charge controller/regulator is key in the system because its optimal operation ensures battery protection. It is essential to ensure that the controller corresponds to the system voltage (12V/24V/48V), and the maximum current of the regulator is greater than the maximum current that the modules can generate in short circuit (Style, 2012). If, when sizing the solar modules to be used, this condition is not met, the modules or the controller must be changed (Macías, Topic 4 - Elements of Autonomous Systems, 2022). With this in mind, we will use Equation 4 to size the ideal controller's maximum current, and based on that data, look for a controller in the market that matches or exceeds this requirement.

$$\text{Maximum controller current} = \frac{\text{Solar Photovoltaic Power}}{\text{Battery Bank Voltage}} \quad (4)$$

Additionally, we need to know how much current the controller should allow to pass to charge the batteries, using the same discharge percentage used in Equation 1, along with the PSH. This minimum controller current is calculated with Equation 5.

$$\text{Controller Current} = \frac{\text{Battery Bank Capacity(Ah)} \times \% \text{ discharge}}{\text{PSH}} \quad (5)$$

Once a model available on the market is selected, we need to know the power that the controller can withstand with Equation 6. This is necessary because it gives us a range or limit for sizing modules.

$$P_{MPPT} = I_{max} \times V_{bat} \quad (6)$$

The modules are the engines or generators of energy in an autonomous photovoltaic system, converting solar energy into electrical energy via the photoelectric effect (Un sistema fotovoltaico autónomos, 2012). So we must have a clear idea of the required energy generation from the modules, with Equation 7.

$$\text{Required Generation} = \text{Battery Bank Voltage} * \text{supply} \quad (7)$$

The five electrical parameters (Open Circuit Voltage, Maximum Power Voltage, Short Circuit Current, Maximum Power Current, and Maximum Power) of a panel are already measured by the manufacturer and given in its datasheet, along with the characteristic curve they create. However, this curve can be affected by temperature or irradiance parameters. In a correct sizing, these changes in voltage must be anticipated according to the temperatures of the area; remembering that the recorded high and low temperatures have a corresponding correction factor, which can be found in NOM-001-SEDE-2018, and are calculated with Equations 8 and 9, respectively

$$V_{max} = V_{OC} * \text{Correction Factor (low temp.)} \quad (8)$$

$$V_{min} = V_{PM} * \text{Correction Factor (high temp.)} \quad (9)$$

Meanwhile, the short-circuit current can increase if there is irradiance greater than 1000 W/in which the module is tested, so we use Equation 10 to cover that variation.

$$I_{max} = I_{SC} * 1.25 \quad (10)$$

This will change the characteristic curve of the module to match what is actually produced in the area where we plan to install it. If the chosen controller is an MPPT, these peaks and variations won't matter as much because this device is designed to always seek the best performance from the panel (Macías, Tema 4- Elementos de sistemas autónomos, 2022).

The different electrical parameters of the module will help us choose the most suitable modules for our system. However, before choosing in the market, we must use Equation 11 to obtain the total power that the modules must have, taking into account the PSH.

$$P_{FV}(W_p) = \frac{\text{Required Energy (Wh)}}{\text{PSH (h)} \times 0.77} \quad (11)$$

After choosing the module to use and the arrangement in which they will be connected, we use Equation 12 to obtain the maximum current delivered by the module to the controller. This data will serve to check that the selected controller will withstand the energy provided by the photovoltaic array.

$$I_{max,mod} = \frac{P_{module} \times \# \text{ panels}}{\text{Battery Bank Voltage}} \quad (12)$$

Once all the parts of the DC autonomous photovoltaic system are measured, we can add the element to switch from direct current to alternating current: an inverter. Inverters, as the name suggests, are responsible for converting direct current to alternating current, transforming it from low voltage to a higher voltage. This process, logically, involves losses of around 10-15%, with efficiencies between 85-90% (Macías, Tema 4- Elementos de sistemas autónomos, 2022).

The inverter, when connected to products in the market that are regulated by law, has recommendations for sizing. These recommendations, given in the Official Mexican Standard, state: "[For] currents of the photovoltaic source circuit, the maximum current must be calculated by [...] the sum of the short-circuit current of the modules in parallel, multiplied by 125 percent" (NOM-001-SEDE-2018). This calculation is reflected in Equation 13, with 125 percent squared to provide greater protection.

$$P_{inversor} = \sum \text{Equipment Power} \times 1.25^2 \quad (13)$$

Once an inverter that fits the power required by the system and complies with NOM safety measures is obtained and chosen, we can find out the current demanded by the inverter with Equation 14. The current demanded by the inverter is essential data for the operation of the autonomous system, as it tells us if our system supplies the proposed load or if we need to resize any part of the system.

$$Demand = I_{max,inv} = \frac{P_{inv}}{V_{bat}} \quad (14)$$

Finally, for the wiring, various factors that can affect the gauge to choose must be taken into account; mainly the required ampacity (with its corresponding adjustment factors), whose formula is described in Equation 15, and the voltage drop, whose corresponding formula is found in Equation 16.

$$Adjusted\ Required\ Ampacity = \frac{\sum I_{SC-parallel} \times 1.25^2}{F_T \times F_C} \quad (15)$$

$$e_T = \frac{2 \times distance \times I_{MP}}{V_{MP}} \times R \quad (16)$$

As with any equation, it is important to keep the units of the data consistent. Otherwise, the result would be incorrect. Additionally, adjustment factors F_1 and F_2 can be obtained from the tables of NOM-001-SEDE-2018 when certain data about the locality in question is available (such as maximum and average temperatures).

Results

Location of the System for the Case Study

The present case study will be conducted for the city of Torreón, Coahuila, Mexico (latitude $25^{\circ}37'$ N and longitude $103^{\circ}23'$). This city is characterized by high levels of solar radiation and mostly clear skies, meaning that the solar radiation reaching a solar panel is high. It is an area where the installation of photovoltaic systems is popular. In fact, the brightest period of the year lasts for 3.3 months, from April 3 to July 14, with an average daily incident energy exceeding 7.2 kWh/m^2 . The brightest month of the year in Torreón is May, with an average of 7.8 kWh , while the darkest is December, with an average of 4.1 kWh (El clima y tiempo promedio en todo el año en Torreón, México, 2021). The solar resource and the expected growth in EV purchases in the area make it a good zone to study the feasibility of an autonomous PV-BESS solar system.

Additionally, we consulted other data for the study location:

- $T_{max}=44^{\circ}\text{C}$
- $T_{min}= -4^{\circ}\text{C}$
- $T_{average}= 22.7^{\circ}\text{C}$

Using Google Earth and the CONAGUA extension, we reviewed data from the nearest meteorological station. In this case, the closest one is at "Presa Coyote" and has data from 1981-2010. We observed that the highest temperature reached was 44°C , recorded in 1996, while the minimum temperature was -4°C , recorded in 1998. These data are highlighted in Figure 3.



Figure 1 Screenshot of the Google Earth program with the CONAGUA informatics extension, showing data taken from 1981-2010 in Torreón, Coahuila.

Source of reference: (Servicio Meteorológico Nacional, 1981-2010)

From the page <https://power.larc.nasa.gov/data-access-viewer/> developed by NASA, we obtained an Excel file shown in Figure 4 for the specific location (coordinates highlighted in green). This file has the average peak solar hour of the region when the solar system is tilted according to latitude. From the data for each month, we took the lowest one, corresponding to December (highlighted in yellow).

We get the data for the city, PSH=5.38 hours.



Figure 4 Screenshot, Excel file describing the PSH of Torreón, Coahuila

Source of reference: (20-year Meteorological and Solar Monthly & Annual Climatologies, 2001-2020)

Study of the load for the system

The charging rate varies among different EV models on the market, depending largely on the charge acceptance rate of the vehicle's battery. This rate is controlled by the energy management system of the batteries in each car.

For example, the 2020 model, Porsche Taycan, which was the best-selling model in Mexico in 2021, limits its charging rate to 50 kW for fast charging. With this rate, the charging station can recharge the Taycan's battery from 10% to 80% state of charge (SoC) in 30 minutes (Charging high-voltage battery, 2020). Additionally, we must take into account that, unlike a gasoline charging station, the charging rate (from the charging station to the vehicle's battery) is not constant over time. For physical and chemical reasons, the charging speed decreases as the charge level approaches 100% (Charging high-voltage battery, 2020).

For example, when the SoC is below 30% at the start of charging, the recharge rate is about 0.72 kWh per minute. However, when the SoC reaches 80%, the recharge rate decreases to 0.16 kWh per minute, which is less than half of the energy rate required for charging at the beginning of the process (economic and environmental viability of off-grid PV-BESS for charging electric vehicles: Case Study of Spain, 2018).

Fast charging stations have a hysteresis effect when the battery reaches a point close to full charge, so a fast charging station can only charge up to 80% of the battery's SoC. Current fast charging stations have a nominal output power of 50 kW and charge the vehicle's battery with direct current (DC) taken from a three-phase electrical grid (Electric Vehicle and Its Interaction with the Electrical Grid, 2010).

In this study, we will consider an EV with a 60 kWh battery, a one-hour fast charging process, and a Terra 54HV UL charging station. This charging station has an approximate price of EUR £25,500, which, as of May 20, is equivalent to MXN \$538,535.58.

We calculate the charging power for the autonomous system taking into account the input data requested by the charging station, obtaining Table 3 showing the power factor data and the nominal input power from the corresponding data sheet.

Electrical Specifications	Terra 54HV
Maximum output power	50 kW continuous
AC input voltage	480Y/ 277 VAC+/- 10% (60 Hz)
AC input connection	3 fases: L1, L2, L3, GND (no neutral)
Nominal input current and nominal input power	64 A, 54 kVA
Recommended upstream breakers	A
Power Factor	>0.96
THD	Comp. IEEE 519; 5%
Short circuit rating	65 kA; 10 kA optional
DC output voltage	CCS-1: 200-920 VDC
DC output current	125 A
Efficiency	95%

Table 1 Electrical Specifications of Terra54HV Charging Station, ABB

Source of reference: (Terra 54HVL UL , 2021) $P = 54000 VA \times 0.96 = 51,840 VA$

We obtain that the charging station requires 51.84 kW of power in one hour.

Sizing of Autonomous System

To continue with the sizing, we will consider that, in a day, two electric cars will be charged with a single charging station. Therefore, the consumption hours are set at 2h. The energy required by the batteries is:

$$\text{Required Energy} = \sum \text{Power of charges} * \text{consumption hours} = 51.84 \text{ kW} \times 2\text{h} = 103.68 \text{ kWh}$$

From this, we size the batteries. First, we size the discharge:

$$\text{Ah Batteries} = \frac{103,680 \text{ Wh}}{48\text{V} \times 0.5 \times 0.77} = 5610.38 \text{ Ah}$$

Specifications	
Brand	Rolls
Modelo	2 OS 33P
Medidas	0.392m×0.211m×0.63m
Area	0.0694m ²
Battery Type	Deep cycle, flooded
Cost per Unit	MXN \$17,451.15 USD \$876
Total Required Batteries	72
Required Area	4.9968 m ²
Total Cost	MXN \$1,256,482.8 USD \$63,072
Life Cycles vs. Charge Deepness	4000 life cycles = 50% discharge




Table 4 Specifications of Rolls battery, 2 OS 33 P
Sources of reference: (Rolls, 2022)

To supply sufficient voltage and amperage with this Battery Types, we obtain the scheme shown in Figure 4.

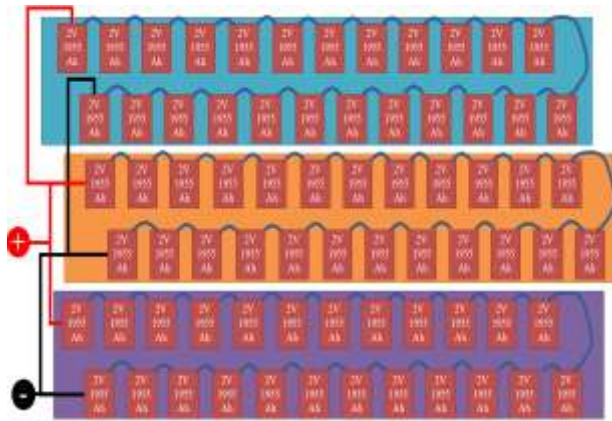


Figure 4 2V battery scheme to reach 48V and 5610 Ah

This scheme includes:

- 24 batteries connected in series = 48 V/1955 Ah
- 3 parallels = 48V/5865 Ah

The battery charging is calculated as follows:

$$Charge = 48V \times 0.5 \times 1955 Ah = 46920 Wh$$

We continue with the sizing of the controller, first calculating the necessary supply that the controller must support, at a minimum, considering the peak solar hours in the area:

$$Supply = \frac{1955 Ah \times 0.5}{5 h} = 195.5 A$$

Taking into account the supply parameter, we look for an MPPT regulator/controller that exceeds this current. Since it is such a large amperage, we will connect multiple controllers in parallel to support the required amount. The chosen model from the market is shown in Table 5.

Specifications	
Brand	VICTRON
Model	Regulador SmartSolar MPPT RS 450V 200A Victron
Dimensions	0.487m×0.434m×0.146m
Battery Voltage	48V
Maximum input voltaje	450V
Maximum charging current	200 ^a
Number of units required	2
Cost per Unit	MXN \$43,958.26 EUR £2,085.96
Total Cost	MXN \$87,916.52 EUR £4171.92




Table 5 Specifications of the SmartSolar MPPT RS 450V 200A Victron regulator
Source of reference: (VICTRON, 2019)

$$P_{controller\ allowed} = Battery\ bank\ voltage \times Controller\ amperage$$

$$P_{controller\ allowed} = 48V \times 400A = 19200W$$

Next, we will size the photovoltaic modules and their arrangement. First, we need to know the energy generation required by the system:

$$Generation\ req = Battery\ bank\ voltage \times Supply$$

$$Generation\ req = 48V \times 195.5A = 9384W$$

Parameters for the modules:

- 9384W < P_{máx} < 19200W
- 195.5A < I_{sc} < 400A
- 48V < V_{Pmáx} < 450V

Considering the above parameters, the selected model with specifications is described in Table 6.

Specifications	
Brand	CanadianSolar
Module	HiKU7, CS7N-670MS
Type	Monocrystalino
Efficiency	21.6%
Maximum Rated Power (Pmax)	670 W
Maximum rated voltage (Vmp)	38.7 V
Maximum rated power current (Imp)	17.32 A
Open Circuit voltage (VOC)	45.8 V
Short-circuit current (ISC)	18.44 A
# modules required	15
Dimensions	2.384m×1.303m×0.035m
Required Area	3.106 m ²
Price per unit	MXN \$4,272.48 USD \$214.5
Total	MXN \$64,087.2 USD \$3,217.5



$$\text{Module current to batteries} = \frac{P_{\text{m\acute{a}x}}}{V_{\text{bat}}} = \frac{10,050W}{48V} = 209.37A$$

Figure 5 shows the installation scheme, including the connection of the battery scheme, along with the controllers and the specified photovoltaic array.

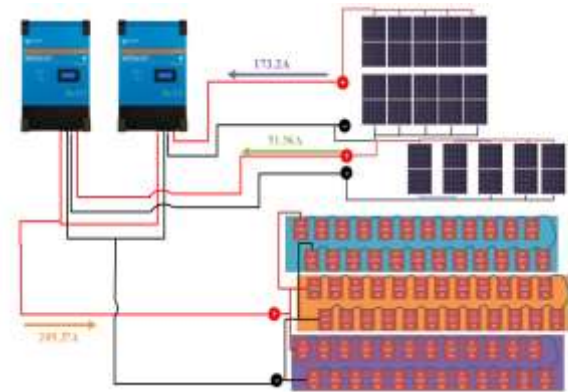


Figure 5 Autonomous Photovoltaic System Scheme, including photovoltaic array, controllers, and battery scheme

Before continuing with the sizing of the inverter and system wiring, we must consider that temperatures and irradiance in the area can change the output values of the panels, so we must consider the changes in the characteristic curve and the output values that this implies.

Table 6 Specifications of the HiKU7, CS7N-670MS solar panel

Source of reference: (CanadianSolar, 2022)

An arrangement in parallel and one in series must be made to cover the energy, voltage, and amperage demands of the system:

- 13 parallels:
- 10 parallels: $I_{\text{m\acute{a}x,mod}} = 10 \times 18.55A = 185.5 A$
- 3 parallels: $I_{\text{m\acute{a}x,mod}} = 3 \times 18.55A = 55.65 A$
- Suma: 241.15 A
- 3 strings/serie: $V_{\text{m\acute{a}x,mod}} = 3 \times 45.8V = 137.4 V$
- Power of 15 panels: $P_{\text{m\acute{a}x}} = 670W \times 15 = 10,050 W$

The amperage that the module provides to the batteries is:

Consulting NOM-001-SEDE-2018, Chapter 6, we obtain the following correction values for voltages, according to the extreme temperature data obtained earlier:

- $-4^{\circ}C=1.12$
- $44^{\circ}C=0.8120$

The tables from which these factors were extracted are shown in Figure 7.

Figure 7 Tables of correction factors for voltages, indicating the obtained values
Source of reference: (NOM-001-SEDE-2018)

NOM-001-SEDE-2018, Chapter 6, Article 690, Section 8, Subsection a, indicates:

"For currents of the photovoltaic source circuit: The maximum current must be calculated by one of the following methods (NOM-001-SEDE-2018):

1. The sum of the short-circuit current of the modules in parallel, multiplied by 125 percent.
2. For photovoltaic systems with a generation capacity of 100 kW or more, a documented photovoltaic system design using a standard industry method and developed by an electrical engineer will be allowed. The calculation of the maximum current value will be based on the average of three hours of the highest current resulting from the simulation of local irradiation of a photovoltaic array, taking into account orientation and elevation."

We then obtain:

- $V_{max} = V_{OC} \times Correction\ Factor = 45.8V \times 1.12 = 51.296V$
- $V_{min} = V_{mp} \times Correction\ Factor = 38.7V \times 0.8120 = 31.42V$
- $I_{max} = I_{SC} \times 1.25 = 18.55 \times 1.25 = 23.18A$

These corrections result in a correction of the original I-V curve of the module, obtaining a graph similar to the one presented in Figure 8, where we see the possible voltage and current surpluses, as well as the possible voltage decrease at high temperatures.

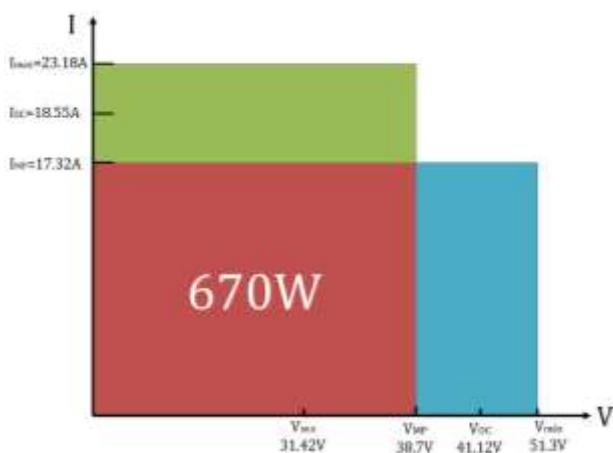


Figure 8 Modified I-V curve with temperature and safety factors for voltage and current, respectively

Finally, the photovoltaic system supplies the following amount of Ampere-hours per day, and we can determine if it satisfies the demand of the batteries.

$$Ah\ per\ day = Current_{controller} \times PSH = 222.5A \times 5 = 1112.5\ Ah$$

$$V_{bat} \times Ah\ per\ day = 48V \times 1112.5Ah = 53400Wh$$

$$53400Wh > 46920Wh$$

Continuing, we obtain the current that the controller would be supplying to the batteries to recharge them. This data will help us size the cables.

$$Current_{controller} = \frac{Photovoltaic\ poer}{Battery\ bank\ voltage} = \frac{10,050\ W}{48\ V} = 209.375\ A$$

The next part of the sizing is the direct current to alternating current inverter since the charging station is designed with AC power.

First, we need to know the maximum Ah that the controller will be able to supply to the inverter:

$$Inverter\ Ah = Controller\ amperage \times HSP = 400A \times 5h = 2000Ah$$

The next part of the sizing is the direct current to alternating current inverter since the charging station is designed with AC power.

First, we need to know the maximum Ah that the controller will be able to supply to the inverter:

$$P_{inverter} = \sum Equipment\ Power * 1.56 = 51,840 \times 1.56 = 80,870W$$

Specifications	
Brand	Growatt
Model	MAX 80KTL3-LV
Dimensions	0.86m×0.6m×0.3m
Input	104,000 W/1100V
Output	80,000W/400V trifásico
Frequency	50Hz/60Hz
Cost	MXN \$96,811.48 EUR £4,584.17




Table 7 Specifications inverter Growatt, MAX 80KTL3-LV

Source of reference: (Growatt, 2018)

We calculate the current demand of the inverter with:

$$Demand = \frac{Max.inverter\ power}{V_{bat.}} = \frac{104,000W}{48V} = 2166.67A$$

The current that the inverter can demand, once the load is applied, is covered by the maximum values of the inverter. Now, we will analyze the best wiring for this installation. The required ampacity of the conductors, with respect to the photovoltaic modules used, is obtained by multiplying the short-circuit current of all modules in parallel by a safety factor of 125% squared. Additionally, two additional factors are considered to modify the required ampacity and, therefore, will change the required gauge in our installation.

These factors are correction within the conduit/channeling (if there are more than two cables in the conduit, there will be losses) and the temperature factor since the wiring is made of a conductor that the ambient temperature can affect. Then we get the following equation:

$$Adjusted\ required\ ampacity = \frac{\sum I_{sc-Parallel} \times 1.25^2}{F_T \times F_C}$$

The piping for the wiring must be separated from the ground by 10cm, and according to NOM-001-SEDE-2018, Table 310-15(b)(3)(c), shown in Figure 9, "Adjustments to ambient temperature for circular conduits exposed to sunlight," we add 17°C to the maximum temperature of the area to then find the temperature adjustment factor.

Distancia por encima del techo hasta la base del tubo conduit milímetros	Sumador de temperatura °C
De 0 hasta 13	33
Más de 13 hasta 90	22
Más de 90 hasta 300	17
Más de 300 hasta 900	14

Figure 9 Table of adjustments to ambient temperature for circular conduits exposed to sunlight on or above roofs
Source of reference: (NOM-001-SEDE-2018)

$$Total\ Temperature = 44°C + 17°C = 61°C$$

With this data, we consult NOM-001-SEDE-2018, Table 310-15(b) (2)(a), "Correction Factors," based on an ambient temperature of 30°C," shown in Figure 10.

Para temperaturas ambiente distintas de 30 °C, multiplique las anteriores capacidades permitidas por el factor correspondiente de los que se indican a continuación:

Temperatura ambiente (°C)	Rango de temperatura del conductor		
	60 °C	75 °C	90 °C
10 o menos	1.29	1.20	1.10
11-15	1.22	1.15	1.12
16-20	1.15	1.11	1.08
21-25	1.08	1.05	1.04
26-30	1.00	1.00	1.00
31-35	0.91	0.94	0.90
36-40	0.82	0.88	0.91
41-45	0.71	0.82	0.87
46-50	0.58	0.75	0.82
51-55	0.41	0.67	0.76
56-60	-	0.58	0.71
61-65	-	0.47	0.60

Figure 10 Correction factors based on an ambient temperature of 30°C
Source of reference: (NOM-001-SEDE-2018)

We obtain that the value of the first Correction Factor is 0.47. Additionally, we will consider that, in the system, each conduit will have a maximum of 2 cables (positive and negative), along with the ground cable. This results in the Conduit Correction Factor as 1. So, with this data, we can obtain the value of the adjusted required ampacity and, consequently, determine the gauge of the cable required.

$$Adjusted\ required\ ampacity = \frac{241.5A \times 1.25^2}{0.47 \times 1} = 801.7A$$

Based on NOM, specifically on Table 310-15(b)(17), "Permissible ampacities of individual insulated conductors for voltages up to and including 2000 volts outdoors based on an ambient temperature of 30°C," shown in Figure 11, we choose an AWG800 gauge to support the required ampacity.

Temperatura ambiente (°C)	Rango de temperatura del conductor					
	60 °C	75 °C	90 °C	105 °C	120 °C	135 °C
10 o menos	1.29	1.20	1.10	1.00	0.90	0.80
11-15	1.22	1.15	1.12	1.05	0.95	0.85
16-20	1.15	1.11	1.08	1.02	0.92	0.82
21-25	1.08	1.05	1.04	0.98	0.88	0.78
26-30	1.00	1.00	1.00	0.95	0.85	0.75
31-35	0.91	0.94	0.90	0.85	0.75	0.65
36-40	0.82	0.88	0.91	0.82	0.72	0.62
41-45	0.71	0.82	0.87	0.75	0.65	0.55
46-50	0.58	0.75	0.82	0.68	0.58	0.48
51-55	0.41	0.67	0.76	0.58	0.48	0.38
56-60	-	0.58	0.71	0.48	0.38	0.28
61-65	-	0.47	0.60	0.38	0.28	0.18

Figure 11 Permissible ampacities of individual insulated conductors for voltages up to and including 2000 volts outdoors based on an ambient temperature of 30°C
Source of reference: (NOM-001-SEDE-2018)

The resistivity of the AWG 800 cable is 0.0377 Ω/km (NOM-001-SEDE-2018), so to determine if this gauge is sufficient for the load and distance, we use the following formula:

$$e_T = \frac{2 \times distance \times I_{MP}}{V_{MP}} \times R$$

Assuming 50 m of wiring, we get:

$$e_T = \frac{2 \times 0.05 \text{ km} \times 17.32 \text{ A}}{39.7 \text{ V}} \times 0.0377 \frac{\Omega}{\text{km}} = 1.64 \times 10^{-4}$$

$$e_T = 0.164\% < 3\%$$

The voltage drop is less than 3%, so the gauge is suitable for the intended distance, as well as for the voltage and ampacity it needs to transmit.

Specifications	
Brand	RNEDA
Gauge	800AWG
Required quantity	50m
Price per meter	MXN \$500
Total	MXN \$25,000



Table 8 Specifications, cable 800AWG

Source of reference: (RNEDA, 2019)

For the sizing of the thermal-magnetic switch, we must take into account the current that the inverter will be supplying at its output, and, therefore, to the charging station.

$$\frac{P_{inverter}}{V_{bat}} = \frac{80,870 \text{ W}}{48 \text{ V}} = 1684.8 \text{ A c}$$

In the market, we look for a thermal-magnetic switch that fits this parameter or exceeds it.

Specifications	
Brand	PowerPact
Model	PowerTag RLF36250U44A
Capacity	600V 2500 ^a
Price	MXN \$58,000




Table 9 Specifications of the PowerPact thermal-magnetic switch

Source of reference: (PowerPact, 2020)

Finally, we reach the sizing of connectors. MC4 connectors will be used, as they comply with article 690-33 of NOM-001-SEDE-2018, Plugs and connectors. MC4 connectors are the most commonly used in the market; the quantity of connectors depends on the number of panels to connect.

Specifications	
Brand	Autosolar
Precio per pair	MXN \$124.05
Required Pairs	15 pares (30 conectores en total)
Total Price	MXN \$1860.75



Table 10 Specifications of MC4 connectors

Source of reference: (Autosolar, 2022)

Finally, the total costs of each element, as well as the complete installation, are shown in Table 11.

	Costs
Charging Station	\$ 538,535.58
Batteries	\$ 1,256,482.80
Controller	\$ 87,916.52
Modules	\$ 64,087.20
Inverter	\$ 96,811.48
Wiring	\$ 25,000.00
Switch	\$ 58,000.00
Connectors	\$ 1,860.75
Total	\$ 2,128,694.33
Total + Labor (10%)	\$ 2,341,563.76

Table 11 Costs of the installation of an autonomous photovoltaic system for a fast charging station

The final installation scheme is shown in Figure 3.3.15, already showing the connections of the battery system with the controllers and the inverter, as well as the power supply from the solar panel systems to the controllers. We also observe how the inverter is connected to the load, in this case, the Terra 54HV UL charging station, and is protected by the thermal-magnetic switch.

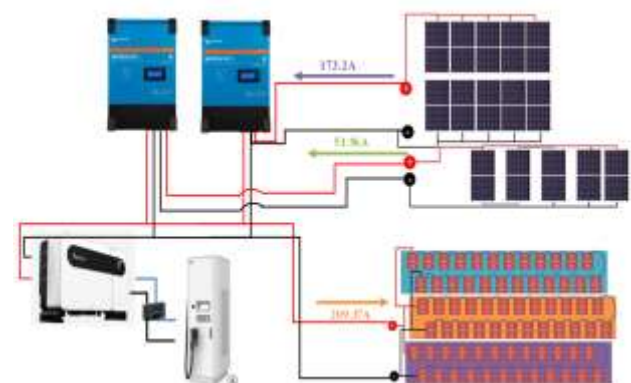


Figure 12 Final scheme of autonomous photovoltaic system installation

Return on Investment, Autonomous System

The return on investment is an economic analysis to determine if the necessary investment for the autonomous system can be recovered or if, on the contrary, it would be just a luxury and a lost investment. This return on investment can be calculated assuming that we will sell the energy at the local marginal price established by CENACE. We must remember that the local marginal price varies according to demand and the time of day, so we obtained an average of the daily consumption of the corresponding node to Torreón, Coahuila, in April 2022. First, we obtained the Node key, being 05TRR-115, as shown in Figure 13.

Figure 13 Screenshot of the document “Catálogo NodosP Sistema Eléctrico v2022”

Source of Reference: (CENACE, 2020)

With the node key, values of the local marginal price (PML) for the node and each hour of the day from April 16 to April 30, 2022, were extracted from the document "PrecioMargLocales SIN MTR Abr02 v2022," also obtained from CENACE. Using these data, the graph shown in Figure 14 was generated.

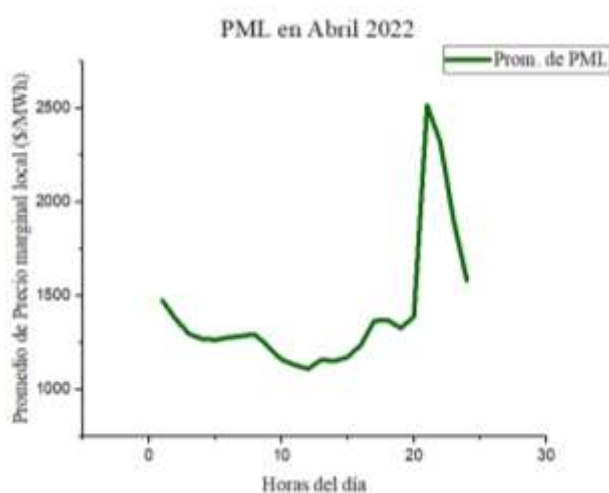


Figure 14 Average Local Marginal Price for node 05TRR-115, from April 16 to 30, 2022

Reference Source: (CENACE, 2020)

From these data, we find that the daily average PML is MXN\$1403/MWh. This value will be used to calculate the return on investment.

For the calculation, let's consider that the fast charging of a single electric vehicle (EV) is approximately 52 kWh, which is equivalent to 0.052 MWh. Thus, the potential profit for each EV fast charge would be:

$$1403 \frac{\text{MXN}\$}{\text{MWh}} \times 0.052 \text{ MWh} = \text{MXN}\$72.9 \approx \text{MXN}\$73$$

If we consider the most optimistic scenario of 2 charges per day, we obtain a daily income of MXN\$146. If we extrapolate this income over 365 days to calculate the annual revenue, we get:

$$\text{MXN}\$146 \times 365 \text{ days} = \text{MXN}\$53,290/\text{year}$$

Therefore, for the return on investment, we will calculate how many years it will take to recover the initial investment:

$$\frac{\text{MXN}\$ 2,341,563.76}{\text{MXN}\$53,290/\text{year}} \approx 44 \text{ years}$$

In the most optimistic scenario, it would take us approximately 44 years to recover the initial investment, without taking into account the maintenance that the installation would require. Furthermore, this timeframe significantly exceeds the lifespan of batteries (estimated at 13 years in good conditions) and the useful life of photovoltaic modules and the inverter (around 25 years) (L. Santiago, 2018).

Acknowledgements

We express our deep gratitude to the Instituto Tecnológico de la Laguna for their invaluable support in providing us with their facilities, enabling the effective conduct of our research and writing.

Financing

This work has been funded by CONACYT [CVU 1271712].

Conclusions

In this study, an energy and economic sizing was carried out for the case of a standalone photovoltaic system in the locality of Torreón, Coahuila, Mexico. The main objective of the work was achieved: theoretically, it was determined that it is possible to install a fast-charging station powered by photovoltaic energy in the region.

However, it would not be a financially viable project in any aspect, as the lifespan of the components is much shorter than the time needed to cover the initial installation expenses of the system. Consequently, it is concluded that, if this project were to be implemented, the initial investment would never be recovered.

References

- A. Orús, Evolución anual del número total de matriculaciones de vehículos eléctricos en España entre 2013 y 2021, 1(2022)
- ABB, Terra 54HVL UL, Datasheet, 1(2021), 1-2
- Autosolar, Conectores MC4, Datasheet, 1(2022), 1
- C. Á. Macías, Tema 1-Principios de Solarimetría, Aplicaciones de Sistemas Fotovoltaicos, 1(2022), 11-29, 40-51
- C. Á. Macías, Tema 4-Elementos de sistemas autónomos, Aplicaciones de Sistemas Fotovoltaicos, 1(2022), 19
- CanadianSolar, HiKU7, CS7N-670MS, Datasheet, 1(2022), 1-2
- CENACE, Precios Marginales Locales Mes Abril, Precios de Energía y Servicios Conexos MTR, 2(2022)
- CONAGUA, Normales Climatológicas, Servicio Meteorológico Nacional, 1(1981-2010)
- D. Azura, Hay autos eléctricos, pero cero enchufes: el dilema del sector automotriz en México, El Financiero, 1(2022)
- F. Nuno, El vehículo eléctrico y su interacción con la red eléctrica, 1(2010)
- Growatt, Inversor MAX 80KTL3-LV, Datasheet, 1(2018), 1
- I. Mendoza, Puntos de recarga rápida en España para coches eléctricos: dónde están y qué precio ofrecen, Motorpassion, 1(2022)
- I. Rodríguez, Electrolíneas: el gran negocio que se frenó por la contrarreforma eléctrica, Expansión, 1(2021)
- J. Larminie, J. Lowry, Electric Vehicle Technology Explained, 2(2012), 19-25, 59-63, 79-85
- J. Montoya Sánchez de Pablo, M. Miravalles López, A. Bret, The Electrical Model, How Green are Electric or Hydrogen-Powered Cars?, 1(2016), 55-65
- K. Chamberlain, Charging Stations, Ultimate Guide for Electric Cars, 2(2020), 38-43
- L. Santiago Azuara Grande, I. Yahyaoui, S. Arnaltes Gómez, Energetic, economic and environmental viability of off-grid PV-BESS for charging electric vehicles: Case Study of Spain, 1(2018), 5-10
- NASA, 20-year Meteorological and Solar Monthly & Annual Climatologies, Data Access Viewer, 1(2001-2020)
- NOM-001-SEDE-2018, Capítulo 6 Equipos Especiales, Artículo 690 SISTEMAS SOLARES FOTOVOLTAICOS, pg 825-841.
- O. Style, Un sistema fotovoltaico autónomo, Energía Solar Autónoma, 1(2012), 2-56
- Porsche, Charging high-voltage battery, Driver's Manual Taycan, 1(2020), 79-86
- PowerPact, PowerTag, R 100KA 3P 600V 2500A, RLF36250U44A, Datasheet, 1(2020), 1
- RNEDA, Cable 800AWG RNEDA, Datasheet, 1(2019), 1
- Rolls, 2 OS 33 P, Datasheet, 1(2022), 1
- SENER, Consumo final de energía por sector, Balance Nacional de Energía, (2020)
- VICTRON, MPPT RS 450V 200A, Datasheet, 1(2019), 1-2
- Weather Spark, Nubes, Energía Solar, El clima y el tiempo promedio en todo el año en Torreón, México, 1(2021)

Simulation model in ProModel to generate proposals for improving the H₂O purification process

Modelo de simulación en ProModel para generar propuestas de mejora del proceso de purificación de H₂O

RUIZ-DIAZ, Montserrat^{†*}, SOTO-LEYVA, Yasmin, BONES-MARTÍNEZ, Rosalía, and SANTOS-OSORIO, Arturo

Tecnológico Nacional de México / Instituto Tecnológico Superior de Huauchinango

ID 1st Author: *Montserrat, Ruiz-Diaz* / ORC ID: 0009-0008-3146-6213, CVU CONAHCYT ID: IT23B214

ID 1st Co-author: *Yasmin, Soto-Leyva* / ORC ID: 0000-0003-2652-7065, CVU CONAHCYT ID: 951464

ID 2nd Co-author: *Rosalía, Bones-Martínez* / ORC ID: 0000-0001-8829-9737, CVU CONAHCYT ID: 368744

ID 3rd Co-author: *Arturo, Santos-Osorio* / ORC ID: 0000-0003-3643-5770, CVU CONAHCYT ID: 951024

DOI: 10.35429/JIE.2023.19.7.53.59

Received September 25, 2023; Accepted December 30, 2023

Abstract

For purification companies, the optimization of H₂O purification processes is of utmost importance because it contributes to the good flow and development of internal operations to satisfy the needs of customers who purchase the vital purified liquid. These organizations take into account that production lines must be used at their maximum capacity, which is why it is necessary to detect the main problems that cause bottlenecks, which generate delays and interruptions in the production cycle. Now, in the purifiers located in the region of Nuevo Necaxa, Puebla, the existence of this type of interruptions has been detected, for which a solution methodology was generated that includes the following phases: 1) Field investigation, 2) Establishment of operational times, 3) Representative layout development in ProModel, 4) Simulation model of the water purification production system, these phases evaluated the compliance of the transformation cycle with the programmed times, detecting the bottlenecks that delay the process, with the main objective of weighting and propose a solution that helps improve and optimize the production of the current management system in purifiers, based on statistical results provided by the ProModel software.

Resumen

Para las empresas purificadoras la optimización de los procesos de purificación del H₂O, es de suma importancia porque aporta al buen flujo y desarrollo de las operaciones internas para satisfacer las necesidades de los clientes que adquieran el vital líquido purificado. Estas organizaciones tienen en cuenta que las líneas de producción deben ser utilizadas en su máxima capacidad, por lo cual resulta necesario detectar las problemáticas principales que ocasionan los cuellos de botellas, mismos que generan atrasos e interrupciones en el ciclo productivo. Ahora bien en las purificadoras ubicadas en la región de Nuevo Necaxa, Puebla se ha detectado la existencia de este tipo de interrupciones, por lo cual se generó una metodología de solución que incluye las siguientes fases: 1) Investigación de campo, 2) Establecimiento de tiempos operativos, 3) Desarrollo de layout representativo en ProModel, 4) Modelo de simulación del sistema de producción de purificadoras de agua, estas fases evaluaron el cumplimiento del ciclo de transformación con los tiempos programados, detectando los cuellos de botella que atrasan el proceso, teniendo como objetivo principal ponderar y plantear una solución que ayude a la mejora y optimización de la producción del sistema de gestión actual en las purificadoras, basándose en resultados estadísticos que proporcione el software de ProModel.

H₂O Purification, Optimization, ProModel Software

Purificación de H₂O, Optimización, Software ProModel

Citation: RUIZ-DIAZ, Montserrat, SOTO-LEYVA, Yasmin, BONES-MARTÍNEZ, Rosalía, and SANTOS-OSORIO, Arturo. Simulation model in ProModel to generate proposals for improving the H₂O purification process. Journal Industrial Engineering, 2023. 7-19: 53-59

* Author's Correspondence (e-mail: montserrat.rd@huauchinango.tecnm.mx)

† Researcher contributing as first author.

Introduction

The water purifiers geographically located in Nuevo Necaxa Puebla supply the vital liquid to a total of 10,213 inhabitants, approximately 2,500 families in the municipal capital. 95% of these purifying companies are dedicated to the proper treatment of water, and 5% only to its distribution and commercialization. However, to ingest this vital liquid, in the experience of Venegas, Tello, Cepeda and Molina (2023), a purification process is required through which bacteria or microorganisms that harm health are completely eliminated. of consumers, taking into account customer satisfaction, quality, effectiveness and efficiency in each of its processes as a priority (Loor, Wilson, Zambrano and Mosquera, 2020).

To comply with each of the variables before mentioned, it is necessary to quantitatively measure the production process, to subsequently detect the sources of origin that cause delays or bottlenecks and implement feasible solutions that resolve the problems or delays of the process or service (Huancas, 2022).

There are various tools that provide viable solutions to the problem described, among which the use of simulation software stands out, being the ProModel software which from the point of view of Dunna, Reyes and Barrón (2006) manages a friendly interface., easily adaptable and specialized to carry out various simulations of transformation, marketing or distribution processes, this technological software is characterized by:

1. Estimate the precise times of the operational/administrative tasks or activities to be carried out (Marmolejo and Marín, 2013).
2. Analyze work days of 8-12-24 hours considering the production levels in each modality.
3. Development of statistical graphs, to generate improvements in the following areas (González y Vivas, 2014):
 - Reduce the specific origin of economic risks.
 - Reduce delays in order deliveries.

- Calculate the level of impact due to mishaps or bottlenecks that directly affect operation.

Once the benefits of simulating with ProModel were analyzed, it was decided to start an effective simulation process for the H₂O water purification cycle, seeking to detect areas for improvement and the elimination or reduction of the sources that generate the main problems. or bottlenecks, taking into account the following two quantitative variables:

1. The effectiveness of each Workstation.
2. The efficiency of the operational staff, finally a proposal is presented that provides a solution to the detected disadvantage, verifying that the Timely and appropriate use of simulation models contributes to organizational success and the generation of business profits.

General objective

Optimize the water purification process of regional companies through the development of a simulation model in ProModel software to identify bottlenecks or delays in the production process and provide a solution proposal that eliminates/reduces the sources that cause them. the problem.

Specific objectives

1. Identify improvements within the production process management system.
2. Obtain statistical results of the activities carried out within the purifier for subsequent decision making.
3. Apply various tools for process analysis.
4. Eliminate/reduce setbacks, delays and bottlenecks that arise within the purifiers.

Methodology to be developed

The primary objective of the H₂O purifiers is to efficiently and effectively supply the community of Nuevo Necaxa as well as the communities and neighborhoods that are around it and within the area of influence; always seeking continuous improvement in all those activities and systems that intervene within it, such as the supply chain processes and the production process, which intervene directly in the water purification cycle (Córdor, 2013). Now, the present application is carried out through the methodological development of the following four phases (Figure 1 Applied methodology):

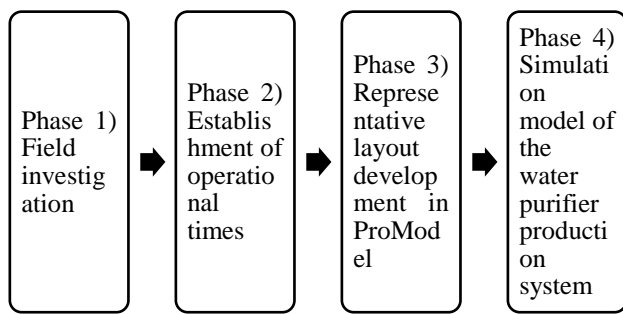


Figure 1 Applied methodology
Source: Own elaboration

Each of the phases mentioned above are described below:

Phase 1) Field investigation:

The previous visit to the purifiers was carried out to observe the operations carried out within these transformation companies, and quantify the stations and/or machines that are used, to identify the monitoring of the entire process that involves purification and processing, water packaging, the result of this first phase, allowed establishing the sequence of standard activities necessary for 100% compliance with the purification process (Figure 2 General Flow Diagram of the purification companies in the area and area of influence).

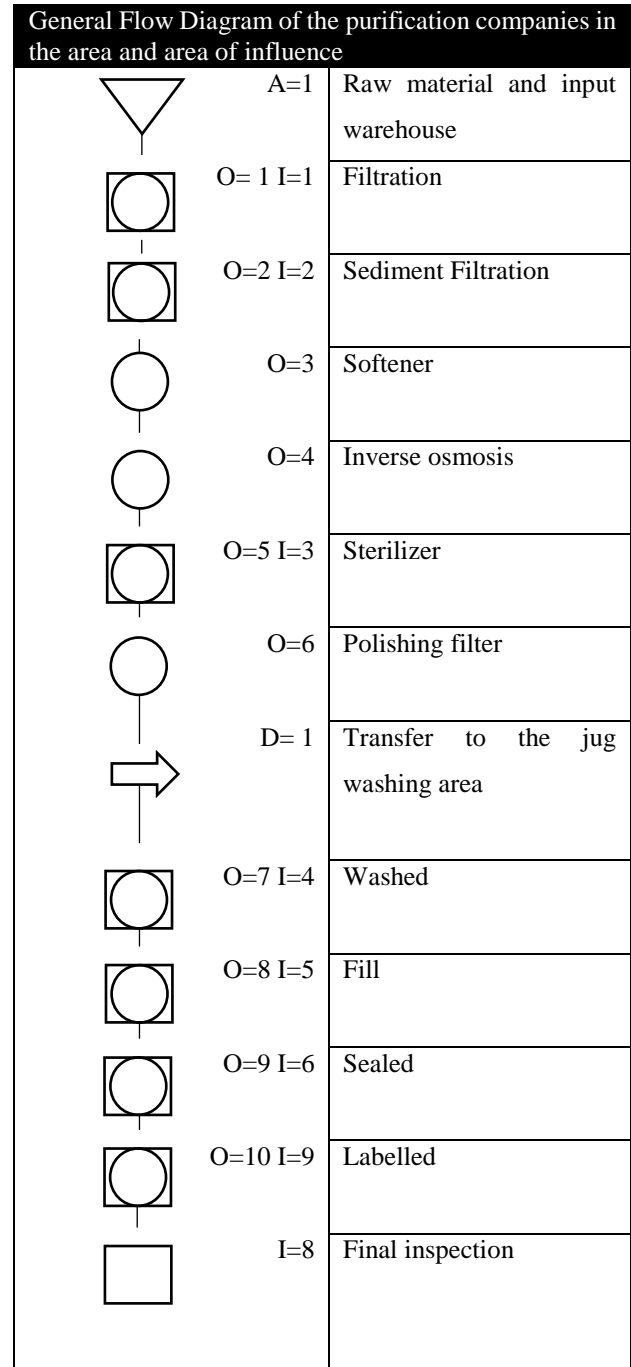


Figure 2 General Flow Diagram of the purification companies in the area and area of influence. **O=Operation I=Inspection D= Movement A=Warehouse
Source: Own Elaboration

Phase 2) Establishment of operational times:

Once they were established each and every operation _ necessary, they proceeded to analyze the water purification process to declare the times suitable for each operation, these times per activity are indicated below (Table 1 Operating times of the H₂O purification process):

Operating times of the H ₂ O purification process		
No.	Operational activity	Cycle time
1	Raw material and input warehouse	2 min
2	Filtration	2 min
3	Sediment Filtration	2 min
4	Softener	2 min
5	Inverse osmosis	3 min
6	Sterilizer	3 min
7	Polishing filter	2.5 min
8	Transfer to the jug washing area	1 min
9	Washed	4.5 min
10	Fill	1 min
11	Sealed	2 min
12	Labelled	4 min
13	Final inspection	1 min

Table 1 Operating times of the H₂O purification process
Source: Own Elaboration

Phase 3) Representative layout development in ProModel

In the development of this third phase, the representative layout of the production process was created in the ProModel software (Figure 3 Layout of the standard purifier process), taking into account that the recognition of these activities occurred in previous stages. mention that purification companies currently work a single workday of 8 hours for 7 days of work, therefore, in the simulation run, the 56 total hours covered must be met to obtain the weekly simulation.



Figure 3 Layout of the standard purifier process
*** Prepared in ProModel software*
Source: Own Elaboration

Phase 4) Simulation model of the water purifier production system:

Once the times already established in the ProModel software were programmed, the first run was carried out, starting at 00:00:00 hours. until the necessary 56:00:00 hours, going through each work day (Figure 4 Simulation run 14:00:00 hours).



Figure 4 Simulation run 14:00:00 hours
***Developed in ProModel software*
Source: Own Elaboration

Results

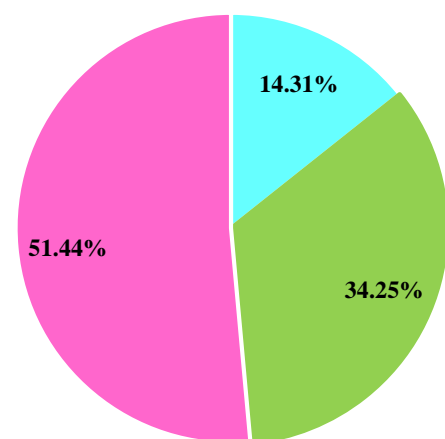
The results obtained from the simulation in the ProModel software are expressed through a series of descriptive statistics, which are explained below:

Result A) Movement logic-Entity locked (Figure 5 Movement logic-Entity locked):

1. Movement logic: The registration of movements is 14.31%, that is, the entity has a total working day of 8 hours, of which 1 hour and 9 minutes is the time in which the jug is in transfer or movement within the cycle. productive.
2. Blocked entity: It is observed that there is a problem, in which it is evident that the production process is unemployed for 51.44% of the working day and only flows for 48.56%, that is, it is flowing for 34.25% and a 14.31% in motion, detecting the existence of a bottleneck that blocks the passage of the entity (water jug) causing downtime in the production cycle, to solve this problem it is suggested to implement a balancing of lines to make the most of the resources human, material and economic that are invested every working day.

Entity States- Carboy

■ % In Movement Logic ■ % In Operation ■ % Locked



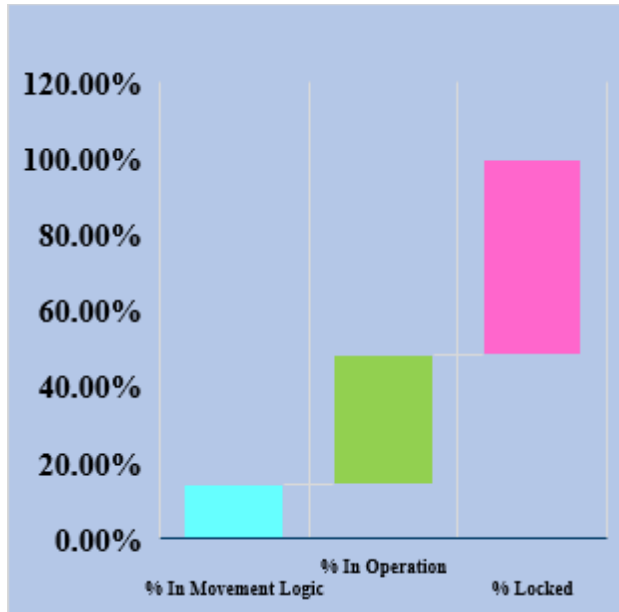


Figure 5 Movement logic-Entity locked
**Prepared in ProModel software
Source: Own elaboration

Result B) Process indicators: The production cycle of the H₂O purification process once the simulation run was carried out records a total time of 3.11 minutes for each full jug, taking into account that the simulation of the process is program for 7 days with a working day of 8 hours a day, the filling of a total of 16,986 weekly is expected, with a record of 2,426.57≈2427 pieces per day, or 303.375≈304 jugs in one hour as required for the production line (Figure 6 Weekly production requirement).

Scoreboard		
Name	Total Outputs	Average Sistem Time (min)
Carboy	16,986	3.11

Figure 6 Weekly production requirement
**Developed in ProModel software
Source: Own elaboration

Therefore, the purifiers have a monthly capacity of 72,810 jugs of water equivalent to 1,456,200 liters of purified water monthly.

Result C) Bottlenecks: It is determined that the labeling operational activity is the bottleneck with a saturation % of 49%, while the other operational activities represent a lower level of saturation, it is recommended to analyze the sterilization operations and washing, because once this bottleneck is solved, an assertive solution will be provided to the other bottlenecks, which will arise by eliminating or reducing the main one (Figure 7 Saturation or bottlenecks in the production line).

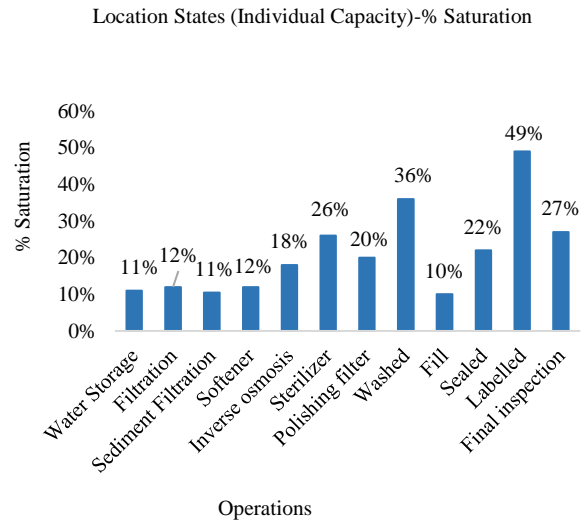


Figure 7 Saturation or bottlenecks on the production line
**Developed in ProModel software
Source: Own elaboration

Result C) Improvement proposal: With 49% of the time that causes delays and bottlenecks, the labeling activity is the one that takes the longest time in the process, which is why the machinery used was analyzed and the corrective maintenance in this area, since the wear of the machinery causes the longest delay time, because the parts that show greater wear do not allow work at higher speeds. Likewise, it is recommended to schedule a monthly preventive maintenance schedule to avoid reprocessing, and stoppages on the production line.

With respect to the operational washing activity, a technique is proposed that consists of the immediate disinfection and use of pressure hoses, because the hoses currently used are handled in slow spray cycles, while for the sterilization area the only improvement possible is to increase the generation of waves without exceeding the limit allowed for the parameters of this process, which indicate a maximum of 253.7 nanometers for the effective disinfection of bacteria, microbes, algae, viruses and biological contaminants that have a propensity to spread rapidly. Although this factor depends directly on the machinery model being handled and the programmable parameters.

Gratitude

To the Higher Technological Institute of Huauchinnago and the Industrial Engineering Division for the facilitations provided for the preparation of this article presented.

Financing

This work has been funded by the ITESHUAU-CA-4 academic body and the Industrial Engineering Division of the Instituto Tecnológico Superior de Huauchinango.

Conclusions

The development of this application allows us to verify the usefulness of ProModel software for the analysis of production systems in real environments. Through the simulation model carried out, the operation of the H₂O purification plants that are located in Nuevo Necaxa Puebla was captured, the optimization of the production process being of vital importance because these transformation companies supply 100% of the population with this vital liquid, taking into account that the standard simulation model developed is and will be very useful for the decision making of these organizations because it will allow the timely detection of the operating stations that generate bottlenecks, which delay the deliveries of orders and cause loss of customers.

It is important to mention that bottlenecks in an H₂O purification system generate significant delays, causing various losses. Specifically, in this application, bottlenecks were detected using the simulation model in the ProModel software, subsequently generating a viable proposal for the solution of the main bottleneck, which exposes a saturation % of 49% and is represented by the operational activity of labeling, in conclusion the use of a standard simulation model provides the process analyst with a means quantitative to assess the efficiency and effectiveness of the operating stations, by calculating the saturation indices and the production requirement scheduled for different working days.

References

Cóndor T, M. E. (2013). Automatización del proceso de llenado de galones de agua en planta purificadora de agua (Bachelor's thesis, QUITO/EPN/2013). Escuela Politecnica Nacional [fecha de Consulta 22 de diciembre de 2023]. Disponible en URL <https://bibdigital.epn.edu.ec/bitstream/15000/6666/1/CD-5062.pdf>

Dunna, E. G., Reyes, H. G., y Barrón, L. E. C. (2006). Simulación y análisis de sistemas con ProModel. Pearson Educación. [fecha de Consulta 21 de diciembre de 2023]. Disponible en URL: https://d1wqtxts1xzle7.cloudfront.net/38953429/simulaci-n-y-an-lisis-de-sistemas-con-promodel_2-libre.pdf?1443678215=&response-content-disposition=inline%3B+filename%3DSimulaci_n_y_an_lisis_de_sistemas_con_pr.pdf&Expires=1703202469&Signature=GDW3tdgKdYzjE5QnOrk6fxVFtVyizs-lnhZb5M3Uh5oqTOLgn2dKcJ5~dtWbDjqTL3-Es~hx0R-e9XDjUD2bVRPV7brkyKVFE~Ec3gv5Ru-yJqGyOIS6cLGLBTT9EGsGD~lRhi1nt5t4ZLj7w6PqNdr5ZqSIxPKSf4OzKzdATv6vu3N374KqAGasIdgwx4SyMG0GzuV0asa5OZWeiukrBddJ7jvy-P-Yena3ZxteQJt5-LugeVPfHVfc08YffiktY7qqrRHEyub5canphlT1oelwxF6OEpOrqPF3plZqJdJofeGE6myqgIiREV9d49zM-6koXVq4Rt7Pk093G-8g__&Key-Pair-Id=APKAJLOHF5GGSLRBV4ZA

González, CD y Vivas, MLT (2014). Comparacion del desempeño de los simuladores arena® y promodel® en un modelo de producción. En Tercera LACCEI Int. Lat. Soy. Caribe. Conf. Ing. Technol (págs. 1-7). Escuela Colombiana de Ingeniería. LACCET'2005 – Information Technology Track. [fecha de Consulta 22 de diciembre de 2023]. Disponible en URL: https://www.laccei.org/LACCEI2005-Cartagena/Papers/IT026_DoncelGonzalez.pdf

Huancas H, C. S. (2022). Propuesta de mejora del procesamiento de granos secos para aumentar la productividad. Universidad Católica Santo Toribio de Mogrovejo. Facultad de Ingeniería Escuela de Ingeniería industrial. [fecha de Consulta 21 de diciembre de 2023]. Disponible en URL: https://tesis.usat.edu.pe/bitstream/20.500.12423/5564/8/TIB_HuancasHuamanCesly.pdf

Loor, E. A. G., Wilson, J. V. C., Zambrano, H. Y. L., & Mosquera, R. A. C. (2020). Plantas purificadoras: Realidad del agua embotellada en Ecuador. *Dominio de las Ciencias*, 6(3), 692-705. Dalnet. [fecha de Consulta 21 de diciembre de 2023]. Disponible en URL: <https://dialnet.unirioja.es/servlet/articulo?codigo=7491411>

Marmolejo, I., y Marín, J. M. (2013). Promodel: Una herramienta alternativa al evaluar el rendimiento de la actividad industrial. *Iberoamerican Journal of Industrial Engineering*, Florianópolis. Universidad Federal de Santa Catarina. [fecha de Consulta 21 de diciembre de 2023]. Disponible en URL: https://www.researchgate.net/profile/Isaias-Simon-Marmolejo/publication/316244025_ProModel_Una_herramienta_alternativa_al_evaluar_el_rendimiento_de_la_actividad_industrial/links/58f76e320f7e9b9a95d5237c/ProModel-Una-herramienta-al-evaluar-el-rendimiento-de-la-actividad-industrial.pdf

Venegas, B., Tello H, M. A., Cepeda C, V., y Molina R, D. (2023). Calidad microbiológica: detección de *Aeromonas* sp y *Pseudomonas* sp en garrafones provenientes de pequeñas plantas purificadoras de agua. *CienciaUAT*, 146-164. DOI: <https://doi.org/10.29059/cienciauat.v17i2.1728> [fecha de Consulta 21 de diciembre de 2023]. Disponible en URL: <https://revistaciencia.uat.edu.mx/index.php/CienciaUAT/article/view/1728/1023>

[Title in Times New Roman and Bold No. 14 in English and Spanish]

Surname (IN UPPERCASE), Name 1st Author†*, Surname (IN UPPERCASE), Name 1st Coauthor, Surname (IN UPPERCASE), Name 2nd Coauthor and Surname (IN UPPERCASE), Name 3rd Coauthor

Institutional Affiliation of Author including Dependency (No.10 Times New Roman and Italic)

International Identification of Science - Technology and Innovation

ID 1st Author: (ORC ID - Researcher ID Thomson, arXiv Author ID - PubMed Author ID - Open ID) and CVU 1st author: (Scholar-PNPC or SNI-CONAHCYT) (No.10 Times New Roman)

ID 1st Coauthor: (ORC ID - Researcher ID Thomson, arXiv Author ID - PubMed Author ID - Open ID) and CVU 1st coauthor: (Scholar or SNI) (No.10 Times New Roman)

ID 2nd Coauthor: (ORC ID - Researcher ID Thomson, arXiv Author ID - PubMed Author ID - Open ID) and CVU 2nd coauthor: (Scholar or SNI) (No.10 Times New Roman)

ID 3rd Coauthor: (ORC ID - Researcher ID Thomson, arXiv Author ID - PubMed Author ID - Open ID) and CVU 3rd coauthor: (Scholar or SNI) (No.10 Times New Roman)

(Report Submission Date: Month, Day, and Year); Accepted (Insert date of Acceptance: Use Only ECORFAN)

Abstract (In English, 150-200 words)

Objectives
Methodology
Contribution

Abstract (In Spanish, 150-200 words)

Objectives
Methodology
Contribution

Keywords (In English)

Indicate 3 keywords in Times New Roman and Bold No. 10

Keywords (In Spanish)

Indicate 3 keywords in Times New Roman and Bold No. 10

Citation: Surname (IN UPPERCASE), Name 1st Author, Surname (IN UPPERCASE), Name 1st Coauthor, Surname (IN UPPERCASE), Name 2nd Coauthor and Surname (IN UPPERCASE), Name 3rd Coauthor. Paper Title. Journal Industrial Engineering, Year 1-1: 1-11 [Times New Roman No.10]

* Correspondence to Author (example@example.org)

† Researcher contributing as first author.

Introduction

Text in Times New Roman No.12, single space.

General explanation of the subject and explain why it is important.

What is your added value with respect to other techniques?

Clearly focus each of its features

Clearly explain the problem to be solved and the central hypothesis.

Explanation of sections Article.

Development of headings and subheadings of the article with subsequent numbers

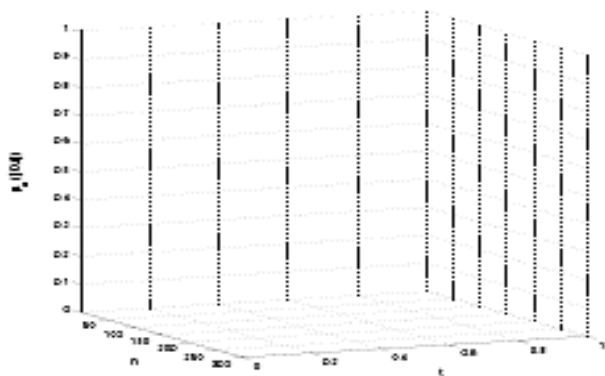
[Title No.12 in Times New Roman, single spaced and bold]

Products in development No.12 Times New Roman, single spaced.

Including graphs, figures and tables-Editable

In the article content any graphic, table and figure should be editable formats that can change size, type and number of letter, for the purposes of edition, these must be high quality, not pixelated and should be noticeable even reducing image scale.

[Indicating the title at the bottom with No.10 and Times New Roman Bold]



Graphic 1 Title and *Source (in italics)*

Should not be images-everything must be editable.

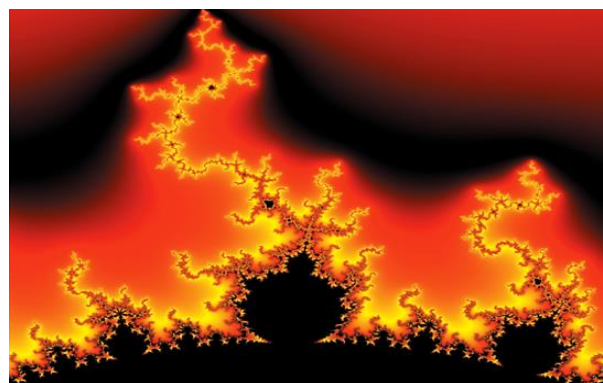


Figure 1 Title and *Source (in italics)*

Should not be images-everything must be editable.

Table 1 Title and *Source (in italics)*

Should not be images-everything must be editable.

Each article shall present separately in **3 folders**:
 a) Figures, b) Charts and c) Tables in .JPG format, indicating the number and sequential Bold Title.

For the use of equations, noted as follows:

$$Y_{ij} = \alpha + \sum_{h=1}^r \beta_h X_{hij} + u_j + e_{ij} \quad (1)$$

Must be editable and number aligned on the right side.

Methodology

Develop give the meaning of the variables in linear writing and important is the comparison of the used criteria.

Results

The results shall be by section of the article.

Annexes

Tables and adequate sources

Thanks

Indicate if they were financed by any institution, University or company.

Conclusions

Explain clearly the results and possibilities of improvement.

- Authentic Signature in blue colour of the Conflict of Interest Format of Author and Co-authors.

References

Use APA system. Should not be numbered, nor with bullets, however if necessary numbering will be because reference or mention is made somewhere in the Article.

Use Roman Alphabet, all references you have used must be in the Roman Alphabet, even if you have quoted an Article, book in any of the official languages of the United Nations (English, French, German, Chinese, Russian, Portuguese, Italian, Spanish, Arabic), you must write the reference in Roman script and not in any of the official languages.

Technical Specifications

Each article must submit your dates into a Word document (.docx):

Journal Name

Article title

Abstract

Keywords

Article sections, for example:

1. *Introduction*
2. *Description of the method*
3. *Analysis from the regression demand curve*
4. *Results*
5. *Thanks*
6. *Conclusions*
7. *References*

Author Name (s)

Email Correspondence to Author

References

Intellectual Property Requirements for editing:

- Authentic Signature in Colour of Originality Format Author and Co-authors.
- Authentic Signature in Colour of the Acceptance Format of Author and Co-authors.

Reservation to Editorial Policy

Journal Industrial Engineering reserves the right to make editorial changes required to adapt the Articles to the Editorial Policy of the Research Journal. Once the Article is accepted in its final version, the Research Journal will send the author the proofs for review. ECORFAN® will only accept the correction of errata and errors or omissions arising from the editing process of the Research Journal, reserving in full the copyrights and content dissemination. No deletions, substitutions or additions that alter the formation of the Article will be accepted.

Code of Ethics - Good Practices and Declaration of Solution to Editorial Conflicts

Declaration of Originality and unpublished character of the Article, of Authors, on the obtaining of data and interpretation of results, Acknowledgments, Conflict of interests, Assignment of rights and Distribution

The ECORFAN-Mexico, S.C Management claims to Authors of Articles that its content must be original, unpublished and of Scientific, Technological and Innovation content to be submitted for evaluation.

The Authors signing the Article must be the same that have contributed to its conception, realization and development, as well as obtaining the data, interpreting the results, drafting and reviewing it. The Corresponding Author of the proposed Article will request the form that follows.

Article title:

- The sending of an Article to Journal Industrial Engineering emanates the commitment of the author not to submit it simultaneously to the consideration of other series publications for it must complement the Format of Originality for its Article, unless it is rejected by the Arbitration Committee, it may be withdrawn.
- None of the data presented in this article has been plagiarized or invented. The original data are clearly distinguished from those already published. And it is known of the test in PLAGSCAN if a level of plagiarism is detected Positive will not proceed to arbitrate.
- References are cited on which the information contained in the Article is based, as well as theories and data from other previously published Articles.
- The authors sign the Format of Authorization for their Article to be disseminated by means that ECORFAN-Mexico, S.C. In its Holding Republic of Peru considers pertinent for disclosure and diffusion of its Article its Rights of Work.
- Consent has been obtained from those who have contributed unpublished data obtained through verbal or written communication, and such communication and Authorship are adequately identified.
- The Author and Co-Authors who sign this work have participated in its planning, design and execution, as well as in the interpretation of the results. They also critically reviewed the paper, approved its final version and agreed with its publication.
- No signature responsible for the work has been omitted and the criteria of Scientific Authorization are satisfied.
- The results of this Article have been interpreted objectively. Any results contrary to the point of view of those who sign are exposed and discussed in the Article.

Copyright and Access

The publication of this Article supposes the transfer of the copyright to ECORFAN-Mexico, SC in its Holding Republic of Peru for its Journal Industrial Engineering, which reserves the right to distribute on the Web the published version of the Article and the making available of the Article in This format supposes for its Authors the fulfilment of what is established in the Law of Science and Technology of the United Mexican States, regarding the obligation to allow access to the results of Scientific Research.

Article Title:

Name and Surnames of the Contact Author and the Co-authors	Signature
1.	
2.	
3.	
4.	

Principles of Ethics and Declaration of Solution to Editorial Conflicts

Editor Responsibilities

The Publisher undertakes to guarantee the confidentiality of the evaluation process, it may not disclose to the Arbitrators the identity of the Authors, nor may it reveal the identity of the Arbitrators at any time.

The Editor assumes the responsibility to properly inform the Author of the stage of the editorial process in which the text is sent, as well as the resolutions of Double-Blind Review.

The Editor should evaluate manuscripts and their intellectual content without distinction of race, gender, sexual orientation, religious beliefs, ethnicity, nationality, or the political philosophy of the Authors.

The Editor and his editing team of ECORFAN® Holdings will not disclose any information about Articles submitted to anyone other than the corresponding Author.

The Editor should make fair and impartial decisions and ensure a fair Double-Blind Review.

Responsibilities of the Editorial Board

The description of the peer review processes is made known by the Editorial Board in order that the Authors know what the evaluation criteria are and will always be willing to justify any controversy in the evaluation process. In case of Plagiarism Detection to the Article the Committee notifies the Authors for Violation to the Right of Scientific, Technological and Innovation Authorization.

Responsibilities of the Arbitration Committee

The Arbitrators undertake to notify about any unethical conduct by the Authors and to indicate all the information that may be reason to reject the publication of the Articles. In addition, they must undertake to keep confidential information related to the Articles they evaluate.

Any manuscript received for your arbitration must be treated as confidential, should not be displayed or discussed with other experts, except with the permission of the Editor.

The Arbitrators must be conducted objectively, any personal criticism of the Author is inappropriate.

The Arbitrators must express their points of view with clarity and with valid arguments that contribute to the Scientific, Technological and Innovation of the Author.

The Arbitrators should not evaluate manuscripts in which they have conflicts of interest and have been notified to the Editor before submitting the Article for Double-Blind Review.

Responsibilities of the Authors

Authors must guarantee that their articles are the product of their original work and that the data has been obtained ethically.

Authors must ensure that they have not been previously published or that they are not considered in another serial publication.

Authors must strictly follow the rules for the publication of Defined Articles by the Editorial Board.

The authors have requested that the text in all its forms be an unethical editorial behaviour and is unacceptable, consequently, any manuscript that incurs in plagiarism is eliminated and not considered for publication.

Authors should cite publications that have been influential in the nature of the Article submitted to arbitration.

Information services

Indexation - Bases and Repositories

LATINDEX (Scientific Journals of Latin America, Spain and Portugal)

EBSCO (Research Database - EBSCO Industries)

RESEARCH GATE (Germany)

GOOGLE SCHOLAR (Citation indices-Google)

MENDELEY (Bibliographic References Manager)

HISPANA (Information and Bibliographic Orientation-Spain)

Publishing Services

Citation and Index Identification H

Management of Originality Format and Authorization

Testing Article with PLAGSCAN

Article Evaluation

Certificate of Double-Blind Review

Article Edition

Web layout

Indexing and Repository

Article Translation

Article Publication

Certificate of Article

Service Billing

Editorial Policy and Management

1047 La Raza Avenue -Santa Ana, Cusco-Peru. Phones: +52 1 55 6159 2296, +52 1 55 1260 0355, +52 1 55 6034 9181; Email: contact@ecorfan.org www.ecorfan.org

ECORFAN®

Chief Editor

SERRUDO-GONZALES, Javier. BsC

Executive Director

RAMOS-ESCAMILLA, María. PhD

Editorial Director

PERALTA-CASTRO, Enrique. MsC

Web Designer

ESCAMILLA-BOUCHAN, Imelda. PhD

Web Diagrammer

LUNA-SOTO, Vladimir. PhD

Editorial Assistant

SORIANO-VELAZCO, Jesús. BsC

Philologist

RAMOS-ARANCIBIA, Alejandra. BsC

Advertising & Sponsorship

(ECORFAN® Republic of Peru), sponsorships@ecorfan.org

Site Licences

03-2010-032610094200-01-For printed material ,03-2010-031613323600-01-For Electronic material,03-2010-032610105200-01-For Photographic material,03-2010-032610115700-14-For the facts Compilation,04-2010-031613323600-01-For its Web page,19502-For the Iberoamerican and Caribbean Indexation,20-281 HB9-For its indexation in Latin-American in Social Sciences and Humanities,671-For its indexing in Electronic Scientific Journals Spanish and Latin-America,7045008-For its divulgation and edition in the Ministry of Education and Culture-Spain,25409-For its repository in the Biblioteca Universitaria-Madrid,16258-For its indexing in the Dialnet,20589-For its indexing in the edited Journals in the countries of Iberian-America and the Caribbean, 15048-For the international registration of Congress and Colloquiums. financingprograms@ecorfan.org

Management Offices

1047 La Raza Avenue -Santa Ana, Cusco-Peru.

Journal Industrial Engineering

“Topological and structural optimization of the brake pedal of a vehicle for the BAJASAE 2023 competition”

CORDERO-GURIDI José de Jesús, ALVAREZ-SANTIAGO Jesús Daniel, MARTINEZ-DIAZ Ana Paola and HERNANDEZ-URBANO Cesar

Universidad Popular Autónoma del Estado de Puebla

“Design of a nozzle for Stratasys uPrint SE Plus 3D printer”

CORTEZ-SOLIS, Reynaldo, ARENAS-ISLAS, David, BETANZOS-CASTILLO, Francisco and FUENTES-CASTAÑEDA, Pilar

Posgrado CIATEQ, A.C.

Tecnológico Nacional de México-TEC Valle de Bravo

“Photovoltaic Autonomous Electric Charging Station”

GARCÍA-CONTRERAS, Cecilia Pamela, ONTIVEROS-SÁNCHEZ, Kenneth Arturo and ALVAREZ-MACÍAS, Carlos

Instituto Tecnológico Nacional de México - Instituto Tecnológico de la Laguna

“Simulation model in ProModel to generate proposals for improving the H₂O purification process”

RUIZ-DIAZ, Montserrat, SOTO-LEYVA, Yasmin, BONES-MARTÍNEZ, Rosalía, and SANTOS-OSORIO, Arturo

Tecnológico Nacional de México - Instituto Tecnológico Superior de Huauchinango

